2014

Characterization of Suppressor of IKKepsilon function using immunofluorescence assays and quantitative colocalization analysis

Kenneth F. Lawrence

CHARACTERIZATION OF SUPPRESSOR OF IKK-ε FUNCTION USING IMMUNOFLUORESCENCE ASSAYS AND QUANTITATIVE COLOCALIZATION ANAYLSIS

A thesis submitted in partial fulfillment of the requirements for the degree of Master of Science at Virginia Commonwealth University

by

KENNETH F. LAWRENCE

B.S., Bridgewater College, 2013

Director: DR. JESSICA K. BELL

Virginia Commonwealth University

Richmond, Virginia

December 2014

Acknowledgements

I would like to take this opportunity to thank everyone who has helped me achieve success in the completion of my degree and thesis. First, I would like to thank my parents, Stephen and Martha Lawrence. They helped me grow into the person I am today, nurturing my curiosity and my drive to see any project I start through to completion. My parents also provided me with a diverse exposure to different facets of academia and life. My experiences growing up were not ordinary, but I thank my parents for that every single day.

I would also like to thank my brothers, Ethan and Charlie Lawrence. My brothers really are two of my closest friends. Ethan is always available to talk when I need to vent frustration or need a break from my studies. He provided comic relief at times and never ask questions or hesitate when I ask for help or advice. Charlie, has a gift for making me laugh, and for making me crazy, but his timing is impeccable. During visits when I came home, he always spent time doing things with me which provided the perfect stress relief at that time. Most importantly, both of them are great at listening when I just needed someone to talk to about life and work in general.

Perhaps most importantly, I would like to thank my lovely fiancée, Katelynn Lieb. She and I have very different personalities, yet in our five years together, she has brought out the best parts of my personality. Looking back, the person I was before I met Katelynn would not recognize me now. Katelynn supported me through the stress and pain of graduate school, always with a smile on her face. There were countless evenings in which I told her I would be home for dinner by 6:00 and then I would work in the lab and not get home until 10:00. She made so many sacrifices to help me and I can never adequately express how much her support and encouragement has meant to me.

I would like to thank the students with whom I shared the lab. Logan Meyer, a fellow student in the lab, shared the common work space with the Bell lab. Logan became a good friend during my time in the program, and was always there when I needed to talk, ask a question, or practice a presentation. Sean McKinley, another Master's student in the Bell lab, also became a good friend. Sean was always willing to help with lab work, work through a problem with me, or just talk for a while. Sean and Logan were both good at helping me prepare for exams and helped me keep on track with the academic aspects of the degree program. Sean and Logan, you have both been wonderful friends and you helped me have fun during my graduate school experience.

I would also like to take the time to thank the members of my committee for their time and the valuable expertise they offered during my work in the laboratory. Dr. Scott Henderson, I would like to thank you for the countless hours you spent training me on microscopy equipment and analysis software. You were always very approachable and willing to help when I had a question or issue I needed to address. Your guidance on the many techniques involved in confocal microscopy and image analysis exposed me to technologies I had never seen before I came to VCU and allowed me to discover my new passion in confocal microscopy. Dr. Jason Carlyon, I would like to extend my gratitude for your questions and suggestions regarding my project. Your comments and questions instigated critical reflection and analysis of my work, helping me to reach a more complete understanding of my research area. You were also integral in providing suggestions for papers to use as reference material when I was trying to better understand the work we were doing with intracellular pathogens.

Finally, but absolutely not least, I would like to thank Dr. Jessica Bell for accepting me into her laboratory and helping me develop as a scientist. When I joined your lab, I was a timid,

quiet person with little independent research experience. You provided me with the time and space in the lab for me to develop into a more outgoing, confident scientist, now capable of independent work in the laboratory. You also provided me with many laboratory skills that served me well on this project, and will continue to serve me well in my professional life. Additionally, your concern and involvement with my academics over this past year and a half were crucial, helping me to keep control of my coursework and learn to study more efficiently. Without your invaluable guidance and mentoring, I would not have been able to complete this project or my degree. So, from the bottom of my heart, you have my deepest gratitude.

Table of Contents

List of Tables

List of Figures

Abbreviations

APC – Antigen Presenting Cell

co-IP – co-immunoprecipitation

DAMP – Damage-Associated Molecular Pattern

dsRNA – Double-stranded RNA

eEF1A – Elongation Factor 1A

FAK – Focal Adhesion Kinase

FGFR1OP2/wit3.0 – Fibroblast Growth Factor Receptor 1 Oncogene Partner 2/Wound Inducible Transcript-3.0

FRET – Fluorescence Resonance Energy Transfer

Hsc – Heat Shock Cognate

Hsp – Heat Shock Protein

IFN – interferon

IKKε – IκB kinase epsilon

IL-10 – Interleukin-10

IRF – Interferon Regulatory Factor

LPS – Lipopolysaccharide

MAP – Microtubule-Associated Protein

MLC – Myosin Light Chain

M.O.I. – Multiplicity of Infection

MTOC – Microtubule Organizing Center

NA – Numerical Aperture

NAP1 – Nucleosome Assembly Protein 1

NK – Natural killer

NLRs – NOD-like Receptors

NPM1 – Nucleophosphomin-1

PAMP – Pathogen-Associated Molecular Pattern

PCC – Pearson's Correlation Coefficient

PCV – Pathogen-Containing Vacuole

poly(I:C) – Polyinosinic acid: polycytidylic acid

PRR – Pattern Recognition Receptor

RFP – Red Fluorescent Protein

RIG – Retinoic acid Inducible Gene

RLR – RIG-like Receptor

ROI – Region of Interest

SCV – *Salmonella*-Containing Vacuole

Sifs – *Salmonella*-Induced Filaments

SIKE – Suppressor of IKKε

SIM – Structured Illumination Microscopy

TANK – TRAF-Associated NFκB activator

TAP – Transporter Associated with antigen Processing

TBK1 – TANK-binding kinase 1

TRAF – TNF Receptor Associated Factor

TIR – Toll-IL-1 Receptor

TLR – Toll-like Receptor

TLR3 – Toll-like Receptor 3

TRIF – TIR-domain-containing adaptor-inducing interferon-β

Abstract

CHARACTERIZATION OF SUPPRESSOR OF IKK-ε FUNCTION USING IMMUNOFLUORESCENCE ASSAYS AND QUANTITATIVE COLOCALIZATION ANAYLSIS

Kenneth F. Lawrence, Master of Science

B.S., Bridgewater College, 2013

A thesis submitted in partial fulfillment of the requirements for the degree of Master of Science at Virginia Commonwealth University.

Virginia Commonwealth University, 2014

Major Director: Jessica K. Bell, Ph.D, Biochemistry and Molecular Biology

During viral infections, Toll-like receptor-3 (TLR3) stimulation initiates signaling to activate transcription of pro-inflammatory cytokines and type-1 interferons. Suppressor of IKK-ε (SIKE) interacts with two kinases in the signaling pathway, IKK-ε and TANK-binding kinase 1 (TBK1), inhibiting the transcription of type I interferons. Recently, this laboratory discovered that SIKE blocks TBK1-mediated activation of type I interferons by acting as a high affinity, alternative substrate of TBK1. Co-immunoprecipitation (co-IP) assays suggested that the SIKE interaction network impinged upon the cytoskeleton and RNA transport. To characterize SIKE's

function within the antiviral response, SIKE's role in RNA transport and cytoskeletal rearrangements was targeted for further study through immunofluorescence assays (IFAs), using traditional confocal microscopy. SIKE was found to colocalize with cytoskeleton components (β-actin and α-tubulin), endosomal and plasma membrane markers (Rab11a, LAMP-1, and LC3), and ribosomes (S6). Additionally, IFA labeling for actin cytoskeleton-associated proteins revealed that SIKE colocalized with α-actinin, β-catenin, ezrin, and Focal Adhesion Kinase (FAK) in both myeloid and epithelial cells. These results were consistent with the hypothesis that SIKE functions in trafficking related to the anti-viral innate immune response.

To further delineate the colocalization of α-actinin, α-tubulin, actin, and S6 colocalization with SIKE, super-resolution microscopy, Structured Illumination Microscopy (SIM), was used. In both cell lines, we found that SIKE colocalized with α-actinin, but did not consistently colocalize with the other markers. Therefore, SIKE localizes with actin, tubulin, and S6 at distances greater than the 85nm resolution achieved using SIM techniques.

To address SIKE function following pathogen challenge, SIKE interactions were examined following two distinct stimuli. Polyinosinic acid: polycytidylic acid (poly(I:C)) was used as a mimic for viral dsRNA challenge. Following poly(I:C) stimulation, SIKE localization from 15 minutes to 24 hours showed little to no change. In addition to mediating a response to viral challenge, TBK1, the kinase that phosphorylates SIKE, maintains Salmonella-containing vacuoles (SCVs) following *S.* enterica serovar *typhimurium* infection. Therefore, changes in SIKE colocalization during *Salmonella enterica* serovar *typhimurium* infection were examined. Because TBK1 is integral to maintenance of the *Salmonella* containing vacuole, the hypothesis was that SIKE may also contribute to the host cell response to this infection. SIKE colocalization with various markers for *Salmonella*-containing vacuoles changes during the time

course of *Salmonella* infection (15 minutes to 18 hours) in a manner that suggested SIKE may play a role in signaling and trafficking related to the host cell's response to this infection. These studies support a SIKE and α-actinin interaction that is consistent with SIKE functioning in the cytoskeleton. Furthermore, SIKE's altered colocalization following *Salmonella* challenge suggest this protein may contribute to cytoskeletal structures that maintain these pathogen-containing vacuoles.

CHAPTER 1: INTRODUCTION

1 Introduction

1.1 The Innate Immune Response

The immune system is the group of cells and organs within the body responsible for preventing and combating disease caused by external mediators [1]. In mammals, including humans, the immune system is subdivided into two parts; the innate immune system, and the adaptive or acquired immune system [1]. Classification of these two immune subsystems relies mostly on the mechanisms and mediators of their action, however, two defining features often used to differentiate between them are the rate of activation and the duration of their response. The innate immune system is associated with a rapid response to threat, becoming activated within minutes of initial detection [1]. The adaptive immune system, however, requires more time and energy to activate [1]. Usually, the time required to fully activate the adaptive immune system is expressed in hours and days rather than minutes [1]. The additional time and energy required to activate the adaptive immune system allow these cells and organs to successfully eliminate pathogens, often through cytotoxic or antibody mediated mechanisms.

While the adaptive immune system is critical to the resolution of disease once a disease state is established, the innate immune system acts in a preemptive capacity. The speed with which the innate immune system becomes activated allows these cells and organs to slow, or even prevent, the spread of disease-causing agents within the host [1]. In addition to response time, another feature used to distinguish the two immune systems is specificity. The innate immune system tends to respond to general, yet conserved threat signals, while the adaptive immune system is activated by extremely specific signals [1]. Although these immune

subsystems differ greatly in many characteristics, both subsystems are vital to immunity. If either subsystem is impaired, it can have far-reaching impacts on the ability of the afflicted organism to protect itself from disease or remove disease-causing agents, often resulting in problems with chronic illness [1]. The importance of each component of the immune system must not be overlooked. However, the remainder of this study focuses on the innate immune system, and therefore, the adaptive immune system will receive relatively little attention moving forward.

The innate immune response provides the body's first line of defense against disease caused by pathogens [1]. Pathogens are a group of microorganisms which are capable of causing disease in a host organism [2]. There are many types of cells that make up the innate immune system. These cells do not requiring mass division and specialization in order to perform their roles, which enables them to immediately respond to pathogen challenge [1]. The components of the innate immune system include physical and mechanical barriers, phagocytic cells, and some cytotoxic cells [1]. These cells all contribute to the innate immune system's primary function, which is to isolate pathogens and prevent their spread throughout the host [1]. Therefore, infection occurs when the pathogen successfully overcomes the innate immune system and establishes itself within the host organism [1]. Although infections do occasionally occur, they are relatively infrequent when one considers the exceptionally high level of exposure to pathogens to which humans are subjected. Humans are exposed to potential pathogens almost everywhere, including microbes that make up the microbiome of the body [2]. These pathogens can come in the form of bacterial, fungal, or protozoan microorganisms, invertebrate pathogens, or viral pathogens. The preventative functions of the innate immune systems help to ensure that humans are not constantly afflicted by infection.

There are many mechanisms by which the innate immune system functions to prevent the spread of pathogens within the body. The skin and mucosal layers (i.e. epithelia) act as barriers, preventing pathogen invasion at the major points of entry into the body. Barrier tissues act in passive means to protect the body from infection; the presence of these tissues is sufficient to allow them to perform their function. However, other components of the innate immune system, typically cells in the tissue or bloodstream, prevent infection by more active means. Phagocytic cells, such as macrophages and dendritic cells, engulf and destroy pathogens, thereby preventing pathogens from interacting with healthy cells in the surrounding tissue [1]. Upon engulfing pathogens, signaling within phagocytic cells becomes activated which causes them to signal to other components of the immune system [1]. Some chemical signals from phagocytic cells can activate additional innate immune cells, while other chemicals enhance the function of already activated innate or adaptive immune cells. These chemical signaling molecules are known as cytokines [1]. Cytokines act upon cells in nearby surrounding tissues to improve the local response to pathogen challenge. Other chemical signals have a greater distance at which they act; these chemical signals are known as chemokines. The purpose of chemokines is to provide a chemical gradient that guides immune cells to the site of pathogen challenge, improving the immune response [1]. In addition to phagocytosis of pathogens and components of pathogens, phagocytic cells are also capable of phagocytizing host cells which have been killed by host mechanisms in response to intracellular pathogen infection. The innate immune system includes some cells that have cytotoxic functions, aimed at killing host cells that have already been infected, preventing the pathogen from replicating and spreading further. Natural killer cells, known as NK cells, are the primary cytotoxic cells of the innate immune system [1]. NK cells recognize host cells infected by intracellular pathogens and signal these cells to undergo

programmed cell death in order to prevent further spread of the pathogen. This approach is quite effective because intracellular pathogens often rely on the cellular "machinery" of living host cells to survive. By killing infected host cells, NK cells, as well as other cytotoxic immune cells, are able to starve intracellular pathogens of biomolecules and host processes required for the pathogen to survive, replicate, and spread. The innate immune system is able to respond in a variety of ways to various general categories of threats. The signals that determine how the innate immune system responds to pathogen challenge are all activated quickly upon recognition of pathogen or infected self-cells. The mechanisms by which innate immune cells identify and recognize threats are vital to determining how the innate immune system will respond to pathogen threats.

Innate immune cells recognize potential threats to the host body through the binding of various ligands to receptors found within the innate immune cells. These receptors are known as Pattern Recognition Receptors (PRRs). PRRs are diverse and are able to recognize a variety of molecules and combinations of molecular patterns, which are known as Pathogen-Associated Molecular Patterns (PAMPs) [1, 3], or Damage-Associated Molecular Patterns (DAMPs) [3]. PRRs are divided into receptor families, based on the types of PAMPs with which they bind. Four major families of PRRs include Toll-like receptors (TLRs), RIG-like receptors (RLRs), NOD-like receptors (NLRs), and C-type lectin receptors [1, 3]. Receptors are classified within these families of receptors based on the types of molecules that are bound by the receptors and the signaling pathways that are activated. PRRs allow the innate immune system to make the distinction between self and non-self when these cells encounter and interact with other cells and molecules within the body [1]. The ability of innate immune cells distinguishing self- versus non-self-entities through PRRs is rooted in the fact that human cells do not express the PAMPs

recognized by PRRs [4]. Although PRRs help immune cells to distinguish self from non-self, these receptors are not specific, relative to receptors found in cells of the adaptive immune system. They are capable of binding to a wide variety of molecular patterns that must simply be close in structure to the intended molecular pattern for that particular receptor. Whereas adaptive immune cells are typically only activated upon binding their specific antigen, innate immune cells can become activated by binding a large host of similar molecules [1]. Due to the variety of molecular patterns capable of activating innate immune cells through PRRs, the innate immune response is able to defend against both bacterial and viral pathogens. For the work in this study, the TLR family is the focal point. Therefore, I will devote the majority of my efforts to examining the functions and activity of TLR pathways.

Although the innate immune system acts to prevent infection from developing, occasionally this function fails. To ensure a robust immune response, the cells of the innate immune system take on additional roles. In particular, phagocytic cells, i.e. macrophages and dendritic cells, perform tasks that enhance the adaptive immune response. These cells phagocytize pathogens, or products of pathogens, and process them into components which are compatible with the receptors of cells involved in the adaptive immune response [1]. By processing these antigens and presenting them to cells of the adaptive immune system, macrophages and dendritic cells act as Antigen Presenting Cells (APCs). APCs play an important role in the interaction of the innate immune response and the adaptive immune response [1]. These cells are crucial to the development of antigen specific B cells and T cells because they provide the antigens to which these cells develop specific receptors [1]. Although the innate immune system is often considered a rapid response to pathogen challenge, the role of APCs in connecting the innate and adaptive immune responses clearly demonstrates that innate

immunity continues to function alongside the adaptive immune system, performing a collaborative effort to effectively protect the body from pathogens, and remove pathogens when protection fails.

1.2 Toll-like Receptor 3 Signaling

The Toll-like Receptors constitute one of the major categories of Pattern Recognition Receptors expressed by innate immune cells. The human genome encodes 10 TLRs which are expressed on a variety of cells [1, 9]. Toll-like receptors have numerous ligands to which they bind and that are capable of inducing their activation [1]. Certain TLRs can be expressed on the plasma membrane, i.e. TLRs 1, 2, 4, 5, and 6, while TLRs 3, 7, 8, and 9 are expressed in the membrane of endosomes [1]. The location of TLRs within cells can indicate their role in innate immunity by suggesting what type of ligand could bind the receptor. While all TLRs play an important role in the function of innate immune recognition and activation, the primary focus of our study is the activity of Toll-like receptor 3.

Toll-like receptor 3 (TLR3) is expressed by dendritic cells [9] and NK cells [1], among other cell types. TLR3 binds double-stranded RNA (dsRNA), activating the innate immune response against viral infection [1, 4, 7]. *In vivo*, dsRNA has been shown to bind TLR3, as well as intracellular receptor targets [8]. TLR3 and its role in innate immune response to viral infection can be studied by using synthetic dsRNA to mimic viral dsRNA [8]. Of the available synthetic dsRNA variations, polyinosinic acid: polycytidylic acid (poly(I:C)) has been shown in past studies to produce the strongest TLR3 activation [8], and therefore, is commonly used as a substitute for viral dsRNA. Once TLR3 has bound dsRNA, a series of signaling events lead to full activation of the antiviral innate immune response.

The structure of TLR3 is important to understanding the mechanism by which this receptor signals, since the structure impacts the events that occur downstream of the receptor during signaling. TLR3 is expressed in the membrane of endosomes, with the ligand-binding domain, or the ectodomain, located in the internal compartment of the endosome [1]. This location enables TLR3 to be exposed to dsRNA products of viral pathogens contained within the endosome after phagocytosis. Due to the symmetry of dsRNA, two TLR3 ectodomains are able to bind a single piece of dsRNA at the same time [1]. Dimerization of TLR3 ectodomains brings together the Toll-IL-1 receptor (TIR) domains, located on the cytoplasmic surface of the endosome, which initiates signaling [1]. Downstream signaling via TLR3 occurs through a series of kinases, which ultimately results in the transcription of genes encoding pro-inflammatory cytokines (Figure 1).

Binding of dsRNA causes TLR3 to recruit TIR-domain-containing adapter-inducing interferon-β (TRIF) to the TIR domains of the receptor dimer [1, 9, 10]. In the type I interferon (IFN) response, TRIF then activates TRAF2/3/6, which is a collection of scaffolding proteins capable of acting upon IκB kinase epsilon (IKKε) and TANK-binding kinase 1 (TBK1) [10, 1, 5, 7]. IKKε and TBK1 are held in complex by a scaffold formed by NAP1 or SINTBAD [10], and act to phosphorylate the interferon regulatory factors (IRF), IRF3 and IRF7 [1, 5]. Phosphorylated IRF3 and IRF7 are transcription factors that translocate to the nucleus, where they induce transcription of type I interferons (IFN-β) [5]. In addition to the production of type I IFNs, activation of TLR3 also leads to the activation of NF-κB and caspase 8 [6, 5, 3]. Activated NF-κB is crucial for IFN-β transcription and the induction of pro-inflammatory cytokines (i.e. IL-6) [3]. Through the induction of apoptotic pathways, TLR3 signaling is able to stimulate programmed cell death of host cells that have become infected by viral pathogens. TLR3-

mediated cell death prevents further replication of viral pathogens within affected host cells by disruption of the host cells' mechanisms for DNA and RNA replication, upon which viruses are fully dependent for their own replication [1]. By eliminating viral pathogens' ability to replicate, TLR3 enables the innate immune cells to prevent further spread of the infection within the host.

The type I IFNs and NF-κB produced during the TLR3 signaling cascade perform additional functions in response to infection. Type I IFNs play a critical role in the activation of other antiviral responses beyond the TLR3 signaling pathway [1]. Similarly, NF-κB is crucial to the production of co-stimulatory molecules responsible for activation of adaptive immune cells [1]. TLR3 signaling is one of numerous signaling pathways initiated during the innate immune response capable of stimulating and enhancing the adaptive immune response.

Figure 1. TLR3 signaling pathway.

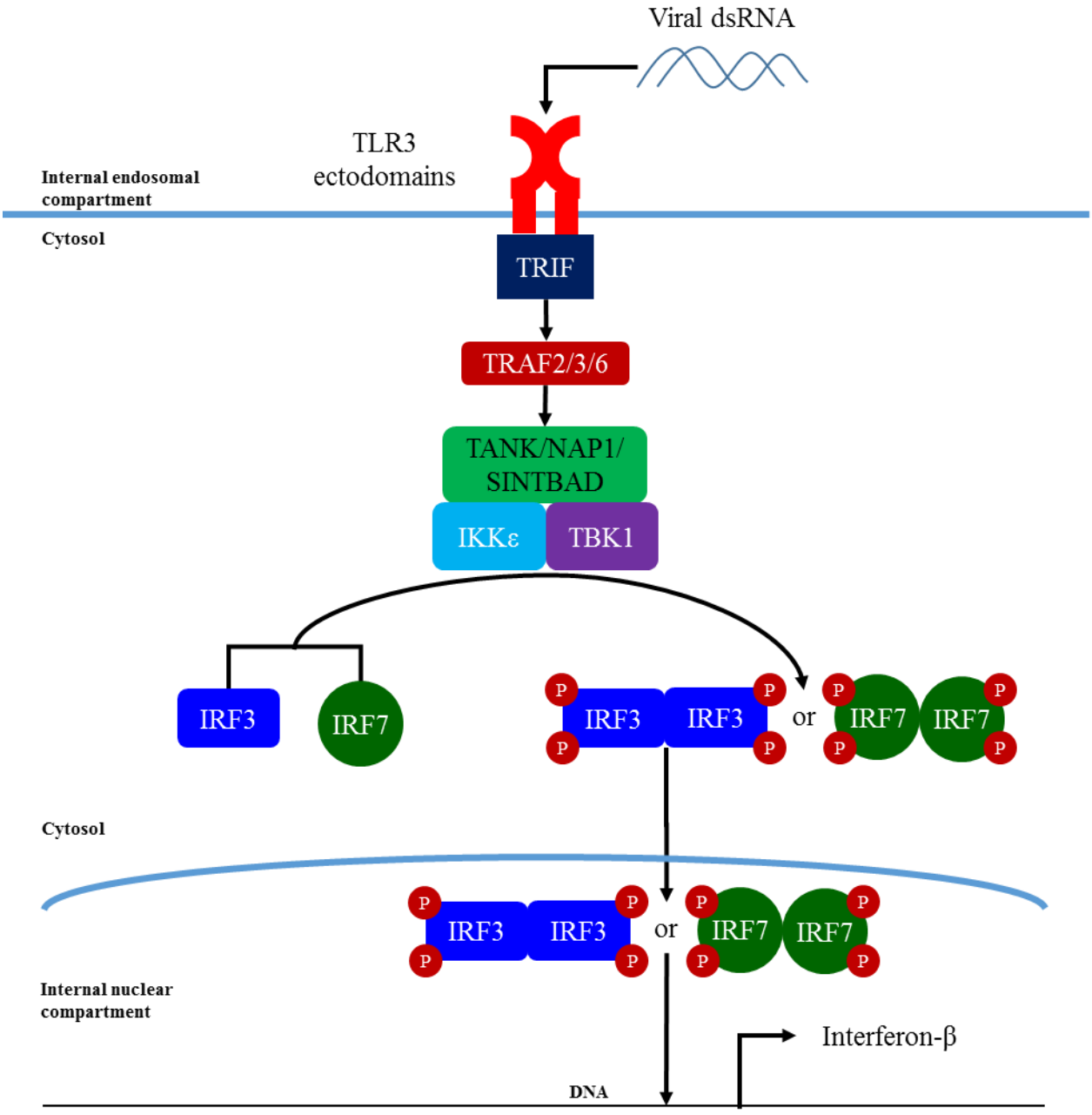

Figure 1. TLR3 signaling pathway. Diagrammatic representation of the events that occur during TLR3 type I interferon signaling. A pair of TLR3 ectodomains bind dsRNA, dimerize, and recruit TRIF to the cytosolic TIR domains. TRIF activates TRAF2/3/6 which then recruits IKKε and TBK1 held in complex by the NAP1/SINTBAD scaffold complex. IKKε and TBK1 then phosphorylate IRF3 and IRF7, which homodimerize and translocate to the nucleus where they stimulate transcription of genes.

1.3 The Role of Suppressor of IKK-ε in Innate Immunity

Suppressor of IKK-ε (SIKE) is a protein, 207 amino acids in length, which interacts with both IKK-ε and TBK1 downstream of TLR3 [5, 7]. SIKE was originally characterized as an endogenous inhibitor of TBK1, preventing the phosphorylation of IRF3 [5]. However, more recent work demonstrated that SIKE actually acts as a substrate of TBK1 [7]. SIKE associates with IKK-ε and TBK1 in the absence of viral pathogen challenge [5]. During viral infection, increased levels of SIKE mRNA indicate SIKE expression may be controlled by transcription factors activated by the anti-viral response [12].

Upon activation of the TLR3 signaling pathway, SIKE is phosphorylated by TBK1. This phosphorylation occurs at six serine residues which are similar to phosphorylation sites found on the TBK1 substrate, IRF3 [7]. The activity of TBK1 upon SIKE gives the appearance that SIKE is inhibiting TBK1 because the normal function of TBK1, phosphorylation of IRF3, is slowed. However, the reality is that SIKE is a substrate for which TBK1 has a higher affinity than it has for IRF3 [7] (Figure 2). Phosphorylation of SIKE is likely to alter the structure and function of the protein, as the addition of a large, negatively charged group often induces conformational changes in a protein's structure. Additionally, because the ability of TBK1 to phosphorylate its native substrate, IRF3, is merely slowed, the phosphorylation of SIKE lowers the affinity of TBK1 for the phosphorylated SIKE molecule. In turn, this leads to the release of SIKE by TBK1, thereby allowing IRF3 to occupy the active site and become phosphorylated. The derease in phosphorylation of IRF3 over time reduces the production of TLR3 signaling products, effectively slowing the TLR3 mediated antiviral response. Although previous work in our laboratory showed that SIKE is a high affinity substrate of TBK1, the function of SIKE after

phosphorylation is unknown. Thus our laboratory began exploration of the function SIKE performs in cells.

Determining the role a protein plays *in vivo* can be approached from two perspectives, the structure of the protein of interest or the interactions of the protein of interest. The structure of a protein can hint at its function through the presence of functional domains and homology to known proteins. Additionally, various methods of mapping a protein's tertiary structure to obtain the protein's structure can provide insight into the function of that protein. On the other hand, the interaction-based determination of a protein's function relies on quite different techniques. Interactions of a protein *in vivo* can be investigated by co-immunoprecipitation (co-IP), using the protein of interest as "bait" to pull down proteins with which the protein of interest interacts, as well as through the use of immunofluorescent labeling and confocal microscopy techniques. Our laboratory employs both structural and interaction based approaches to determining the function of SIKE. However, my research focuses on the interactions in which SIKE participates *in vivo*. Therefore, further explanations will revolve around identifying SIKE's function through its interaction network.

Previous work in the Bell laboratory used co-immunoprecipitation studies and tandem mass spectrometry to identify several SIKE interaction partners. These studies identified four main categories of interactions SIKE had with other proteins in cells, which allowed several functions to be proposed for SIKE (Figure 3). Based on an interaction identified between SIKE and nucleophosphomin-1 (NPM1) [55], a chaperone during ribogenesis, SIKE may play a role in ribogenesis. A second category of interactions identified between SIKE and various proteins involved in mRNA transport, including ALY [55] and Hsp70 [55], suggested that SIKE may play a role in mRNA trafficking. Another group of interactions identified between SIKE and

elongation factor 1A (eEF1A), which is a protein chaperone involved in facilitating translation [56], and also in bundling actin [56], was consistent with the NPM1 interaction, but also linked SIKE to the cytoskeleton. The fourth category of interaction identified between SIKE and γ-actin, indicated that SIKE may play a role in cytoskeleton rearrangement. This fourth function is also supported by the fact that eEF1A is also shown to interact with the actin cytoskeleton. Once these interactions were identified, experiments shifted to examining the localization of SIKE within cells to confirm these observations.

In addition to determining the interaction network of SIKE *in vivo*, our laboratory examined the basal localization of SIKE. The original localization patterns of SIKE within cells showed a pattern dependent upon cell type. In epithelial cells, SIKE localized to stress fiber-like structures and cytosolic puncta, but was not seen in the nucleus. On the other hand, in myeloid cells, SIKE was seen to localize to cytosolic puncta as well as nuclear puncta, but was not observed in stress fiber-like structures. These observations played an integral role in the development of current work examining the function of SIKE.

Figure 2. SIKE interaction with the TLR3 signaling pathway.

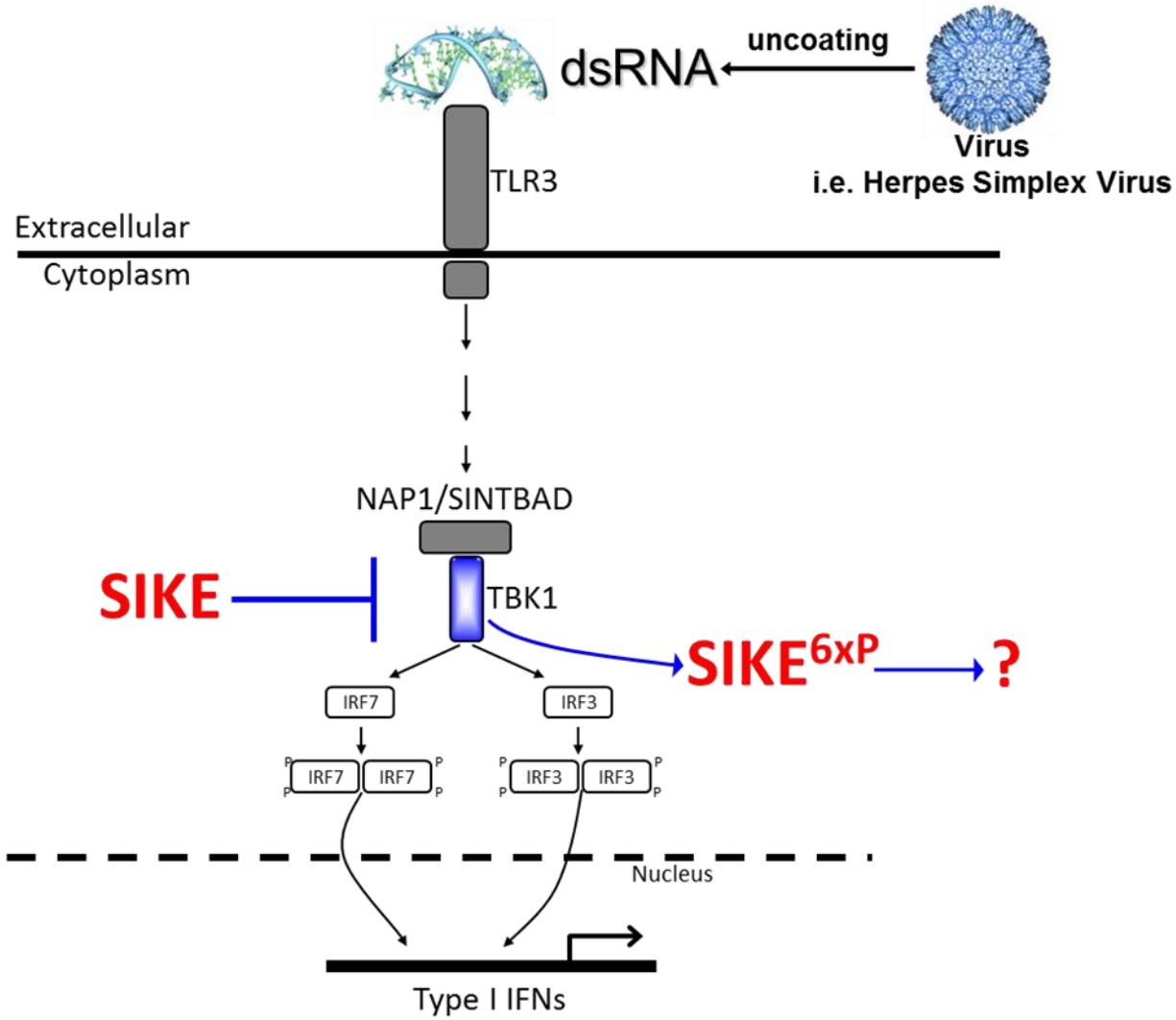

Figure 2. SIKE interaction with the TLR3 signaling pathway. Diagrammatic representation of SIKE's interaction with TBK1 in the TLR3 signaling pathway. Viral dsRNA binds to TLR3, activating the signaling cascade which activates TBK1. Traditionally, TBK1 phosphorylates IRF3 and IRF7, allowing them to translocate to the nucleus and induce transcription of type I IFNs. When SIKE interacts with TBK1, the higher affinity of TBK1 for SIKE than for IRF3 and IRF7 gives the appearance of inhibition of TBK1. However, the TBK1 actually phosphorylates SIKE instead of IRF3 and IRF7. The function of phosphorylated SIKE is yet to be determined.

Figure 3. SIKE interaction network.

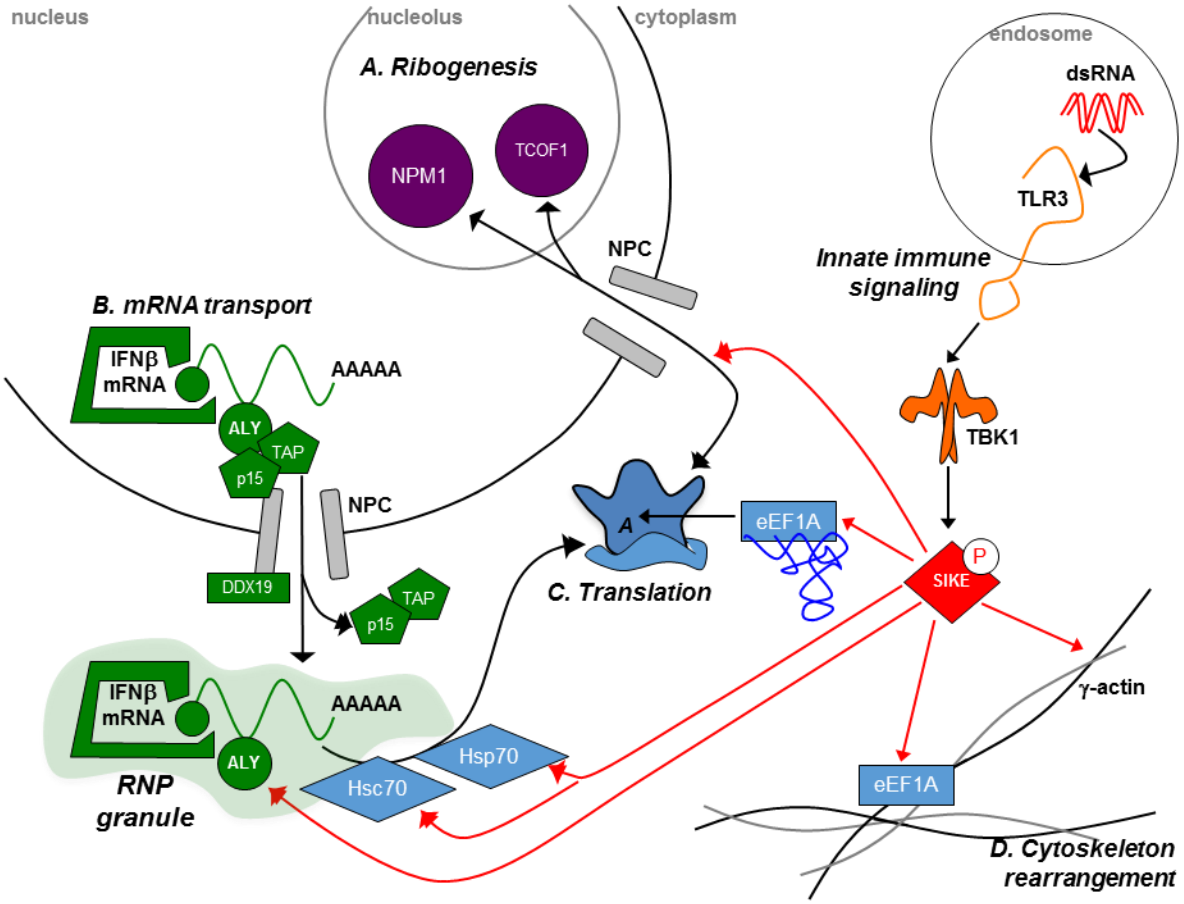

Figure 3. SIKE interaction network. Cartoon depicting the interactions of SIKE as identified by co-IP and tandem MS/MS experiments. (A-D) co-IP using SIKE as the bait identified four categories of interactions. (A) SIKE was shown to interact with NPM1, a key molecule in the process of ribogenesis, suggesting SIKE may also play a role in ribogenesis. (B) SIKE was pulled down with ALY, a key chaperone during mRNA transport, suggesting SIKE may also play a role in mRNA transport. (C) SIKE was pulled down with eEF1A, Hsc70, and Hsp70, which are important facilitators of translation, suggesting SIKE may play a role in initiating translation. (D) Interactions identified between SIKE and γ-actin, as well eEF1A, indicate SIKE may play a role in cytoskeleton rearrangement.

1.4 Signaling During *Salmonella enterica* Infection

TLR3 signaling is known to occur exclusively in response to binding of dsRNA. However, many signaling pathways in immunity have components that overlap in function or act in multiple pathways [1]. TBK1, a key component of the TLR3-mediated antiviral response, is also involved in the signaling that occurs during infection with *Salmonella enterica* serovar *typhimurium*. Previous studies have shown that TBK1 is essential for the maintenance of different types of pathogen-containing vacuoles (PCVs), including *Salmonella*-containing vacuoles (SCVs) [13]. TBK1 knockout and knockdown experiments show that PCVs in TBK1 deficient host cells often break down and release pathogens into the cytosol of the host cell, thereby failing to isolate the pathogen from the host cell [13]. TBK1 associates with the PCV during the later stages of the maturation of the endosomal structures associated with the PCV [13]. The associations TBK1 forms with PCVs and the importance of this kinase to the maintenance of these vacuoles suggest that interaction partners downstream of TBK1 may also play a role in the maintenance of PCVs (Figure 4). Since our lab concentrates on SIKE, a downstream interaction partner of TBK1, the possibility that other TBK1 associated proteins also interact with the PCV is intriguing. If our protein were to interact with the TBK1 associated with the PCV, the stage of infection at which the interaction occurs could lead to discerning the function SIKE performs with regard to this host defense.

From the moment *S. enterica typhimurium* is phagocytized, the endosomal compartment is undergoing a maturation process. Throughout the course of infection, the SCV interacts with various endosomes, acquiring different marker proteins, which enable the infection to be categorized into stages [14, 15]. In addition to markers directly associated with the SCV, the progression of *S. typhimurium* infection is also coupled with the up-regulation of certain

intracellular markers within the host cell which do not directly associate with the SCV [14, 15]. The changing landscape of markers within host cells enable distinguishing among three major stages of infection.

At the earliest stages of infection, within 30 minutes of initial infection [14], early endosome markers are associated with the SCV [14, 15]. Included in these early endosome markers associated with the SCV are: EEA1 [14], Rab5a, b, and c [14, 15], and Rab4 [15]. These markers are associated with endosomes recently formed following phagocytosis, which are trafficking inward through the cytosol from the plasma membrane. As the infection reaches the later stages, these markers eventually dissociate from the SCV, marking the transition from an early SCV to the later stage SCVs.

During the intermediate stage of SCV maturation, between 30 minutes and 5 hours post-infection, various late endosome and recycling endosome markers associate with the SCV. These markers include: Rab7, Rab11a and b [14, 15], and Rab2 [15]. Also associated with the SCV at the intermediate stages of maturation are LAMP markers [14], which are associated with the lysosomes. The markers associated with the intermediate stage of SCV maturation indicate a shift toward the host cell making an effort to resolve the infection by targeting the SCV for degradation. Late endosome markers are associated with endosomes which are nearing their final destination within cells, while the increase in lysosomes suggest the host cell is preparing to destroy the invading pathogen.

Finally, during the late stage of *S. enterica typhimurium* infection, markers such as Rab7 [14, 15], Rab9, and LAMP markers [14] associate with the SCV. *Salmonella*-induced filaments (Sifs) are other structures seen at the late stages of infection. Sifs are endosomal compartments known to associate with the Microtubule Organizing Center (MTOC), and microtubules within

the host cell [15]. Sifs are distinguished by the collection of microtubules radiating toward the edges of the cell with the SCV at the center. In this later stage, the increased presence of late endosome and lysosome markers indicate further efforts on the part of the host cell to clear the pathogen. Additionally, the presence of Sifs indicate that the *Salmonella* has begun to repurpose the host cellular functions.

Figure 4. TBK1 and maintenance of *Salmonella*-containing vacuole.

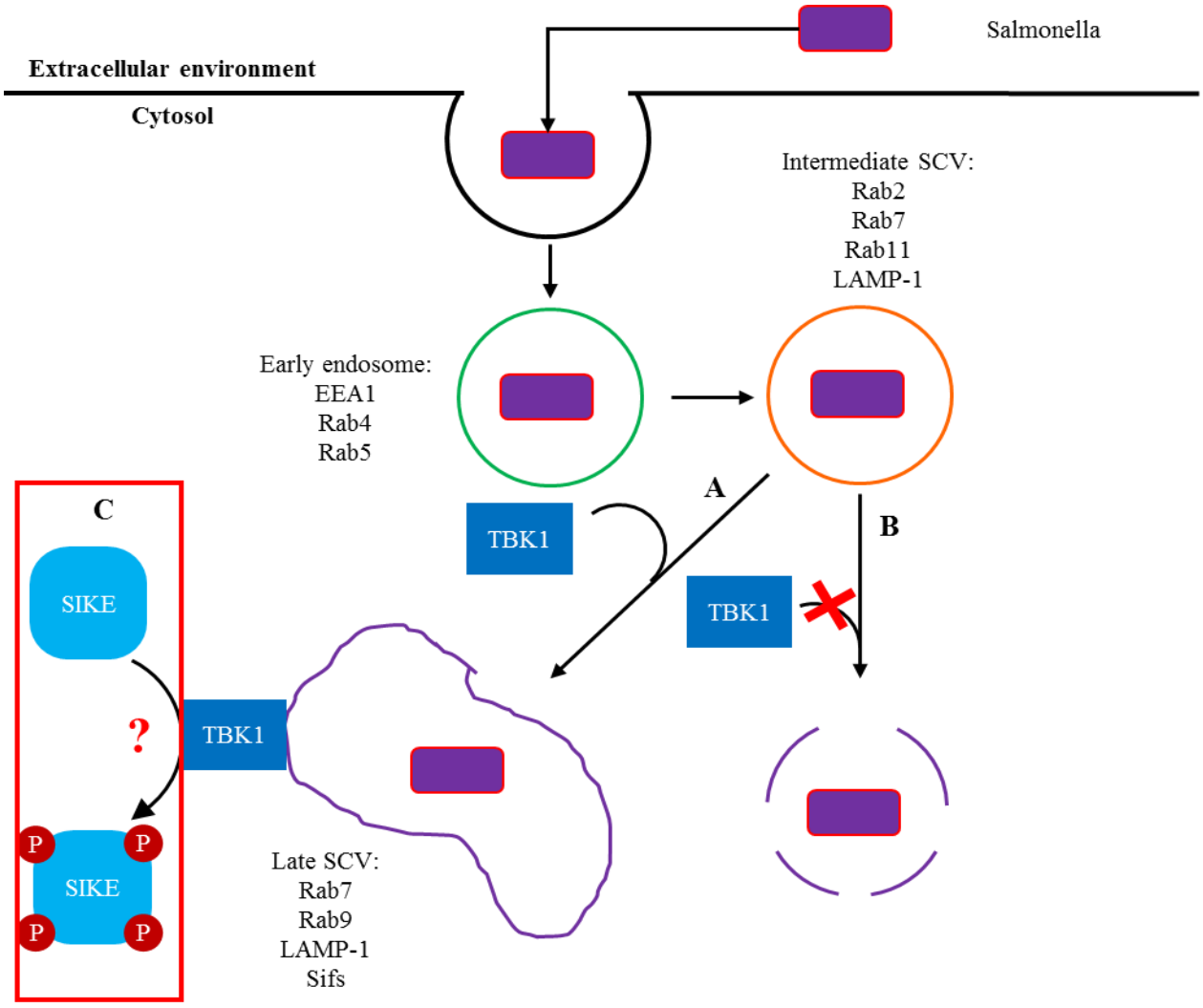

Figure 4. TBK1 and maintenance of *Salmonella*-containing vacuole. Schematic representation of the progression of *Salmonella* infection. *Salmonella* is phagocytized by the cell and progresses through early endosomes and late endosomes. (A) At the transition from late endosome, TBK1 associates with the *Salmonella*-containing vacuole and aids the maintenance of this structure. This action is part of the host defense, which keeps *Salmonella* separated from the cytosol, preventing unchecked growth and replication. (B) In cells in which TBK1 is not present or functioning properly, the SCV degrades, releasing the *Salmonella* into the cytosol and preventing the effective immune response to the infection. The interaction of TBK1 with the SCV and its importance to SCV maintenance indicate that downstream partners of TBK1 may also be crucial to SCV maintenance. (C) Although it is unknown, SIKE may play an important role in the maintenance of the SCV, following phosphorylation by TBK1 associated with the SCV.

1.5 Quantitative Analysis of Colocalization

Colocalization is described as two molecules being present in close proximity, typically the same location, within a cell [16]. In the vast majority of studies, colocalization is examined by looking for the presence of overlap between two color channels in a digital image of a cell labeled for immunofluorescence [16]. The colors in the two channels are the result of excitation of a molecule, known as fluorophore, which causes it to release photons of light with a particular energy content, which determines the specific wavelength of the photon [16, 17]. The different wavelengths of light emitted by fluorophores are often detectable as different colors by the human eye. Typically, green and red fluorophores are employed for use in two color channel studies. When overlap occurs between the signals of photons in these wavelengths, it can be seen as yellow when present in an image. However, in most studies, the proteins examined are present at different levels. The different levels of these proteins mean that they could colocalize without producing yellow signal, which is why quantitative analysis of colocalization is necessary. Many studies of colocalization rely on the presence of this yellow signal to determine if two molecules colocalize [16]. The resolution of the microscope defines the minimum distance at which two objects can be seen as separate from one another. Resolution depends on many factors but is mainly determined by the numerical aperture (NA) of the objective lens used and the wavelength of light used to illuminate the sample. Typically, confocal microscopes are able to achieve a resolution of about 250nm [30]. When the objects emitting the signals are closer to each other than the microscope can resolve, overlap of the signals is observed [30]. At this distance, the separation between the objects is unresolved and thus the two objects are inferred to be colocalized. During image collection, the researcher establishes values for many parameters, such as signal saturation, which can alter the perceived presence of colocalization by

visualization alone. The wide array of factors impacting the perception and presence of colocalization make it difficult to rely solely on the visual appearance of overlap to determine colocalization.

As confocal microscopy developed, attempts to devise methods of quantifying colocalization developed simultaneously. In 1993, a paper by Manders, et al. defined several coefficients and mathematical formulas that could be used to quantify colocalization in dual-color confocal images [17]. Building from the Pearson's Correlation Coefficient, which was an established tool in analysis of patterns [17], a series of coefficients were presented which could further describe colocalization. These coefficients attempted to make quantification of colocalization possible through minimizing the impacts of less precise parameters involved in image collection (Table 1). Some of these coefficients eliminated the impact of signal intensity on their value, while others were designed to incorporate the effects of intensity on the final outcome. The final result of this work was a set of tools that scientists studying colocalization could use in order to quantify their data, and remove some of the subjective components associated with colocalization studies. The subjective components of assessing colocalization lie in the historic reliance upon assessment of colocalization based on the perception of an overlap color (e.g. yellow in dual-labeled red and green images). The tools developed by Manders are available, in the form of computer programs, to most scientists attempting quantitative analysis of colocalization. A wide variety of software is currently available for performing quantitative analyses of colocalization. Although each software is quite different from the others, they all function based on the work of Manders, using the coefficients from the seminal paper to analyze and quantitate colocalization.

Perhaps the most crucial aspect of quantitative analyses of colocalization is the defining of threshold values. A threshold value is a value of intensity in each color channel, which is defined by the researcher as the intensity of the minimum positive signal in that color channel [18]. The threshold values provide the computer program performing the computational portion of analysis with a value that defines which intensities are to be used in calculating the various colocalization coefficients. Only pixels in a particular channel with an intensity value in that channel above the threshold value are included in the computation of the colocalization coefficients pertaining to that color channel. Pixels possess signal intensity values for all color channels present in a particular image. Those pixels that possess signal intensity value above the threshold value in both channels are considered to be colocalized pixels. Therefore, setting thresholds are extremely influential, because the values of the threshold settings determine which pixels of an image are included in the calculation of the colocalization coefficients.

The setting of thresholds introduces another facet of subjectivity to the process of quantitative analysis of colocalization. Threshold setting is important because it determines a specific intensity value for each channel of an image that defines the separation between specific and nonspecific labeling by that signal [57]. Currently, there is a distinct lack of widely accepted computational or technology based methods to determine the appropriate threshold values for analyzing an image. Methods for determination of thresholds include manual and automated techniques. Manual techniques rely on the researcher's ability to identify the minimum intensity value considered a positive signal for each signal channel. Automated methods, including Costes automatic threshold, rely on the use of algorithms to calculate threshold values for images [57]. The main difficulty involved in the use of automated techniques is the lack of universal ability to properly apply theses methods. Each program or calculation has advantages and

disadvantages, but currently, none have been developed which are universally accepted. Therefore, most colocalization studies that rely upon quantitative analysis are influenced heavily by the person performing the analysis. Their determination of thresholds can greatly influence the outcome of quantitative analysis of colocalization. However, improvements in image collection, careful threshold adjustment, and proper training in image analysis techniques, coupled with an understanding of the available coefficients to describe colocalization in a quantitative manner can serve to minimize the impact of subjectivity on the final outcome.

In addition to the impacts of various components of quantitative analysis colocalization, colocalization is strongly impacted by the approach employed in labeling a sample. Labeling techniques, such as labeling with antibodies, expression of fluorescent tagged protein, or staining using organic dyes, each impact the observed result in imaging studies. Additionally, labeling techniques can directly impact thresholds for quantitative colocalization analysis based on the background signal produced by various labeling molecules. For instance, staining with organic dyes can be produce excess background signal if the staining is performed too long or if the excess dye is not appropriately washed away prior to mounting. The presence of background signal can also be affected by nonspecific labeling by antibodies. However, proper application of quantitative colocalization analysis methods can minimize the problems associated with these factors affecting thresholds and background signal. In my research, the primary focus was the amount of overlap between SIKE and its interaction partners. Additionally, when SIKE was found to interact with these molecules, we were interested in how they interacted, i.e. to what degree they colocalized and whether there is a substantial correlation between the localization of the two proteins. Little of my research concerned the intensity of the signal in either channel of our images, so moving forward I will spend little time dealing with colocalization coefficients

that are sensitive to signal intensities (i.e. the k_1 and k_2 coefficients). We thought it was more important for our investigation at this stage to focus on how much SIKE colocalized with various markers, irrespective of intensity. However, I would like to emphasize that we did not ignore or throw away data pertaining to coefficients of colocalization affected by intensity. We considered these data, but decided against using them to structure the focal points of our studies.

Table 1. Coefficients for quantitative analysis of colocalization.

Coefficient	Formula	Characteristics
Pearson's Correlation Coefficient	$r_p = \frac{\sum_i (R_i - R_{aver}) \cdot (G_i - G_{aver})}{\sqrt{\left[\sum_i (R_i - R_{aver})^2 \cdot \sum_i (G_i - G_{aver})^2\right]}}$ *	• Defines correlation between two channels • Range -1 to 1
Overlap Coefficient	$r = \frac{\sum_i R_i \cdot G_i}{\sqrt{\left[\sum_i (R_i)^2 \cdot \sum_i (G_i)^2\right]}}$ *	• Gives overlap between two channels • Not sensitive to differences in signal intensities between channels • Ratio of objects strong influence • Range 0 to 1
Overlap coefficient k_1	$k_1 = \frac{\sum_i R_i \cdot G_i}{\sum_i {R_i}^2}$ *	• Examines overlap of only red channel with green channel • Sensitive to differences in intensity of green channel • Range 0 to 1
Overlap coefficient k_2	$k_2 = \frac{\sum_i R_i \cdot G_i}{\sum_i {G_i}^2}$ *	• Examines overlap of only green channel with red channel • Sensitive to differences in intensity of red channel • Range 0 to 1
Colocalization coefficient M_1	$M_1 = \frac{\sum_i R_{i,\,coloc}}{\sum_i R_i}$ *	• Examine colocalizing intensities in red channel • Not sensitive to differences in signal intensity • Range 0 to 1
Colocalization coefficient M_2	$M_2 = \frac{\sum_i G_{i,\,coloc}}{\sum_i G_i}$ *	• Examine colocalizing intensities in green channel • Not sensitive to differences in signal intensity • Range 0 to 1

*Equations were taken from original Manders et. al paper from 1993 [17].

Table 1. Coefficients for quantitative analysis of colocalization. Table describing the coefficients from the research of Manders et. al. Each coefficient has characteristics which lend it value for analysis under different circumstances. The far left column gives the name of each coefficient, while the center column gives the mathematical formula used to calculate each coefficient. The far right column defines the key characteristics of each coefficient. Mathematical terms: $\sum_i$ = sum of intensities, R_i = intensity values in the red channel, R_{aver} = average intensity of red channel, G_i = intensity values in the green channel, G_{aver} = average intensity of green

channel, $R_{i,\ coloc}$ = intensity of colocalizing signal in the red channel, and $G_{i,\ coloc}$ = intensity of colocalizing signal in the green channel.

1.6 Current Study

My work with SIKE is an attempt to discern the function of SIKE by examining the associations of this protein within cells. In conjunction with the result of the tandem mass spectrometry and co-IP experiments, the initial localization patterns of SIKE were used to determine a panel of ten common intracellular markers for which to begin examination of SIKE colocalization partners. The original ten markers included cytoskeletal markers, endosomal markers, and RNA-associated markers. The cytoskeletal markers were β-actin and α-tubulin. The original endosomal markers included LC3, LAMP-1, Rab5, Rab7, and Rab11a. The original RNA-associated markers were Edc4, PABP, and S6. Analysis of the data obtained for these ten markers led to the selection of five additional cytoskeletal markers: α-actinin, β-catenin, caveolin-1, ezrin, and Focal Adhesion Kinase (FAK). Later, we also examined myosin light chain (MLC). We also examined three possibilities to identify the cytosolic puncta: PSMA7, PMP70, and TBK1. Our early data also led us to examine two additional RNA-associated markers in order to attempt to identify the nuclear puncta observed in myeloid cells. These two markers were fibrillarin and nucleophosphomin-1 (NPM1).

My research focused on quantitating the levels at which SIKE colocalized with various intracellular markers. Based on the patterns of SIKE localization in cells and the interactions identified by co-IP, we examined SIKE colocalization with our selected markers. Once images were obtained by confocal microscopy, the colocalization was quantified using one of two software programs. In addition to studying the levels of SIKE colocalization in normal conditions, we also examined SIKE localization and colocalization during pathogen challenge. Pathogen challenge conditions were studied by infection time course experiments using either

dsRNA to mimic viral infection or a red fluorescent protein (RFP) expressing strain of *S. enterica typhimurium* to establish *Salmonella* infection.

The examination of SIKE localization during viral challenge was primarily concerned with determining whether there was a change in the pattern of SIKE localization over the course of pathogen challenge. The work for this part of the study relied predominantly on analysis of SIKE localization over the time course of an infection. Using a variety of time points, images were collected over the defined time frame and analyzed to detect changes in SIKE localization. Once images were collected, segmentation analysis was used in an attempt to determine to which types of structures SIKE appeared to localize during viral infection. Ultimately, this work was not fruitful using fixed slides from specified time points. On the other hand, fixed cells infected with *Salmonella enterica* serovar *typhimurium* and fixed at different time points during the infection, then labeled for various markers provided insight into SIKE function during *Salmonella* infections.

Chapter 2: Materials and Methods

2 Materials and Methods

2.1 Mammalian cell culture

Three cell lines were used for *in vivo* study of SIKE colocalization. The DOV13 ovarian epithelial cancer cell line and the RAW264.7 mouse macrophage cell line were already present in the laboratory. The CCD-18Co colon epithelial cell line was purchased from American Type Culture Collection (ATCC).

DOV13 and RAW264.7 cell lines were cultured in complete media composed of RPMI 1640 supplemented with 10% fetal bovine serum, 20mM L-glutamine, 1X non-essential amino acids, 10mM sodium pyruvate, 100mM HEPES, 50units/mL penicillin, and 50µg/mL streptomycin. CCD-18Co cells were cultured in Eagle's Minimum Essential Medium supplemented with 10% fetal bovine serum, 50units/mL penicillin, and 50µg/mL streptomycin. Cells used for immunofluorescence labeling and microscopy were cultured for fewer than 20 passages. All cells were cultured at 37°C and 5% CO_2.

2.2 Stable cell lines

Stable cell lines expressing fluorescently labeled SIKE were prepared for use in live cell imaging over the course of dsRNA challenge. pCDNA3.1 SIKE sYFP2 and pCDNA3.1 mTURQ SIKE constructs were previously constructed in our laboratory. pCDNA3.1 vector carries a hygromycin resistance gene for selection following mammalian cell transfection. DOV13 and RAW264.7 were transfected with 4µg pCDNA3.1 SIKE sYFP2 or mTURQ SIKE using lipofectamine 2000 following manufacturer's protocol (Invitrogen/Life Technologies).

Transfected cells were selected by addition of 50μg/mL hygromycin (previously determined) to the media. Frozen stock of cells grown under 3 weeks of hygromycin selection were created for future analyses. We intended to establish stable cell lines which expressed these fluorescent-tagged proteins in order to characterize changes in SIKE localization over the course of dsRNA challenge.

2.2.1 DNA amplification and purification

100μg of stock DNA for GFP-tagged constructs of Rab4, 5, 10, 11, 14, 22, and 35 (Carlyon laboratory at Virginia Commonwealth University, Richmond, Virginia) were used to transform alpha-bronze *E. coli* cells as per manufacturers protocol (Bioline). Transformed *E. coli* were plated on LB agar plates supplemented with 50 μg/mL kanamycin. One colony from each transformed batch of *E. coli* was selected and grown in 100 mL LB broth culture containing 50μg/mL kanamycin. Flasks were cultured overnight at 37°C and 200 rpm in a shaker. Cells were harvested from culture by centrifugation 4000 rpm for 7 minutes. Pellets were then stored at -20°C. Purification of plasmid DNA was completed following the manufacturer's instructions (Qiagen EndoFree Plasmid Maxi Kit).

2.3 *Salmonella enterica* serovar *typhimurium* strain SL1344 cell culture

The RFP-expressing *S. enterica typhimurium* strain, SL1344, was a gift from the Detweiler laboratory, University of Colorado Boulder, Boulder, Colorado. The SL1344 strain contained the StrR plasmid with the pDsRed gene. Selection markers for this strain included streptomycin resistance and ampicillin resistance genes.

2.3.1 RFP expression based selection

The SL1344 strain was originally grown on LB agar plates containing 30μg/mL streptomycin and 100μg/mL ampicillin to select a single colony for liquid culture. Plates were incubated at 37°C overnight and observed the next day. Colonies were then selected for highest RFP expression, as determined by the vibrant pink appearance of colonies, and streak plated on fresh LB/strep/amp plates. Selection was performed over two cycles, resulting in 10 culture plates with high RFP expression. From these colonies, the 10 most vibrantly pink colonies were selected and used to make glycerol stocks, which became the stocks of SL1344 for all future experiments.

2.3.2 SL1344 culture and mammalian cell infection

Prior to infection, SL1344 was cultured in 5 mL LB broth containing 300 μg/mL streptomycin and 100 μg/mL carbenicillin overnight at 37°C and 200 rpm in a shaker, until the cultures had reached an O.D. = 1. An O.D. = 1 provided us with 5×10^8 bacteria/mL of culture, allowing us to calculate the multiplicity of infection, or M.O.I. In addition to previously described selection, we explored reducing the temperature at which the SL1344 was grown in liquid culture to enhance RFP expression. Cultures were grown until turbid, at which point the temperature was reduced to 16°C, then grown overnight. Reducing the temperature at which SL1344 was grown was intended to slow the process of protein folding, providing the bacteria with more time to properly fold the RFP protein. Success or failure of this method was determined by performing test infections of cells in culture and pelleting the remaining bacterial culture to observe the color of the pellet. Based on the success of this method, all subsequent SL1344 cultures were grown until turbid at 37°C in 5 mL LB broth cultures containing

300μg/mL streptomycin and 100μg/mL carbenicillin, then grown overnight at 16°C and 200rpm in the shaker.

The day prior to infection, DOV13 (25,000 cells/mL) and RAW264.7 (10,000 cells/mL) were plated into 6 well plates containing glass coverslips (Fisher #1.5 (170μm thick)). The SL1344 culture was started early in the morning the day prior to infection, grown to turbidity and then incubated overnight at 16°C and 200rpm. Early experiments used an M.O.I. of 20 for the DOV13 cell line and 50 for the RAW264.7 cell line, but few cells were found to be contain SL1344. Later experiments used an M.O.I of 1000 for DOV13 infections and 2500 for RAW264.7 infections which improved number of cells containing multiple bacteria for imaging purposes. SL1344 were allowed to infect mammalian cells for 1 hour and then media was removed, cells were rinsed one time with 1X PBS and then cultured in complete media containing 100μg/mL gentimicin to kill any bacteria remaining outside mammalian cells.

On the day of infection, optical density at 600nm of SL1344 was measured and culture adjusted to $O.D._{600nm} = 1$. The number of cells in 1 well/cell line was counted. Using the number of cells/well and the density of SL1344 (1 $O.D._{600nm} = 5 \times 10^8$ bacteria/mL), the volume of bacterial cell culture for a given multiplicity of infection was determined. Prior to SL1344 infection, cell media was refreshed with media sans antibiotics. The appropriate volume of bacterial cell culture was added to the infection media by diluting the bacteria to the appropriate M.O.I. with media containing RPMI 1640, 10% fetal bovine serum, 200mM L-glutamine, and 5mM HEPES. 2 mL of this media was added to each well of the mammalian cell cultures, and the cells were incubated for 1 hour at 37°C and 5% CO_2. Coverslips intended for use at 0 minute time points were incubated for the 1 hour with media containing only RPMI 1640, 10% fetal bovine serum, 200mM L-glutamine, and 5mM HEPES; SL1344 was not added to this media.

After 1 hour, the infection media was replaced with 2mL in each well of complete media supplemented with 100 μg/mL gentamycin to stop the infection. Cells were cultured in this media at 37°C and 5% CO_2. Coverslips were fixed by removing media, rinsing one time with 1X PBS, then incubating for 10 minutes in ice cold 4% formaldehyde in PBS. Fixed coverslips were stored in hydrated chambers at 4°C in 1X PBS. Time points included 0 minutes, 15 minutes 30 minutes, 1 hour, 5 hours, and 18 hours after stopping the infection.

2.4 dsRNA challenge

Double-stranded RNA challenge experiments were performed using poly(I:C) dsRNA as a substitute for viral dsRNA. Mammalian cells were cultured overnight and then challenged with 50μg/mL poly(I:C). Cells were fixed at 0 minutes, 15 minutes, 30 minutes, 1 hour, 2 hours, 8 hours, 12 hours, and 24 hours post-poly(I:C) challenge. Cells used for the 0 minute time point were not challenged with poly(I:C), but were fixed at the same time poly(I:C) was added to all other wells.

2.5 Immunofluorescence assays

2.5.1 Coverslip preparation

Coverslips were prepared prior to use in immunofluorescence by acid cleaning. #1½ coverslips were separated and placed in a beaker. In a fume hood, 200mL of nitric acid and 100mL of HCl were mixed, added to the beaker containing the coverslips, and swirled occasionally for 2 hours. The mixture was then decanted into waste beaker and a small amount of water was added. After fumes dissipated, cold water was run over the coverslips until pH 5.5 – 6.0 was reached. Coverslips were then stored in a jar containing 70% ethanol. When preparing for cell culture, coverslips were removed from the jar one at a time, using tweezers,

and flamed over an ethanol burner to remove excess 70% ethanol, then placed in individual 35mm wells.

2.5.2 Immunofluorescent labeling of cells in culture

Mammalian cells were cultured in 6 well tissue culture plates. Tissue culture plates were prepared by placing one acid washed coverslip in each well. 2mL of cells were added to each well. For immunofluorescence, DOV13 cells were plated at a density of 25,000 cells/mL, while RAW264.7 cells were plated at a density of 10,000 cells/mL.

2.5.2.1 Fixing cells

Cells grown on coverslips were fixed by removing the culture media and rinsing in 1 mL 1X PBS. After removing the 1X PBS, cells were fixed in 1 mL ice cold 4% formaldehyde in PBS for 10 minutes, at room temperature. Cells were then rinsed in 1 mL 1X PBS if proceeding to immunofluorescent labeling, or stored in 2 mL 1X PBS at 4°C.

2.5.2.2 Primary antibody labeling

After cells were fixed, they were either stored in 2 mL 1X PBS in each well or washed once with 1X PBS before proceeding with the labeling procedure. All labeling procedures were performed at room temperature unless otherwise indicated. Cells were permeabilized in 1 mL 0.1% Triton-X-100 (Fisher) in 1X PBS for 10 minutes, with gentle rotation. Cells were then washed three times in 2 mL 1X PBS, with gentle rotation. Cell were blocked in 1 mL 5% goat serum in 1X PBS for 1 hour with gentle rotation. 200 μL of primary antibody diluted in 5% goat serum in PBS was placed on Parafilm, in a humidity chamber, and coverslips were placed, inverted (i.e. cell side down), on top of primary antibody solution. In dual-labeled experiments,

both primary antibodies (from different species) were added simultaneously. Primary antibodies were diluted as follows:

A. Rabbit α-SIKE1 (Sigma), 2 ng/μL (stock 0.5 mg/mL) in 5% goat serum in 1X PBS
B. Mouse α-β-actin(8H10D10) (Cell Signaling), 1:600 in 5% goat serum in 1X PBS
C. Mouse α-α-actinin (Sigma), 1:300 in 5% goat serum in 1X PBS
D. Mouse α-β-catenin(E-5) (Santa Cruz Biotech., Inc.), 1:250 in 5% goat serum in 1X PBS
E. Mouse α-caveolin-1 (Sigma), 1:1500 in 5% goat serum in 1X PBS
F. Mouse α-Edc4(F-1) (Santa Cruz Biotech., Inc.), 1:200 in 5% goat serum in 1X PBS
G. Mouse α-ezrin (ThermoFisher), 1:200 in 5% goat serum in 1X PBS
H. Mouse α-FAK (Pierce), 1:500 in 5% goat serum in 1X PBS
I. Mouse α-fibrillarin(Nop1p) (Invitrogen), 1:500 in 5% goat serum in 1X PBS
J. Mouse α-CD107a(LAMP-1) (BioLegend), 1:250 in 5% goat serum in 1X PBS
K. Mouse α-MAP LC3β(G-2) (Santa Cruz Biotech., Inc.), 1:200 in 5% goat serum in 1X PBS
L. Mouse α-phospho-myosin light chain 2(Ser19) (Cell Signaling), 1:200 in 5% goat serum in 1X PBS
M. Mouse α-NAK [TBK1] (ThermoFisher), 5 μg/mL (stock 500 μg/mL) in 5% goat serum in 1X PBS
N. Mouse α-PABP(A-4) (Santa Cruz Biotech., Inc.), 1:200 in 5% goat serum in 1X PBS
O. Mouse α-PMP70 (Sigma), 1 μg/mL (stock 1000 μg/mL) in 5% goat serum in 1X PBS
P. Mouse α-PSMA7(M01) (Abnova), 2 μg/mL (stock 500 μg/mL) in 5% goat serum in 1X PBS
Q. Mouse α-Rab4 (BD Transduction Laboratories), 1:300 in 5% goat serum in 1X PBS

R. Mouse α-Rab5(D-11) (Santa Cruz Biotech., Inc.), 1:200 in 5% goat serum in 1X PBS
S. Mouse α-Rab7(D-4) (Santa Cruz Biotech., Inc.), 1:200 in 5% goat serum in 1X PBS
T. Mouse α-Rab9 (ThermoFisher), 1:500 in 5% goat serum in 1X PBS
U. Mouse α-Rab11a(D-3) (Santa Cruz Biotech., Inc.), 1:200 in 5% goat serum in 1X PBS
V. Mouse α-S6 ribosomal protein (54D2) (Cell Signaling), 1:25 in 5% goat serum in 1X PBS
W. Mouse α-α-tubulin(DM1A) (Cell Signaling), 1:4000 in 5% goat serum in 1X PBS

Cells were incubated overnight with primary antibodies at 4°C. The following morning, coverslips were returned to 6 well tissue culture plates with 2 mL 1X PBS in each well.

2.5.2.3 Secondary antibody labeling

Cells were washed in 2 mL 1X PBS three times, with gentle rotating. Then, they were incubated for 1 hour with 1 mL secondary antibody solution with gentle rotating, while covered. In dual-labeled experiments, secondary antibodies were added simultaneously. Secondary antibodies were diluted as follows:

A. Goat α-rabbit IgG (Alexa Fluor® 488 conjugate) (Cell Signaling), 1:1000 in 5% goat serum in 1X PBS
B. Goat α-mouse IgG (Alexa Fluor® 555 conjugate) (Molecular Probes), 1:1000 in 5% goat serum in 1X PBS
C. Goat α-mouse IgG (Alexa Fluor® 568 conjugate) (Molecular Probes), 1:1000 in 5% goat serum in 1X PBS
D. Goat α-mouse IgG (Alexa Fluor® 633 conjugate) (Molecular Probes), 1:1000 in 5% goat serum in 1X PBS

E. Goat α-mouse IgG (Alexa Fluor® 647 conjugate) (Molecular Probes), 1:1000 in 5% goat serum in 1X PBS

In dual-labeled studies, goat α-rabbit AF488 was used alongside either goat α-mouse AF555 or goat α-mouse AF568. *Salmonella* infection studies involved triple-labeled experiments, and therefore goat α-rabbit AF488 was used alongside either goat α-mouse AF633 or goat α-mouse AF647. All steps carried out after secondary antibody incubation were performed with cells covered, to prevent photobleaching of fluorophores. Following incubation with secondary antibodies, cells were washed in 2 mL 1X PBS three times, with vigorous rotating. In later experiments examining actin, cells were not labeled with the mouse α-actin primary antibody. Instead, phallotoxins conjugated to fluorophores were used. Phallotoxin labels were diluted as follows:

A. Alexa Fluor® 555 phalloidin (Moleular Probes), 1:40 in 5% goat serum in 1X PBS

Cells were labeled with AF555 phalloidin by placing 200μL of diluted AF555 phalloidin on Parafilm, in a humidity chamber, and placing coverslips, inverted, on top of diluted phalloidin. Cells were then incubated for 20 minutes at room temperature, while covered. After incubation, AF555 phalloidin labeled coverslips were returned to wells with 2 mL 1X PBS and procedure continued with three washes with 1X PBS. Cells were stringently washed in 1 mL 0.1% Triton-X-100 in 1X PBS with vigorous rotating (vigorous indicates ~75 rpm, normal ~50rpm) to remove any nonspecific labeling. Cells were washed three times in 2 mL 1X PBS with vigorous rotating. At this point, coverslips intended for use in Structured Illumination Microscopy (SIM) were mounted on microscope slides. Otherwise, cells were counter-stained for DNA with Hoechst stain. Hoechst stain was diluted and administered as follows:

A. Bisbenzimide H 33342 (Sigma), 10 µg/mL (stock 1 mg/mL) in 1 mL 1X PBS

Counter-staining in 1X PBS was performed for one minute. Cells were then washed three times in 2 mL 1X PBS with vigorous rotating, before being mounted on slides.

2.5.2.4 Coverslip mounting

After immunofluorescent labeling was complete, coverslips were mounted on microscope slides. Microscope slides were washed with 100% ethanol and wiped with a KimWipe to dry. Most coverslips were mounted using the SloFade® Gold antifade reagent (Molecular Probes). Mounting these coverslips was accomplished by placing a drop of SloFade® on the microscope slide and removing the coverslip from the well and wicking away excess PBS. The coverslip was then placed, inverted, on top of the drop of SloFade® and excess SloFade® was wicked away using a KimWipe. The coverslip was sealed to the microscope slide using nail polish around all edges. Sealed microscope slides were laid flat to allow nail polish to harden and stored in microscope slide boxes at 4°C.

Coverslips intended for SIM experiments were mounted using ProLong® Gold antifade reagent (Molecular Probes). Mounting these coverslips was accomplished by placing a drop of ProLong® Gold on the microscope slide and removing the coverslip from the well and wicking away excess PBS. The coverslip was then placed, inverted, on top of the drop of ProLong® Gold. The microscope slides were stored, lying flat, in microscope slide boxes at room temperature for at least 24 hours prior to imaging to allow the ProLong® Gold time to cure.

2.5.3 Imaging of immunofluorescence labeled cells

Imaging of microscope slides was performed in the VCU Microscopy Facility housed in the Department of Anatomy and Neurobiology, Virginia Commonwealth University, Richmond,

Virginia. Dual-labeled microscope slides were imaged using the Zeiss LSM700 confocal microscope system (> 5 images/marker, Zeiss Zen 2011 Black Edition, version 7.0). Triple-labeled microscope slides were imaged using the Zeiss LSM710 confocal microscope system, which employs the QUASAR array detector (3 images/marker/time point/trial, Zeiss Zen 2011 Black Edition, SP3, version 8.1). This detector allows for sufficient separation between color channels in triple-labeled experiments. Images collected using these two systems were captured using the 63x objective lens on each microscope. Detector offsets and gains for the images collected on both systems were set using the "Range Indicator" option in the software and the parameters were adjusted to minimize the red and blue pixels (maximum and minimum gray values) in order to make use of the full range of gray levels for each channel in each image. Images on both microscopes were collected in sequential scanning mode: dual-labeled images were collected with the blue and red channels together, and the green channel was collected independently, triple-labeled images were collected with the blue and red channels together, and the green and far red channels together. Dual-labeled images were collected using Zeiss LSM700 filters: short pass 490 for the blue channel, long pass 560 for the red channel, and short pass 555 for the green channel. Lasers used to excite the fluorescent molecules in the dual-labeled experiments include the 405nm (blue channel), 488nm (green channel), and 555nm (red channel). Triple-labeled images were collected using Zeiss LSM710 filters: 410-483 for the blue channel, 580-629 for the red channel, 493-561 for the green channel, and 638-747 for the far red channel. Lasers used to excite the fluorescent molecules in the triple-labeled experiments include the 405nm (blue channel), 488nm (green channel), 561nm (red channel), and 633nm (far red channel). Pixel dimensions and z-step parameters were set according to Nyquist Sampling Criteria (2 pixels or z-slices per unit of resolution). Structured Illumination Microscopy was

performed using the Nikon N-SIM system (5 images/marker, Nikon NIS-Elements Advanced Research, version 4.2). SIM images were collected using the Apo TIRF 100x objective lens. Samples were illuminated using lasers of 488nm (green channel) and 561nm (red channel). Pixel dimensions and z-step parameters were set according to Nyquist Sampling Criteria (2 pixels or z-slices per unit of resolution). SIM images were collected using SIM 488 filter (EX 480/40x, DM 495, EM 518/58m) and SIM 561 filter (EX 561/20x, DM 570, EM 605/90m). Early experiments relied on single z-plane images, however, all experiments following the original ten markers made use of full cell z-stack images.

2.6 Quantitative analysis of colocalization

Quantitative analysis of colocalization was performed on all images obtained. Two-dimensional, or single-slice, images were analyzed using the "Coloc" function of the Zeiss Zen software (Zen 2011 Black Edition, SP2, version 8.0). Thresholds were determined using the scatterplot depicting intensities of either selected channel. The channels included in the scatterplot were set to the same color channel, producing a line of slope = 1 representing the pixels in that channel. The crosshair on the scatterplot was then moved along the line until the indicator color (e.g. white) was present in all pixels of that channel considered to be positive for that signal. Once the thresholds were determined for each color channel in each image, the output coefficients were recorded. All data were saved in ".czi" file format, with data tables also exported from the Zen software as text files. Regions of Interest (ROIs) were defined to examine differential SIKE colocalization within cells.

Three-dimensional images were analyzed using the Volocity software (Volocity 6.3, version 6.3.0, Perkin-Elmer). Analysis was performed using a series of commands to build a protocol for analyzing images. The protocol began by defining the threshold of each color

channel. The threshold was then used in conjunction with the "Find Objects" command to define objects in the image which were above threshold in each color channel. The thresholds were determined by adjusting the intensity value associated with "Find Objects" until all voxels considered to be positive for the signal in each channel were occupied by the corresponding indicator color associated with that channel. Once the objects in both channels were defined, the "Intersect" command was selected to define the regions of overlap between above threshold objects in each channel. For each image, the total volume (in μm^3) of each category of objects was recorded. Using the volume of objects identified by the "Intersect" command and the volume of objects defined by each "Find Objects" command, variations of the Manders M1 and M2 coefficients were calculated, shown below.

$$Coloc.of\ channel\ = \frac{volume\ of\ intersecting\ objects(\mu m^3)}{volume\ of\ total\ objects\ in\ channel(\mu m^3)}$$

2.6.1 Segmentation analysis of dsRNA challenge images

Segmentation analysis was performed on images from the DOV13 dsRNA challenge time course at time points 0 minutes, 30 minutes, and 2 hours. This analysis was used to identify changes in SIKE localization induced by dsRNA challenge. The analysis was performed using the Volocity software. The key to successful segmentation analysis was the fine-tuning of the protocol used to analyze the images. The SIKE associated with the plasma membrane was measured. A Region of Interest was traced near the edge of the cell, following the contours of the plasma membrane. The image was then cropped twice, once to include the exterior of the ROI boundary, and once to include the interior of the ROI boundary. Cropping these images removed signal not included in the ROI. Therefore, when examining the ROI that included the

plasma membrane, the middle of the cell was removed from the image. On the other hand, the plasma membrane region was removed when examining the interior ROI. The membrane-associated SIKE was quantified by measuring the volume of total SIKE in the exterior ROI. The cropped image with the interior of the ROI was used to examine the localization of SIKE to structures other than the plasma membrane. A variety of filters were used to define the structures formed by SIKE. The final protocol applied to the interior of the ROI first measured the total SIKE signal in the cell, based on signal intensity. Signal intensity was determined for each image individually. The most fine-tuned protocol developed defined SIKE puncta based on volume. The volume of SIKE puncta was defined as less than 2.5 μm^3. SIKE fibers were defined as SIKE structures with volume greater than 2.5μm^3 and a longest axis greater than 9μm. The remaining SIKE not defined as puncta or fibers was categorized as miscellaneous SIKE. Data gathered using the most recent protocol we developed was compiled and plotted on a graph to examine the significance of the results.

CHAPTER 3: RESULTS

3 Results

3.1 Suppressor of IKK-ε localization in epithelial and myeloid cell types

Previous work in the Bell laboratory made use of co-IP tandem MS/MS assays to identify potential interaction partners of SIKE in HEK293 cells and RAW264.7 cells. These assays immunoprecipitated FLAG-tagged SIKE and examined the proteins associated with SIKE by tandem MS/MS. Based on these results, a number of shared interactions among different experimental conditions were outlined between SIKE and various proteins within cells. The proteins that were shown to interact with SIKE included cytoskeletal proteins such as actin and tubulin, and RNA-associated proteins such as ALY/REF, Hsp70 and HSP90, and nucleophosphomin.

Following the co-IP experiments, the *in vivo* localization patterns of SIKE were examined by immunofluorescent labeling and confocal microscopy. Immunofluorescent labeling for SIKE demonstrated that SIKE localized differentially, dependent on cell type (Figure 5). Labeling for SIKE in DOV13, an ovarian epithelial cancer cell line, indicated that SIKE localizes to cytosolic puncta and stress fibers, but not to the nucleus (Figure 5A). In RAW264.7, a mouse macrophage cell line, labeling demonstrated that SIKE localizes to cytosolic and nuclear puncta, but not to stress fibers (Figure 5B). After demonstrating a group of interaction partners and the cellular localization patterns of SIKE, we sought to define its specific colocalization partners *in vivo*.

Due to concerns that our ovarian epithelial cancer cell line may not represent an immunologically relevant platform for examining SIKE's interaction network *in vivo*, we

obtained an additional epithelial cell line, CCD-18Co colon epithelial cells. We found that the pattern of SIKE labeling observed in CCD-18Co was similar to the labeling pattern for SIKE observed in DOV13 (Figure 6). In order to determine whether SIKE localization changed depending on cell density, we prepared coverslips from all three cell lines in which cells were allowed to grow to confluence before fixing. We determined that SIKE localization in cells at confluence was similar to the pattern of SIKE localization observed at sub-confluent conditions (Figure 6). Therefore, we concluded that SIKE localization was not dependent on the density of a cell culture.

Figure 5. SIKE localization is cell-type dependent.

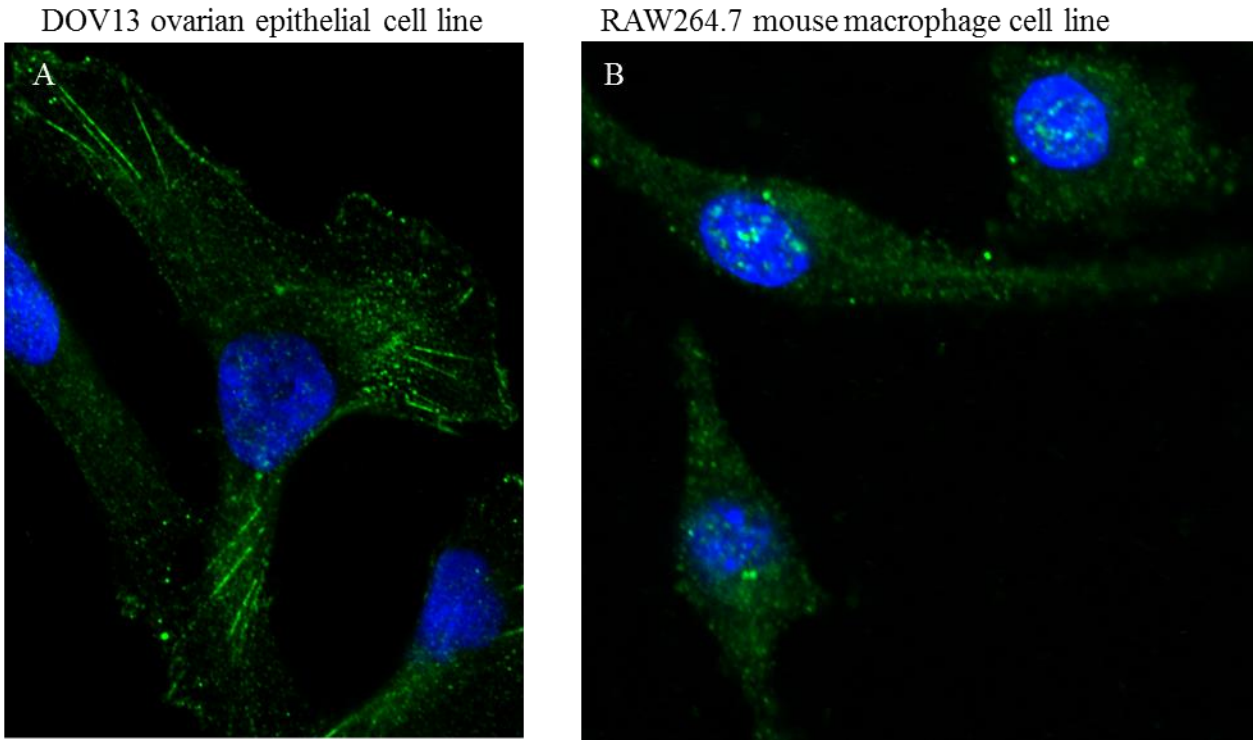

Figure 5. SIKE localization is cell-type dependent. DOV13 and RAW264.7 labeled for SIKE (green) and counterstained for DNA (blue, Hoechst). (A) In epithelial cells, SIKE localizes to cytosolic puncta and stress fibers, but does not localize to the nucleus. (B) In myeloid cells, SIKE localizes to cytosolic and nuclear puncta, but does not form stress fibers.

Figure 6. SIKE localization is consistent between epithelial cell lines, and is not impacted by cell density.

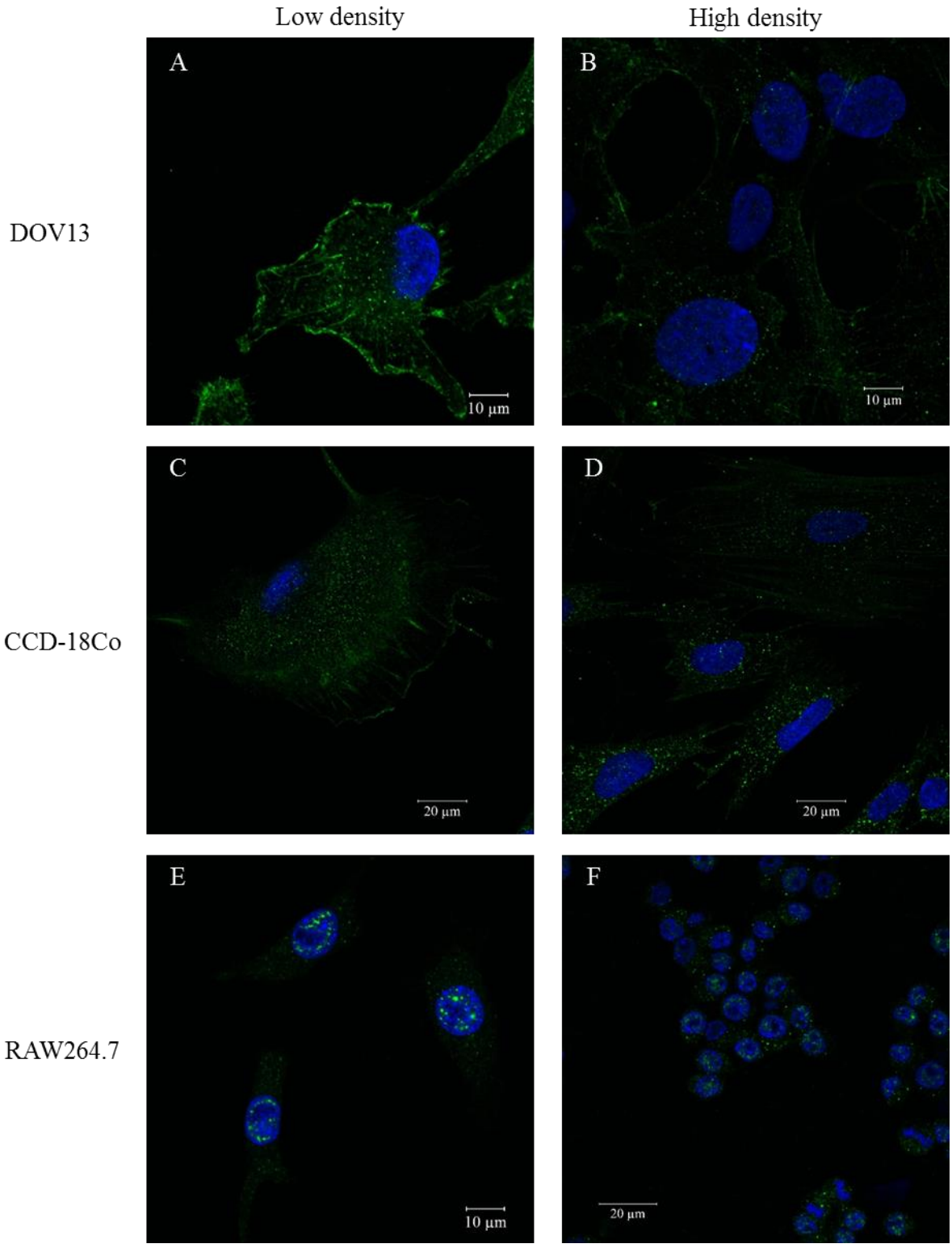

Figure 6. SIKE localization is consistent between epithelial cell lines, and is not impacted by cell density.

DOV13, CCD-18Co, and RAW264.7 labeled for SIKE (green) and counterstained for DNA (blue, Hoechst).

DOV13 at (A) low cell density and (B) confluence compared to CCD-18Co at (C) low cell density and (D) confluence. SIKE localizes to both cytosolic puncta and stress fibers in DOV13 and CCD-18Co. These structures are also visible at low cell density and confluence in both epithelial cell lines. RAW264.7 labeled for SIKE at (E) low cell density and (F) confluence. SIKE localizes to cytosolic and nuclear puncta, but not stress fibers, in RAW264.7 cells grown at low cell density and confluence. Images were captured by confocal microscopy, using optimized gain and laser power settings for each image.

3.2 Suppressor of IKK-ε colocalization with cellular markers

Based on the interactions identified by co-IP and the localization patterns of SIKE observed in cells, a panel of ten standard intracellular markers were selected. We performed immunofluorescent labeling of DOV13 and RAW264.7 cells for SIKE and each of the 10 markers. Microscope images of immunolabeled cells were analyzed visually for colocalization between SIKE and the selected markers. Subsequent quantitative analysis of colocalization in images labeled for the original markers provided data that was used to select additional markers to refine our understanding of SIKE's interactions in the cell. For certain SIKE structures, we used the patterns of SIKE localization and the initial quantitative data to select additional markers to attempt to identify structures that were not positively identified using the original markers. Final analysis of the compiled results of the colocalization analysis allowed us to propose potential roles SIKE may fulfill in the TLR3 signaling pathway.

3.2.1 Panel of cellular markers

The original ten markers we assessed are markers of general cellular structures and organelles. These markers fit into three distinct categories of subcellular structures: endosomal markers, RNA-associated markers, and cytoskeletal markers. We began our colocalization experiments by seeking to determine the types of organelles and cellular structures with which SIKE colocalized. After the analysis of SIKE colocalization with the original ten markers was complete, we selected six additional cytoskeletal markers, three additional cytosolic puncta markers, and two nuclear puncta markers in an effort to refine our understanding of SIKE's colocalization partners *in vivo*.

3.2.2 Puncta markers

The puncta markers that we examined were categorized into endosomal and RNA-associated markers. The endosomal markers we tested were Rab5 (early endosomes [19]), Rab7 (late endosome [20]), Rab11a (recycling endosomes [21]), LAMP-1(lysosome [22]), and LC3 (autophagosome [23]). Varying levels of colocalization were observed between SIKE and the endosomal markers. SIKE was not observed to localize with Rab5, Rab7, LAMP-1 or LC3 in epithelial cells (Figure 7A, B, D, E) or myeloid cells (Figure 8 A, B, D, E); however, colocalization was observed between SIKE and Rab11a in both epithelial cells (Figure 7C) and myeloid cells (Figure 8C).

In addition to endosomal markers, RNA-associated markers including Edc4 (processing bodies [24]), PABP (stress granules [25]), and S6 (ribosomes [26]) were investigated as potential SIKE colocalization partners in the cell. SIKE did not appear to colocalize with Edc4 or PABP in either cell line (Figure 9 A and B, Figure 10 A and B), but we did observe colocalization between SIKE and S6 in both epithelial cells (Figure 9C) and myeloid cells (Figure 10C).

Figure 7. SIKE colocalizes with Rab11a, but not with other endosomal markers in DOV13 cells.

A

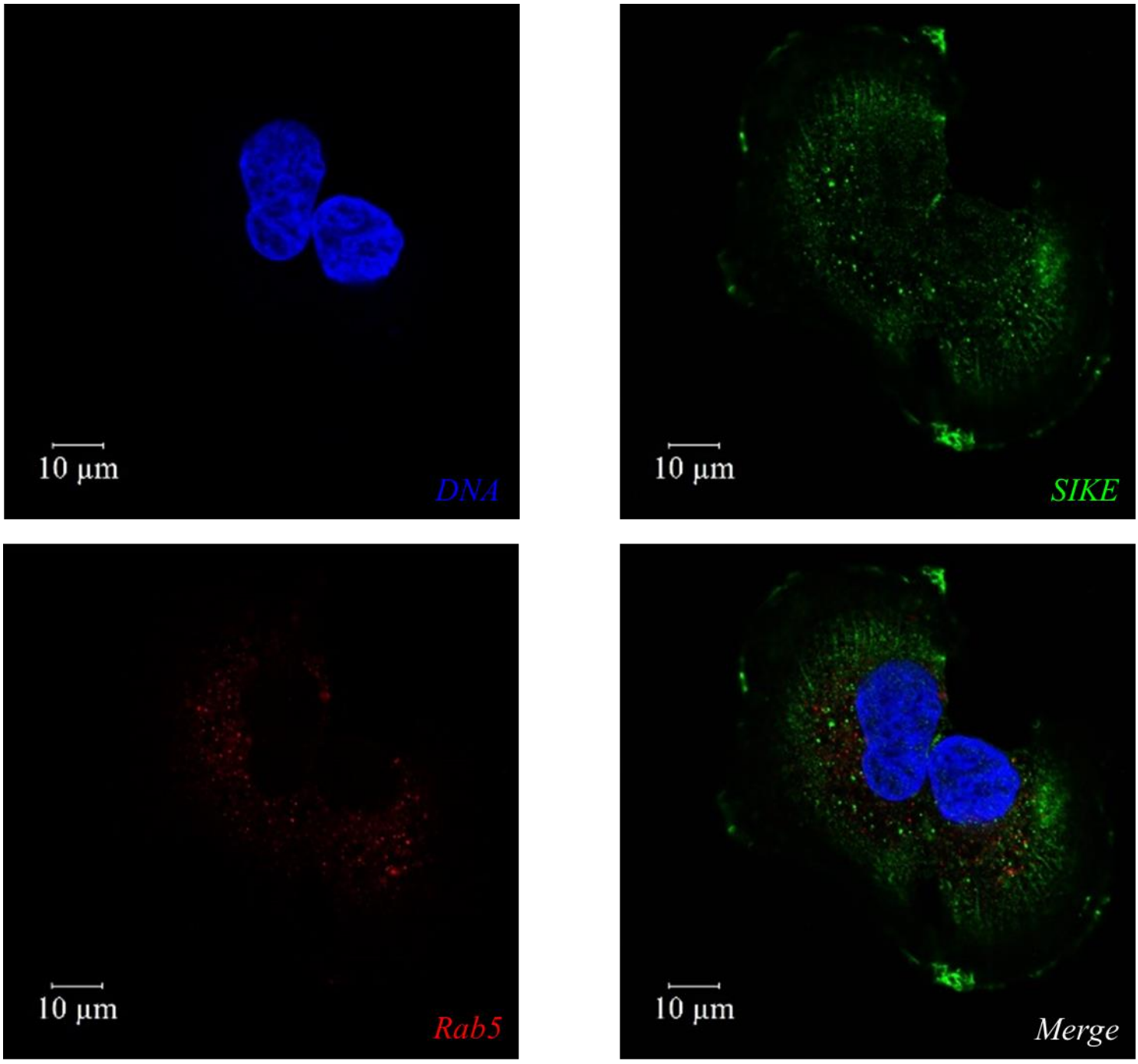

B

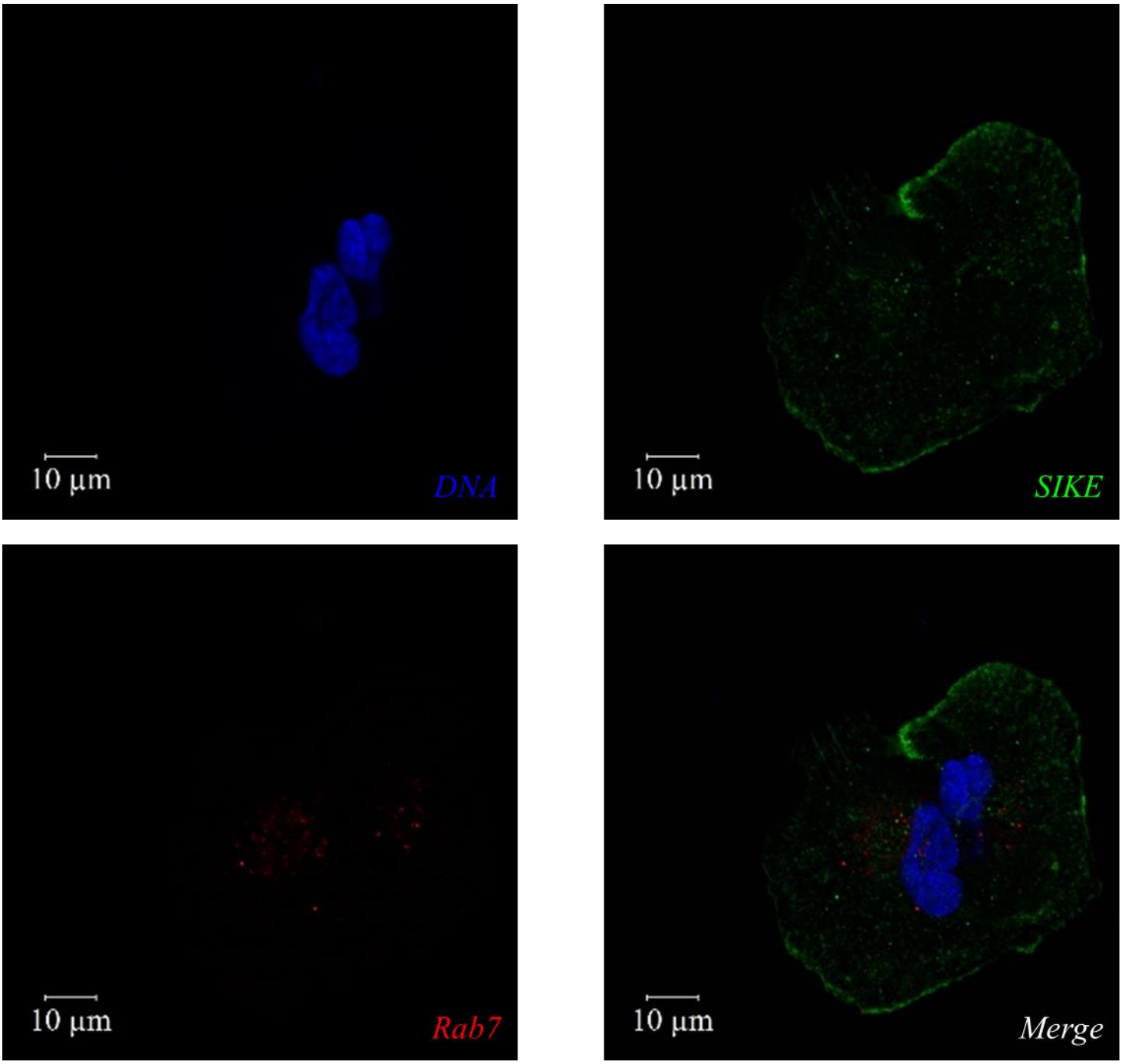

C

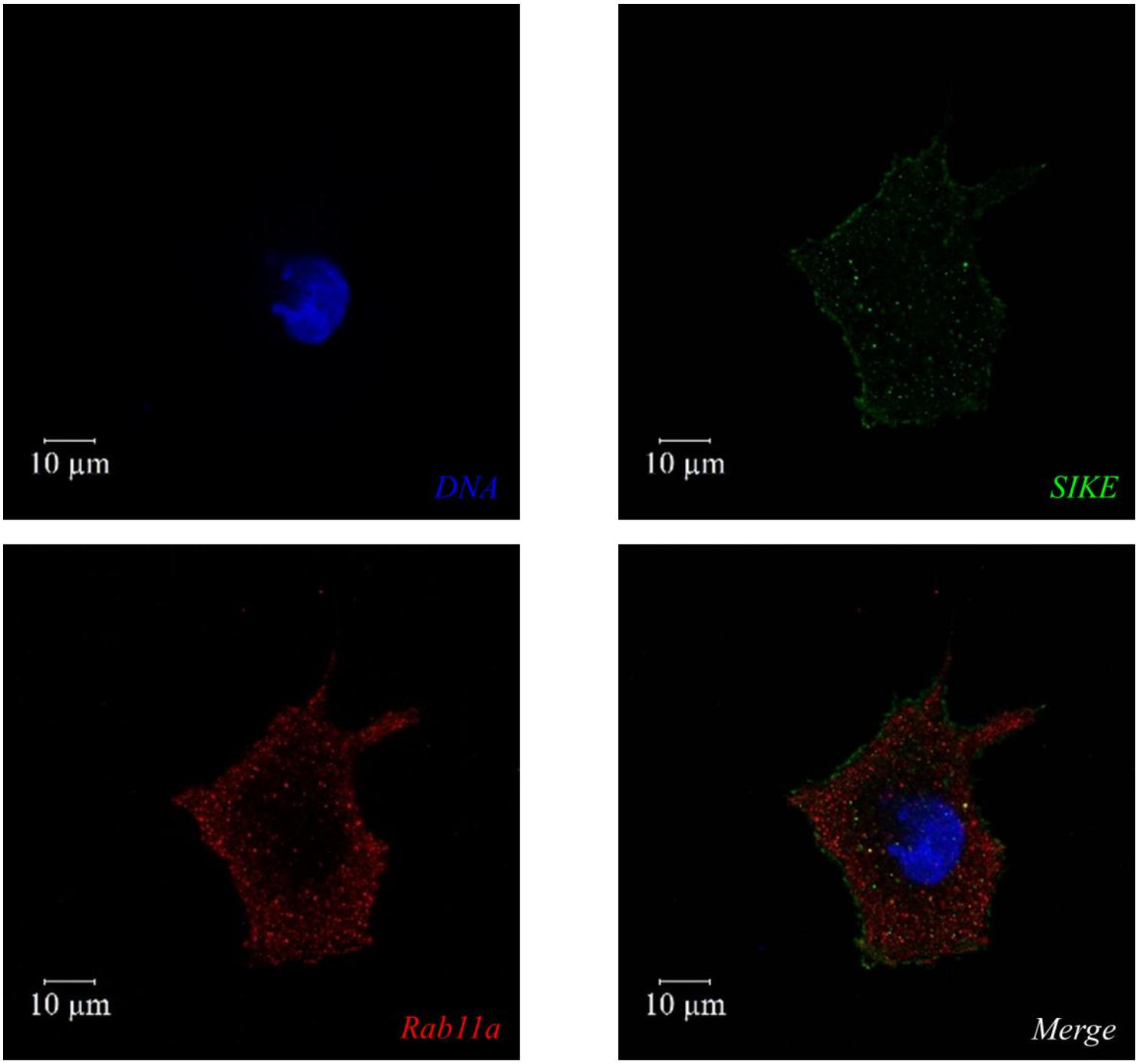

D

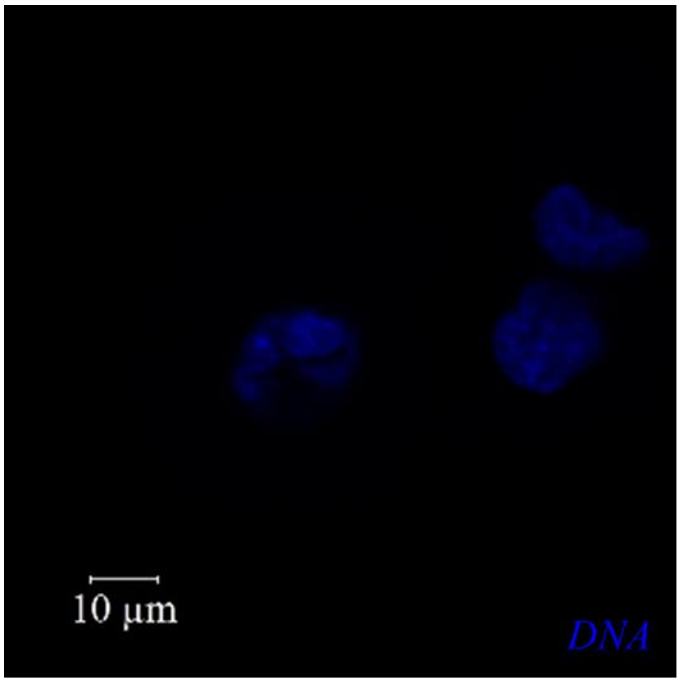

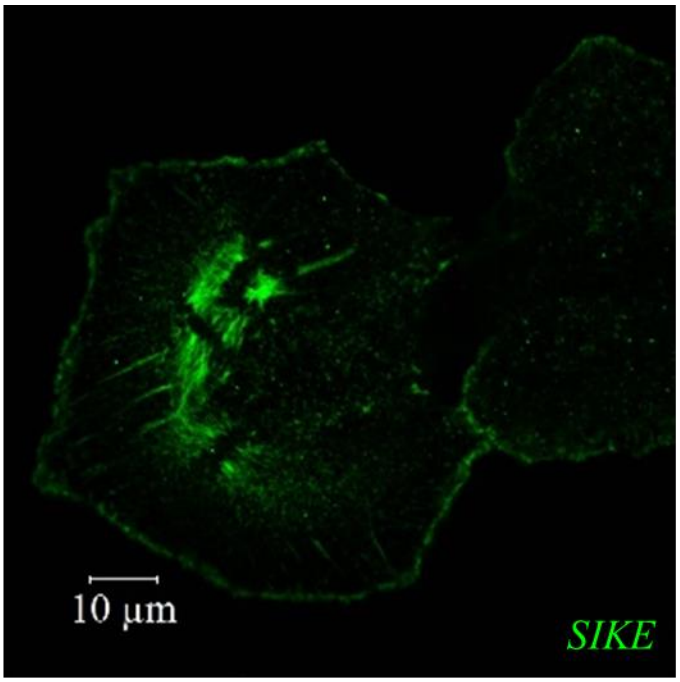

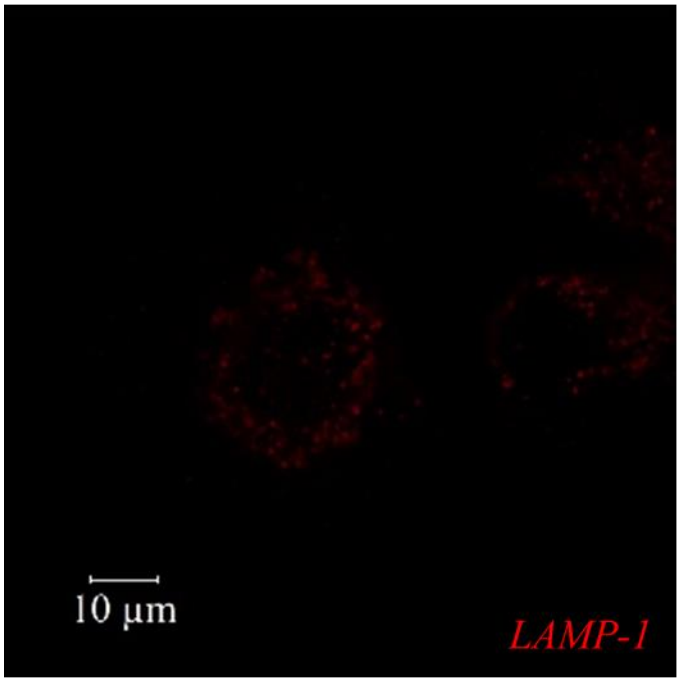

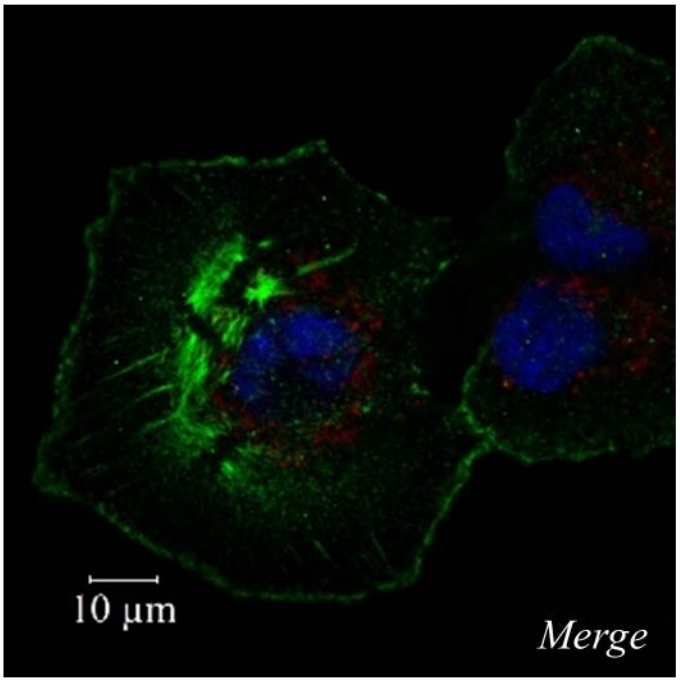

E

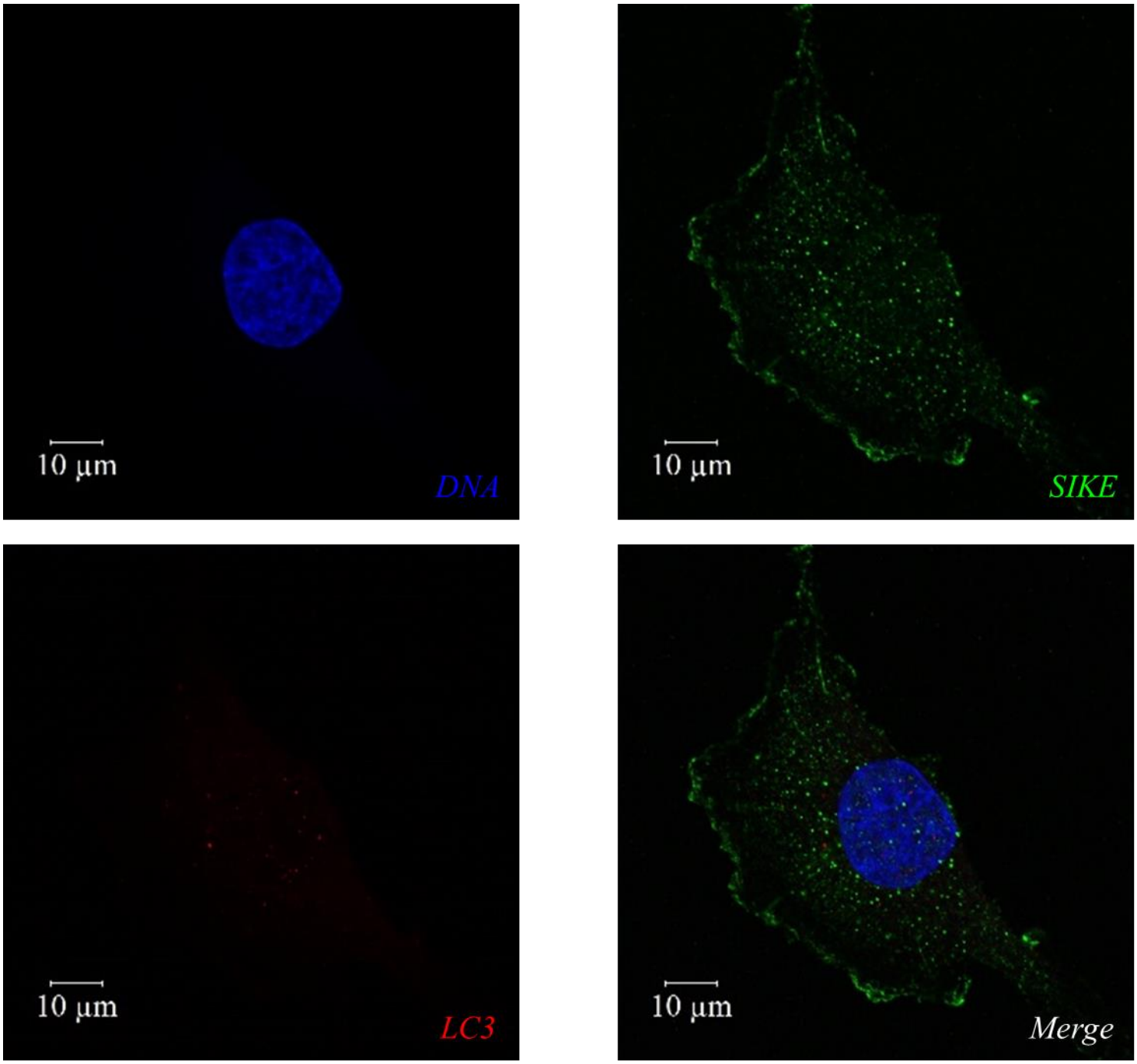

Figure 7. SIKE colocalizes with Rab11a, but not with other endosomal markers in DOV13 cells. DOV13 labeled for SIKE (green) and indicated endosomal markers (red). Cells were counterstained for DNA (blue, Hoechst). Images were captured by confocal microscopy, using optimized gain and laser power settings for each image.

Figure 8. SIKE colocalizes with Rab11a, but not with other endosomal markers, in RAW264.7 cells.

A

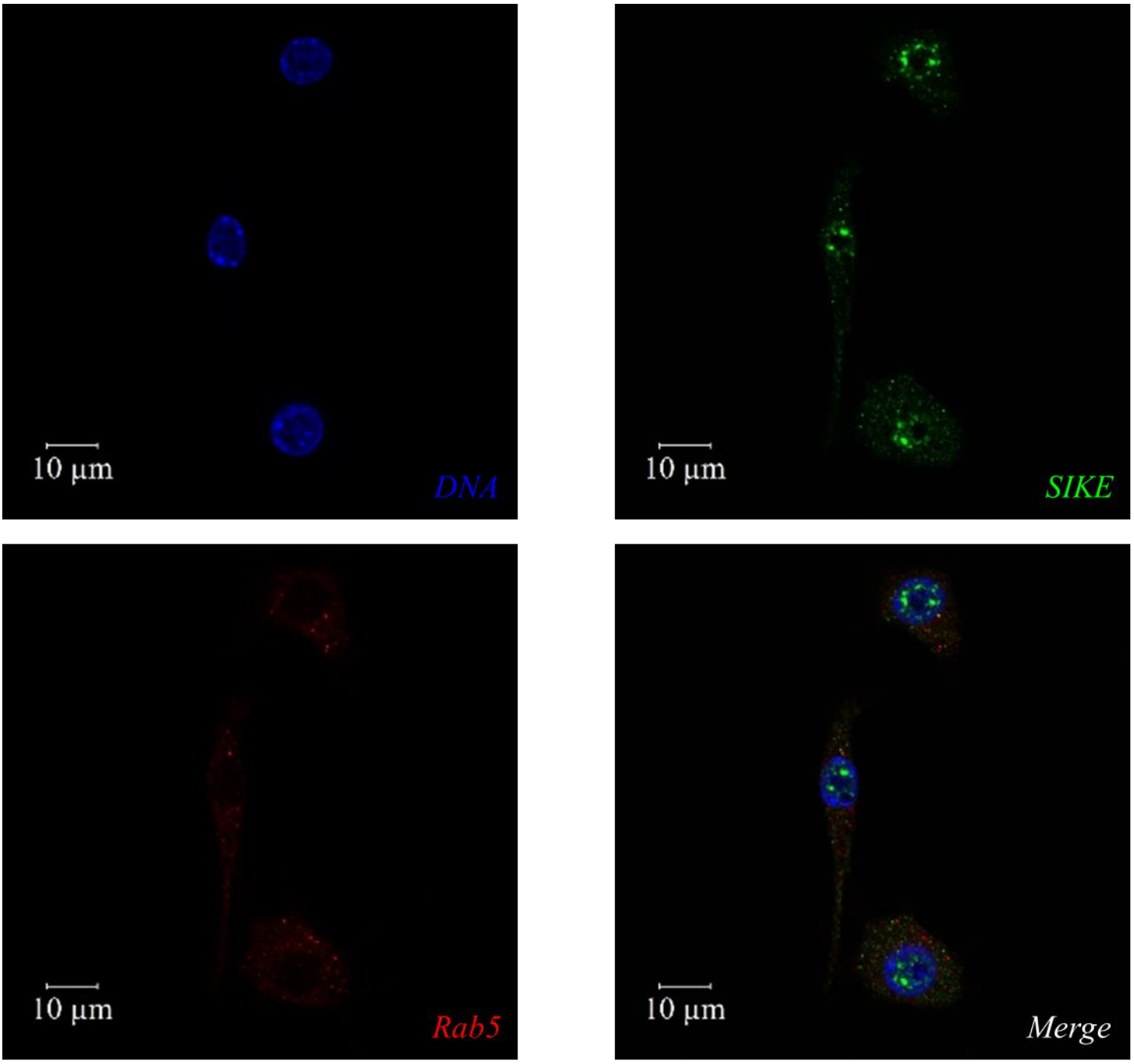

B

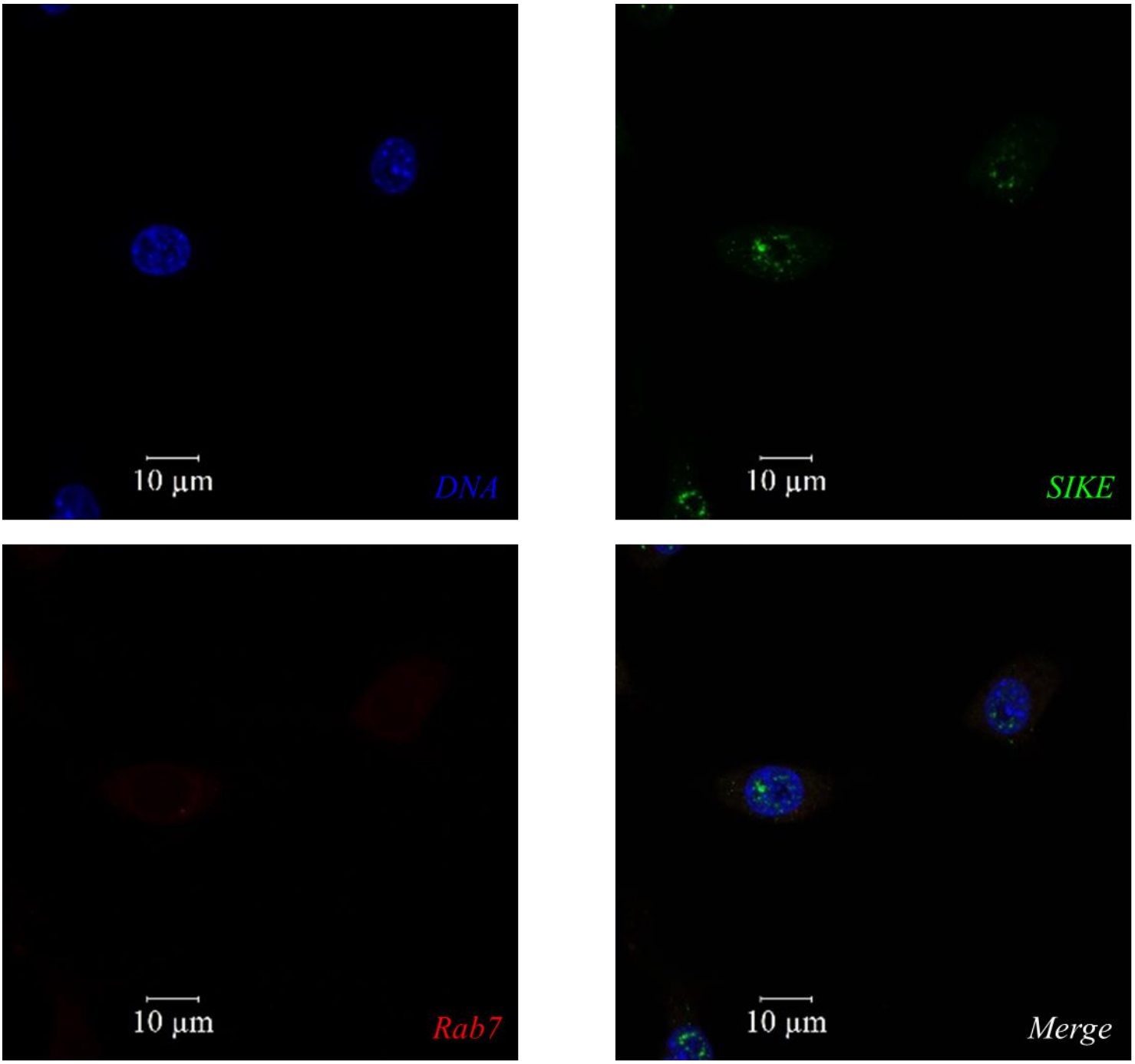

C

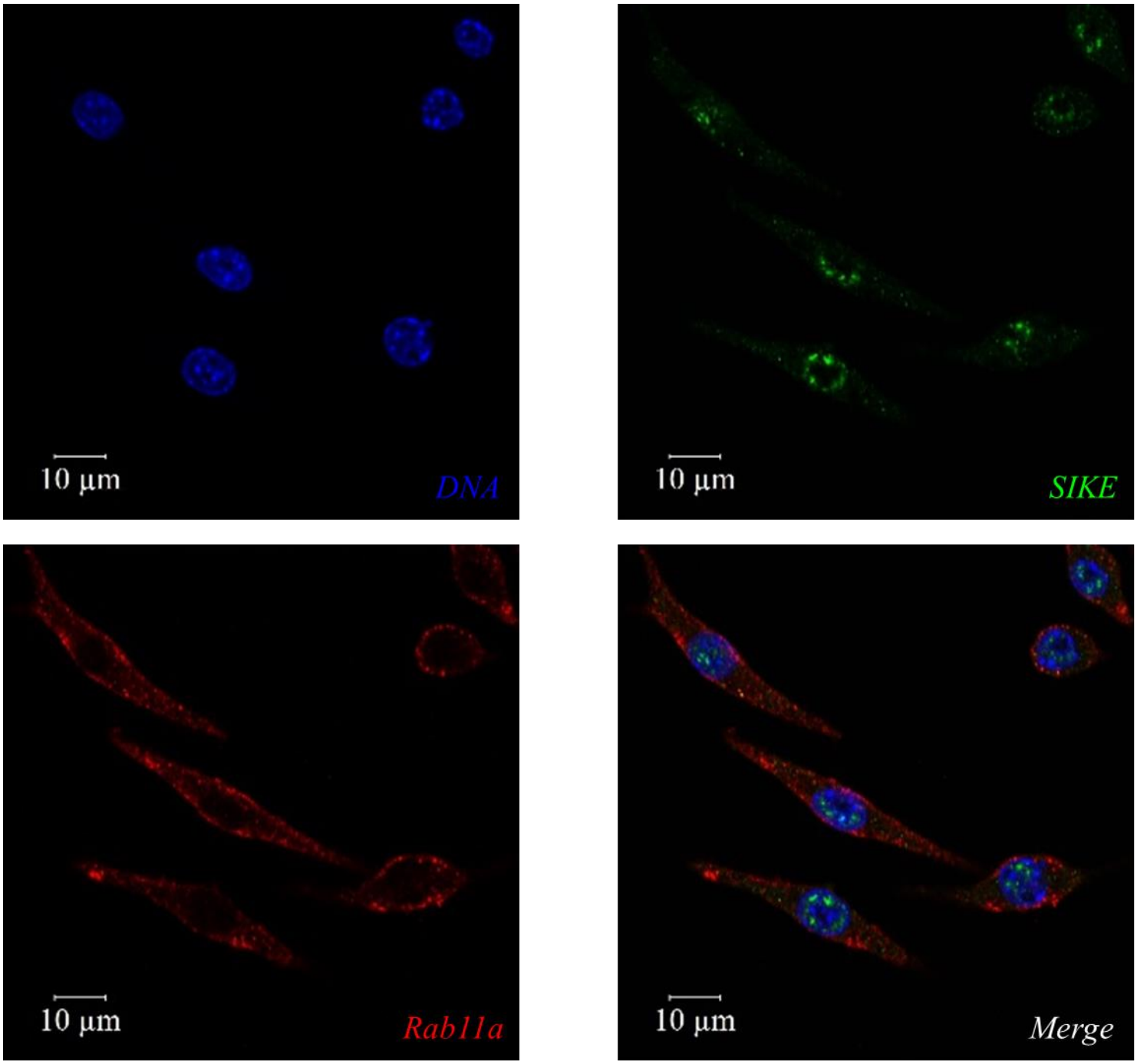

D

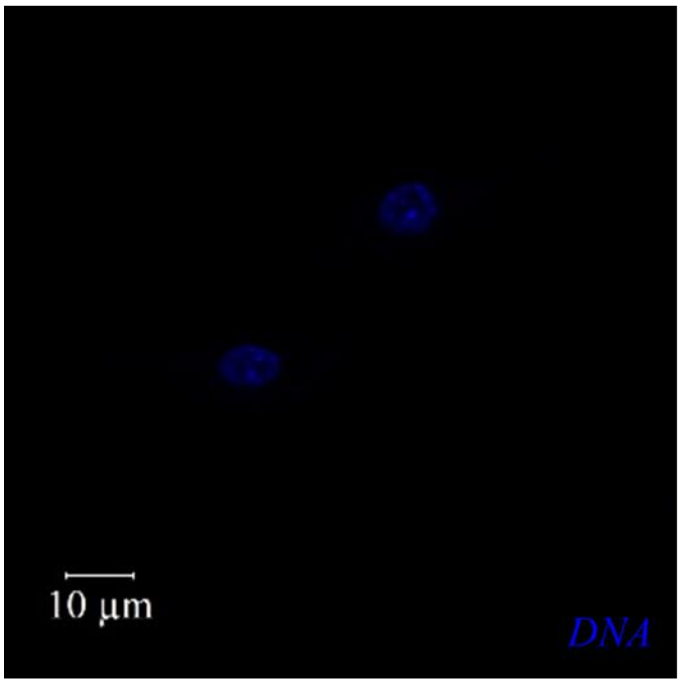

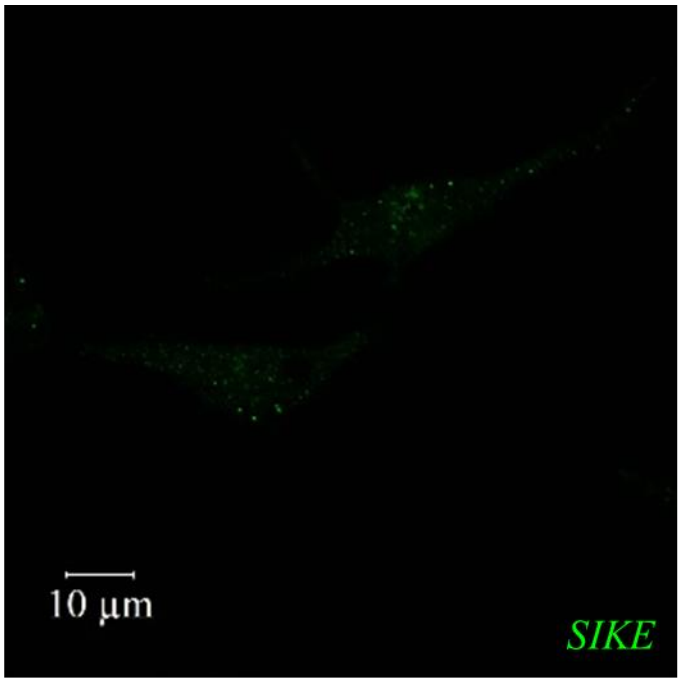

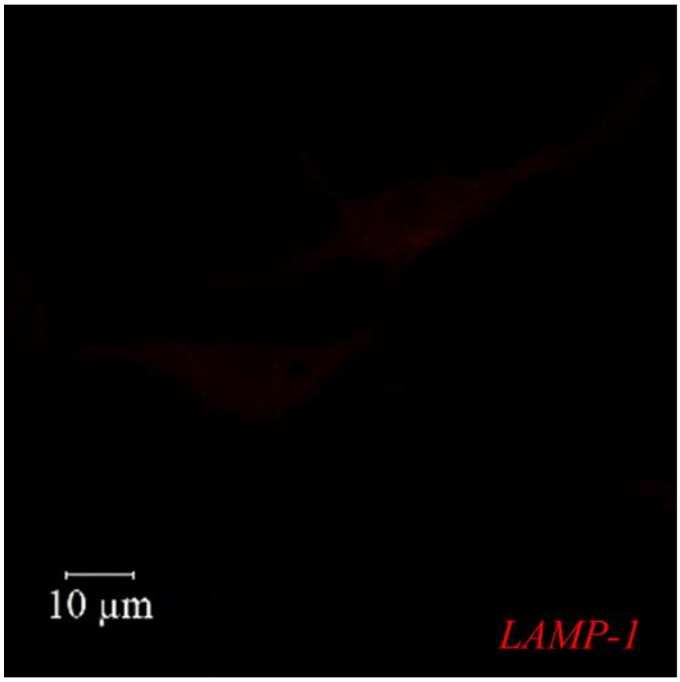

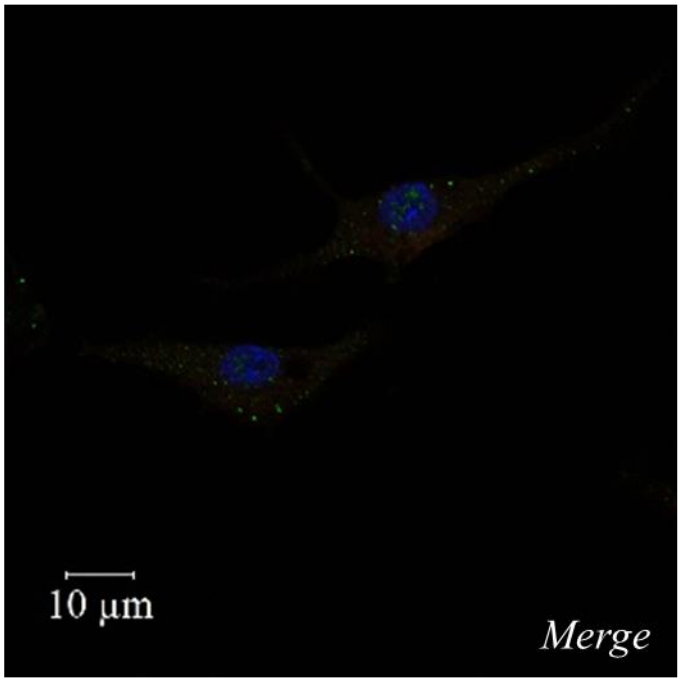

E

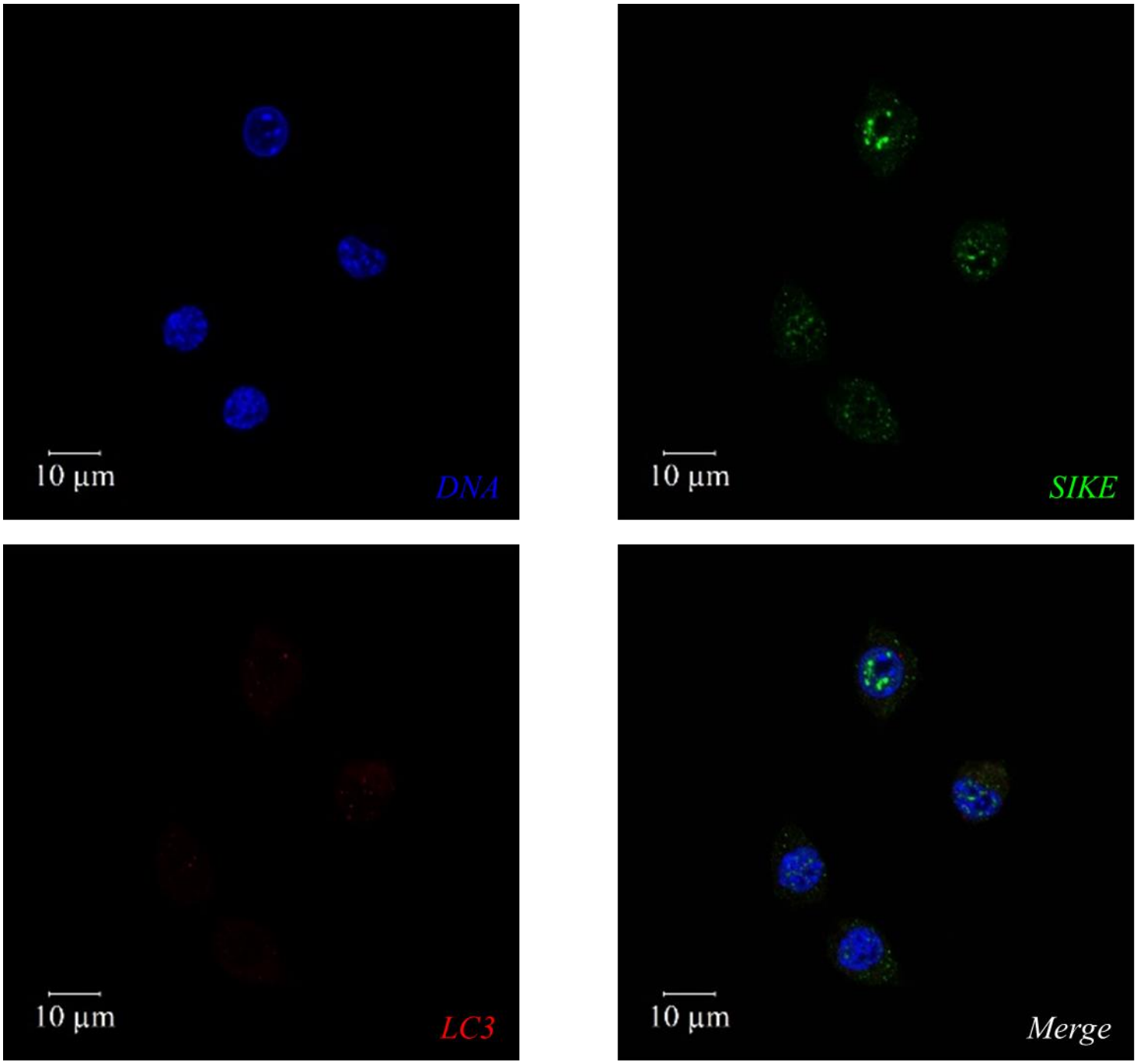

Figure 8. SIKE colocalizes with Rab11a, but not with other endosomal markers in RAW264.7 cells.

RAW264.7 labeled for SIKE (green) and the indicated endosomal markers (red). Cells were counterstained for DNA (blue, Hoechst). Images were captured by confocal microscopy, using optimized gain and laser power settings for each image.

Figure 9. SIKE colocalizes with S6, but not with other RNA-associated markers in DOV13 cells.

A

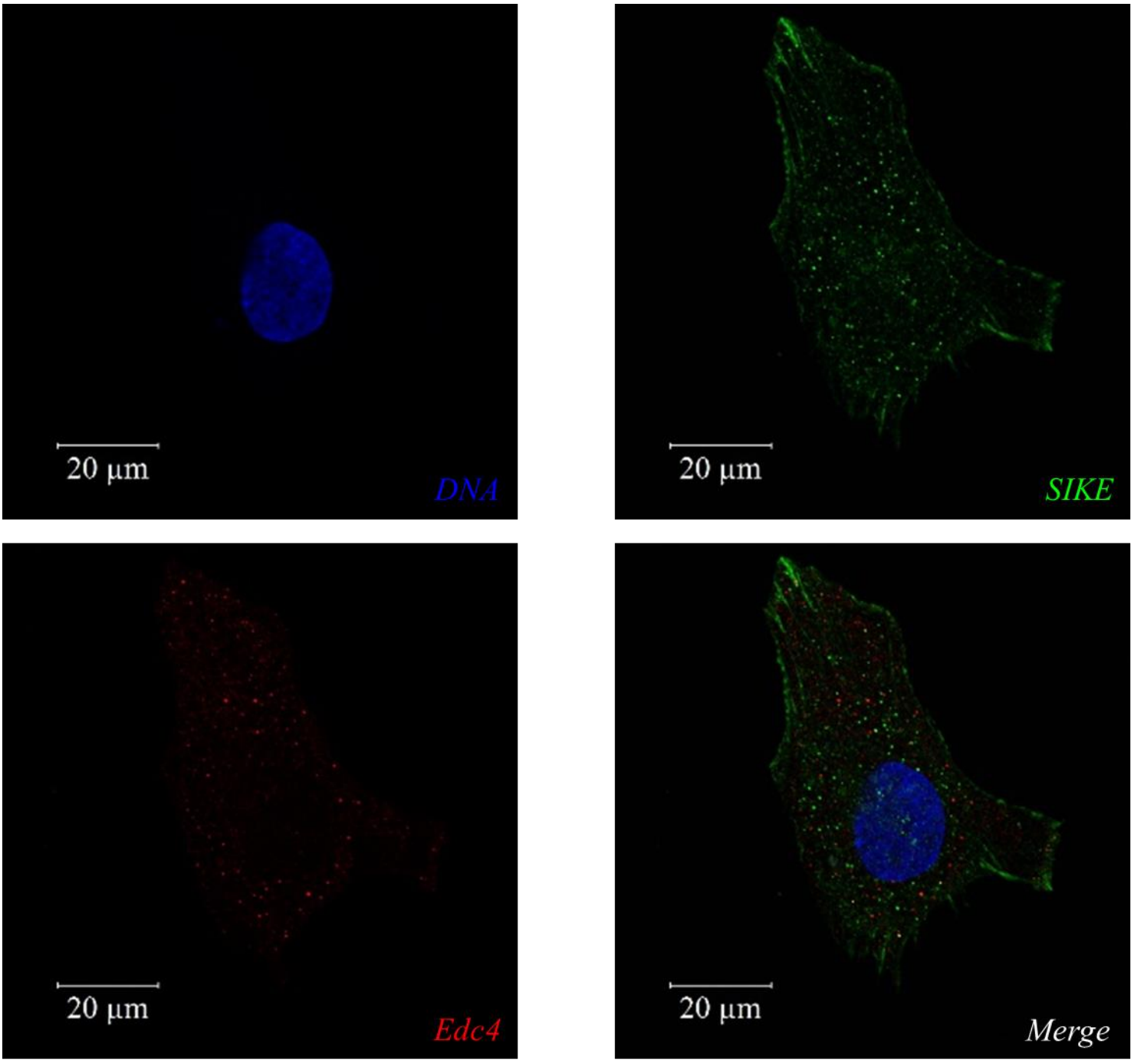

B

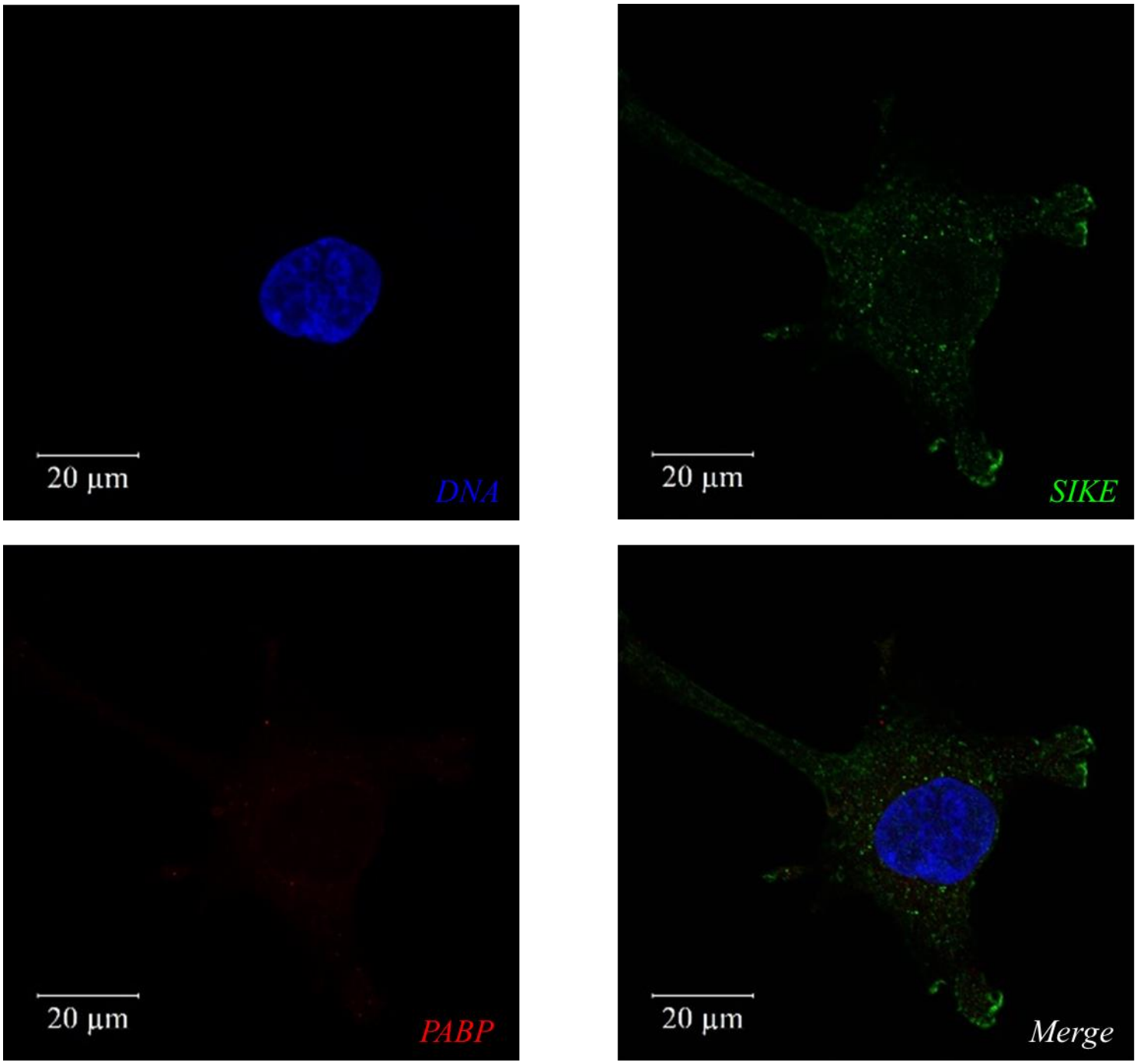

C

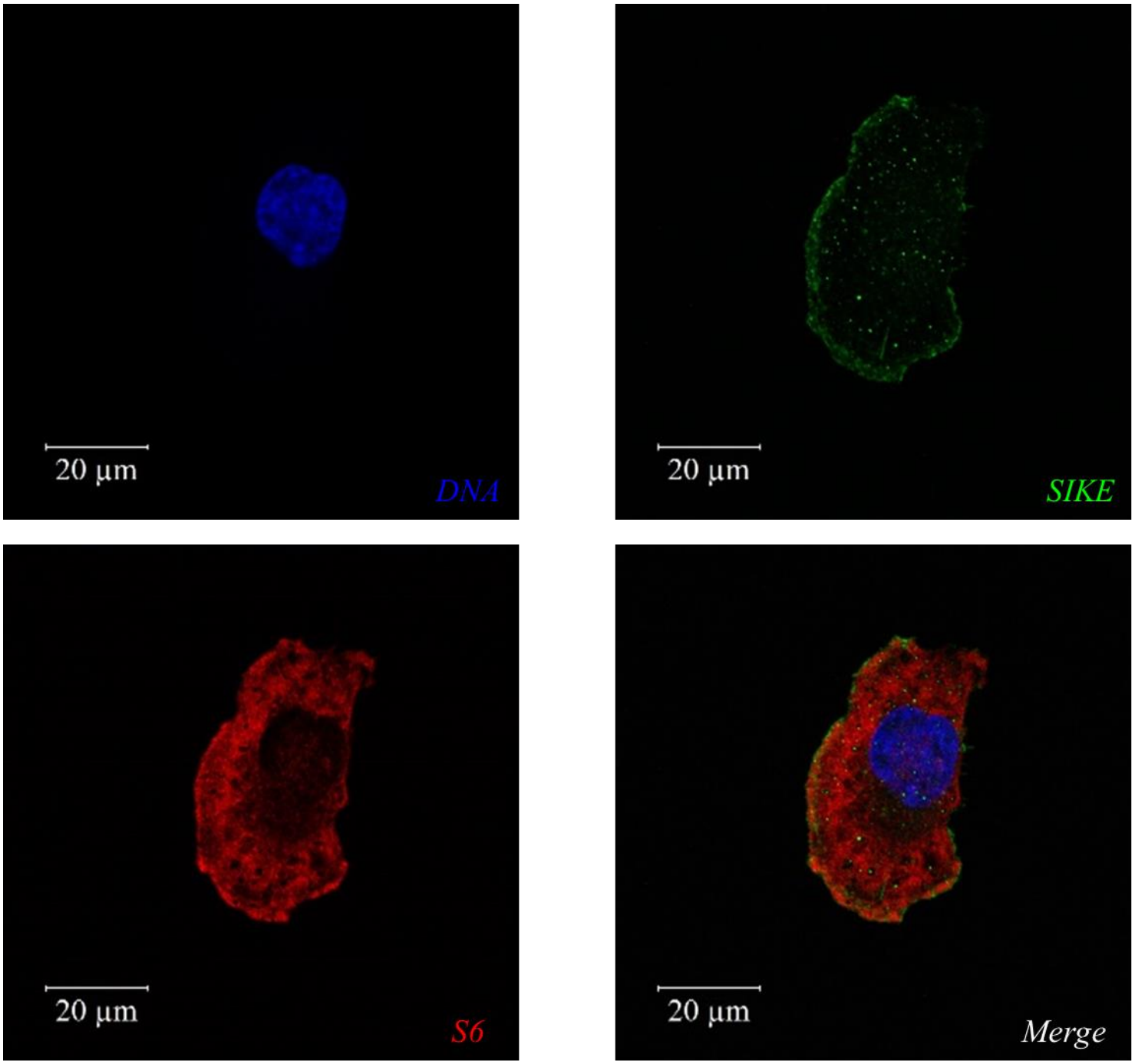

Figure 9. SIKE colocalizes with S6, but not with other RNA-associated markers in DOV13 cells. DOV13 labeled for SIKE (green) and the indicated RNA-associated markers (red). Cells were counterstained for DNA (blue, Hoechst). Images were captured by confocal microscopy, using optimized gain and laser power settings for each image.

Figure 10. SIKE colocalizes with S6, but not with other RNA-associated markers in RAW264.7 cells.

A

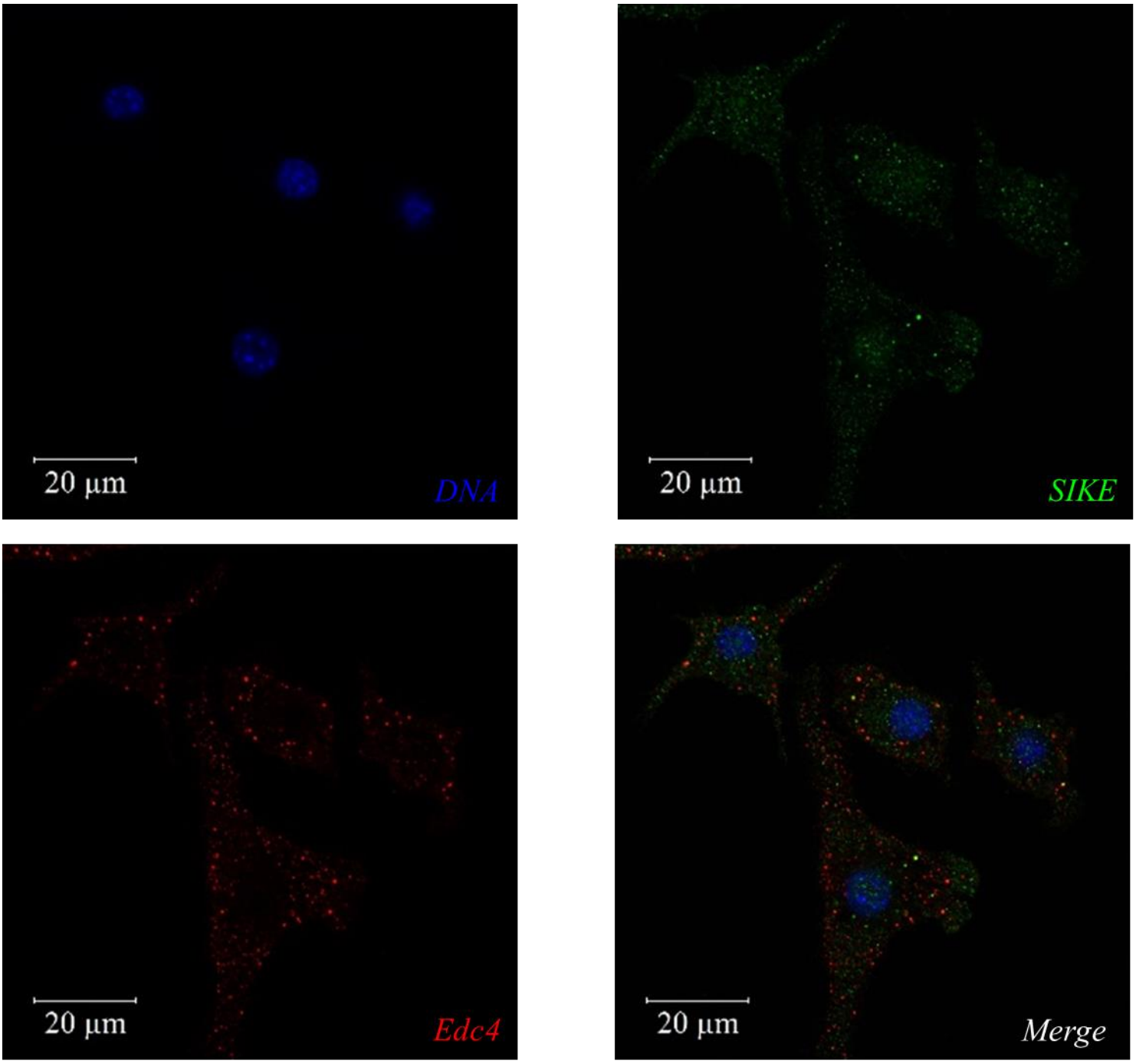

B

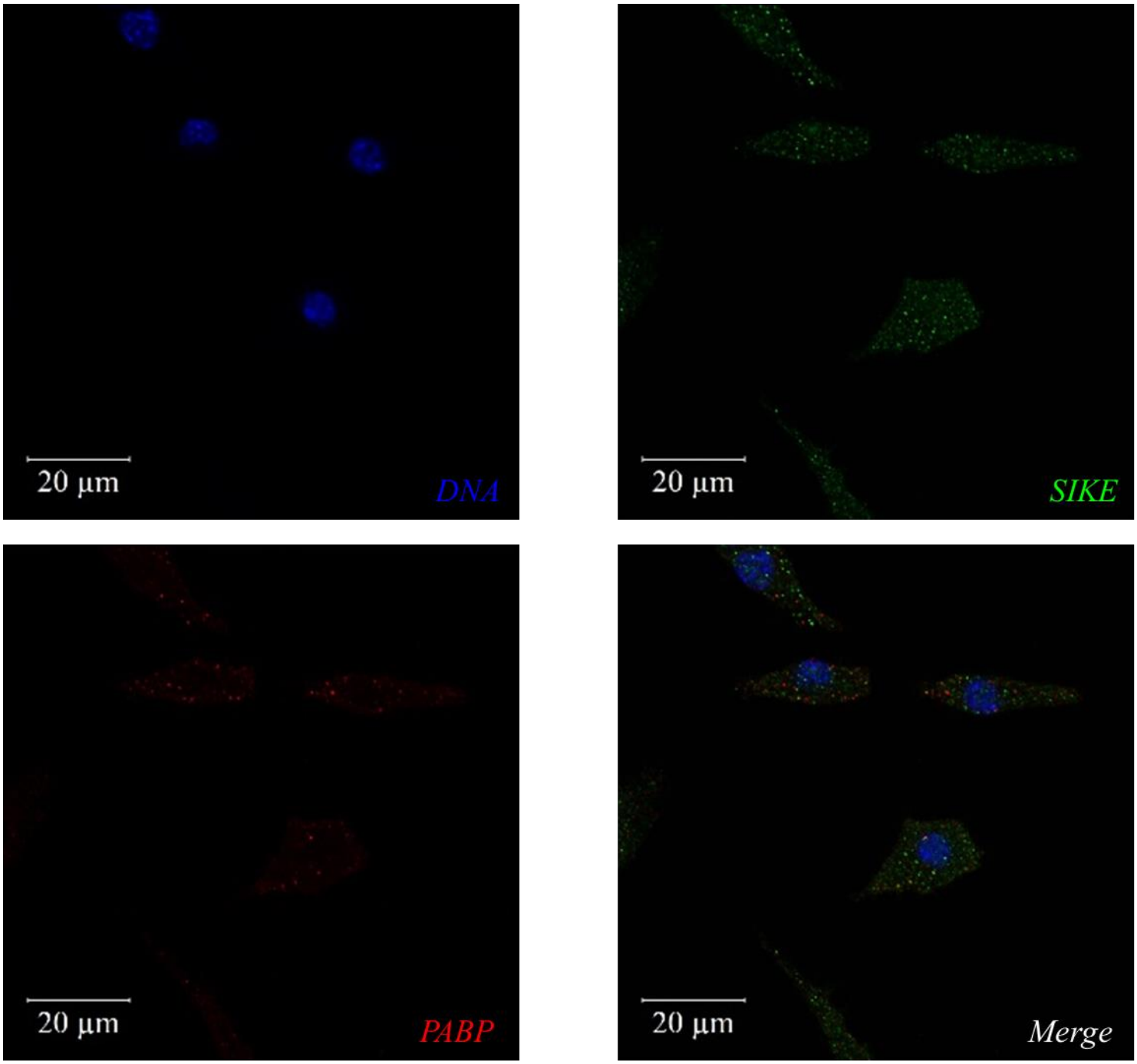

C

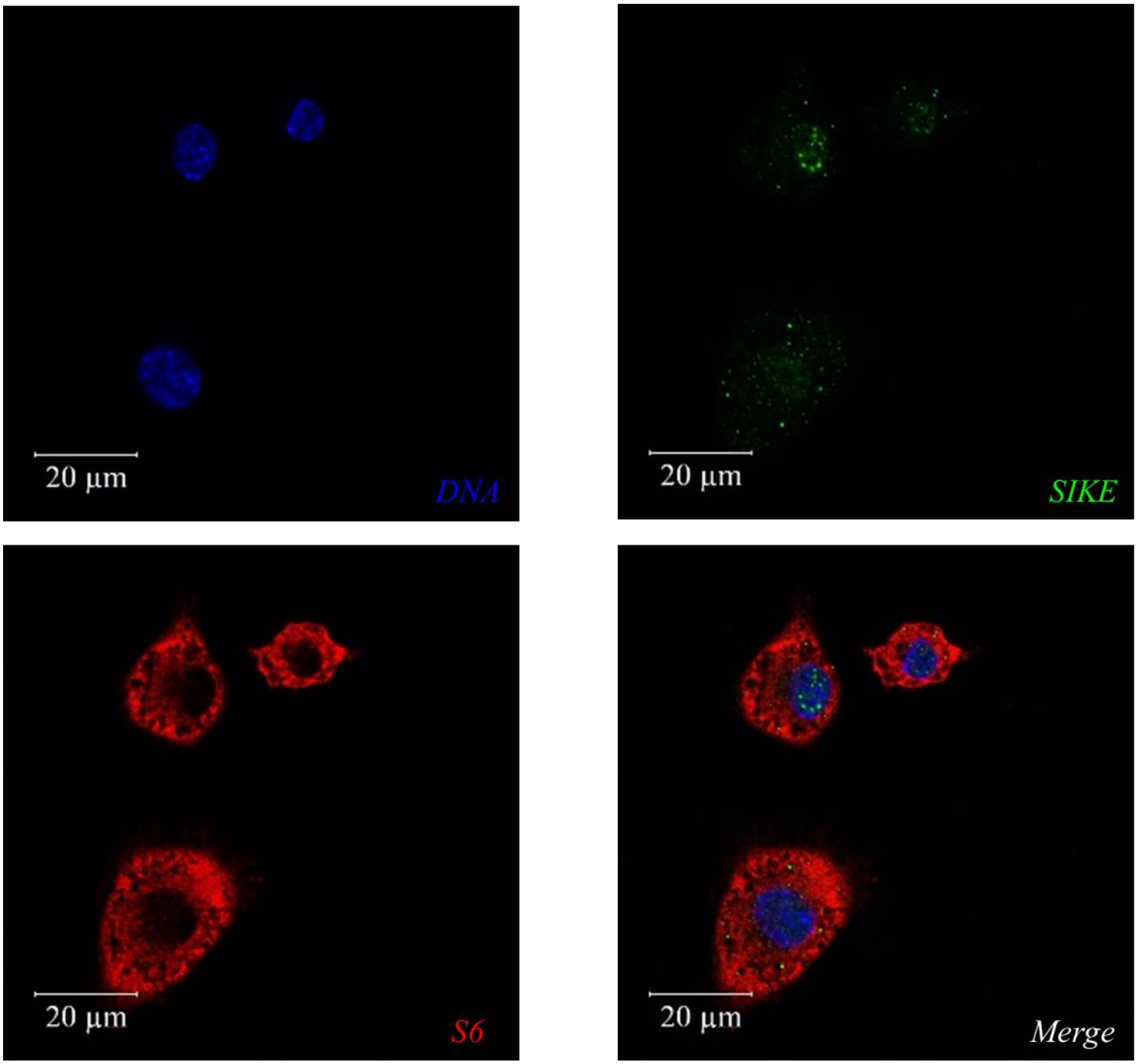

Figure 10. SIKE colocalizes with S6, but not with other RNA-associated markers in RAW264.7 cells.

RAW264.7 labeled for SIKE (green) and the indicated RNA-associated markers (red). Cells were counterstained for DNA (blue, Hoechst). Images were captured confocal microscopy, using optimized gain and laser power settings for each image.

3.2.3 Cytoskeletal markers

Colocalization with two cytoskeletal markers, β-actin and α-tubulin, was examined in both cell lines in order to determine the interactions between SIKE and the cytoskeleton. At first, β-actin was labeled for using a mouse anti-β-actin primary antibody and a goat α-mouse secondary antibody conjugated to Alexa Fluor® 555. We found that labeling with this antibody did not produce the expected pattern of actin labeling (Figure 11). As an alternative, the use of Alexa Fluor® 555 conjugated phalloidin was tested as a method to label the actin cytoskeleton for the colocalization studies. Phalloidin, a phallotoxin that preferentially binds to the actin cytoskeleton [28], was found to be a suitable substitute for the original β-actin antibody because it produced much stronger signal during imaging, and demonstrated the expected localization pattern associated with the actin cytoskeleton (Figure 11). Based on the improvements in actin labeling achieved using phalloidin, we relied on images in which we labeled for actin using phalloidin to draw our conclusions. It was noticed that SIKE and actin appeared to colocalize strongly in regions we thought to be the focal adhesions, especially in epithelial cells. This became important later in the research when we wanted to refine our understanding of the interactions between SIKE and the actin cytoskeleton.

Another cytoskeleton structure that was consistent with SIKE labeling in epithelial cells was the tubulin cytoskeleton. To examine this potential interaction, we labeled for α-tubulin. SIKE appeared to colocalize with α-tubulin in both epithelial and myeloid cells (Figure 12). Combined with the results of our actin labeling, we concluded that SIKE colocalized with both the actin and tubulin cytoskeleton (Figure 12). Based on visual observations made from our confocal microscopy images, we determined that more accurate means of characterizing

colocalization were required. Therefore, we sought to confirm these findings by quantitative analysis of colocalization.

Figure 11. Phalloidin produces more accurate actin cytoskeleton labeling than the β-actin antibody.

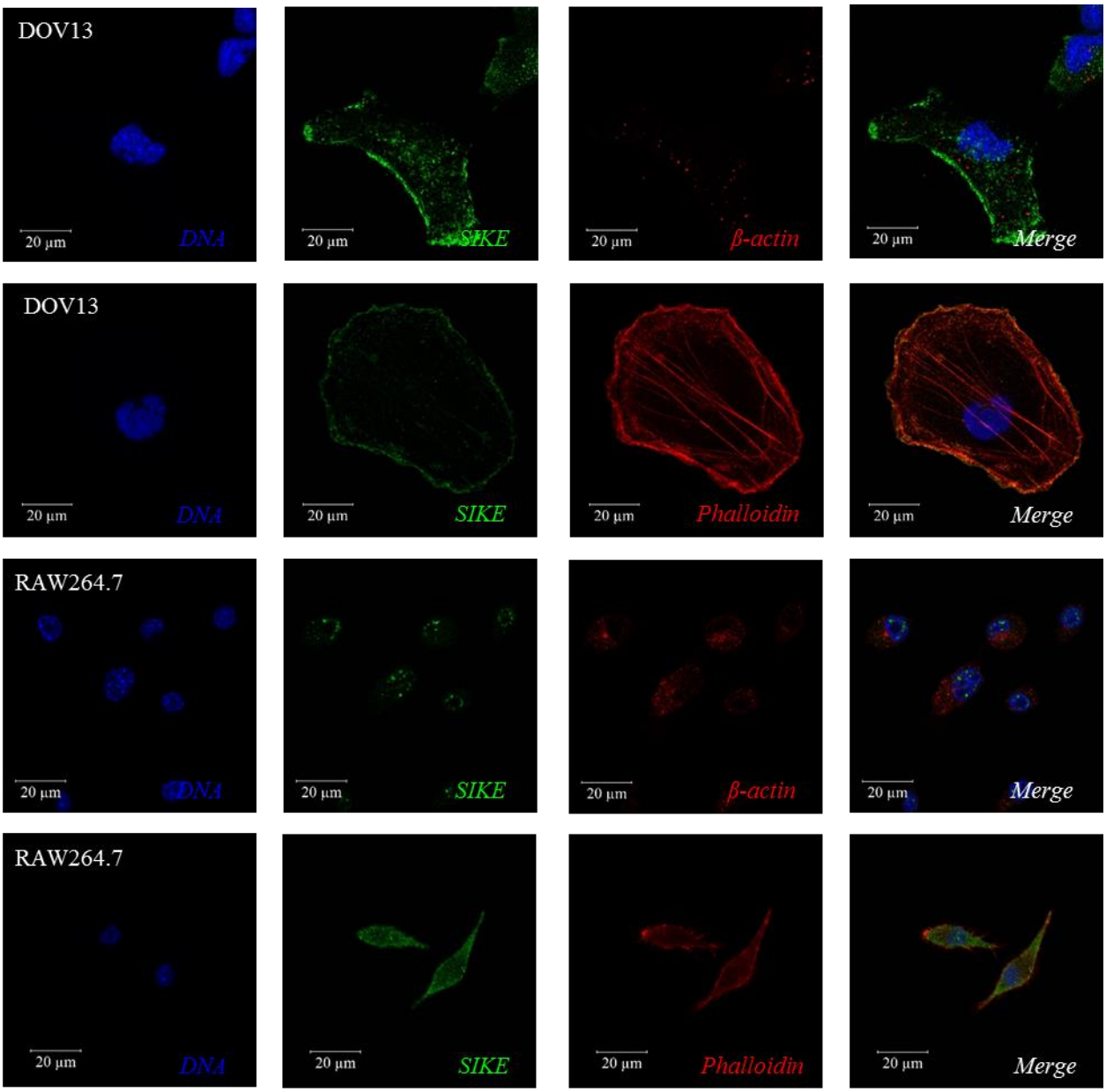

Figure 11. Phalloidin produces more accurate actin cytoskeleton labeling than the β-actin antibody. DOV13 and RAW264.7 labeled for SIKE (green) and actin (red) using either: primary antibody against β-actin and fluorescent secondary antibody or fluorophore conjugated phalloidin. In both cell lines, labeling with anti-β-actin antibody did not produce the expected labeling patterns of actin fibers, instead appearing to form puncta that are not characteristic of actin cytoskeleton structure. On the other hand, labeling with phalloidin produced the expected labeling patterns. Cells were counterstained for DNA (blue, Hoechst). Images were captured by confocal microscopy, using optimized gain and laser power settings for each image.

Figure 12. SIKE colocalizes with the actin and tubulin cytoskeletons in both epithelial and myeloid cell lines.

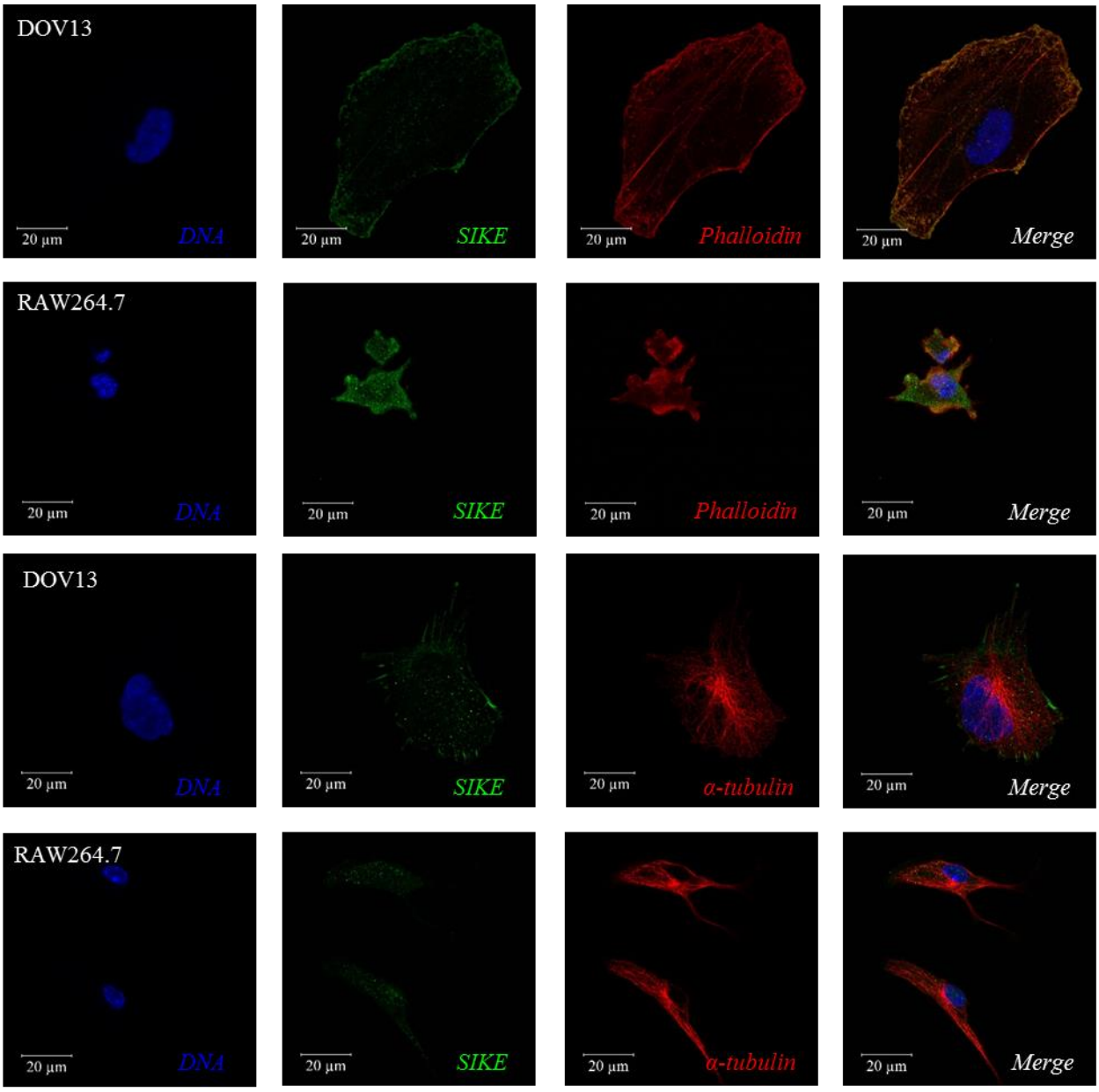

Figure 12. SIKE colocalizes with the actin and tubulin cytoskeletons in both epithelial and myeloid cell lines.

DOV13 (first and third rows) and RAW264.7 (second and fourth rows) labeled for SIKE (green) and either actin (red, first and second rows) or α-tubulin (red, third and fourth rows). Cells were counterstained for DNA (blue, Hoechst). Images were captured by confocal microscopy, using optimized gain and laser power settings for each image.

3.2.4 Quantitative colocalization data for original markers

Upon completion of the visual analysis of SIKE colocalization with the first ten markers, we used quantitative image analysis software to more accurately determine the degree of colocalization between SIKE and these markers. The quantitative analysis required thresholds to be determined for each channel individually for each image due to laser power and gain optimization. Analysis provided several coefficients with which colocalization could be characterized. Our project was primarily focused on examining the colocalization between the signals produced by SIKE and the cellular markers, irrespective of intensity. Therefore, we placed the greatest importance on the values of the Colocalization Coefficients 1 and 2 from the Zeiss Zen software (comparable to Manders M1 and M2 coefficients; Table 1) in completing our quantitative analysis. In order to determine how SIKE colocalized with the various markers, we performed quantitative analysis of colocalization on whole images, then using researcher defined Regions of Interest.

Several observations were made based on quantitative analysis of SIKE colocalization with the original ten markers. First, SIKE colocalized most strongly with the actin and tubulin cytoskeletons, but in a cell type-dependent manner (Table 2). SIKE colocalized more strongly with the actin cytoskeleton in the epithelial cell line, while SIKE colocalized with the tubulin cytoskeleton more strongly in the myeloid cell line. Additionally, we determined that SIKE colocalized with LAMP-1 and LC3 differentially based on cell type. We found that SIKE colocalized with LAMP-1 in epithelial cells, but not in myeloid cells (Table 2). We also found that SIKE colocalized with LC3 in myeloid cells, but not in epithelial cells (Table 2). On the other hand, we determined that SIKE colocalized with Rab11a and S6 equally strongly in both epithelial and myeloid cells (Table 2). After discovering these trends, we attempted to identify

specific components of the cytoskeleton structures with which SIKE colocalized, while also striving to improve the identification of the cytosolic puncta in both cell lines and the nuclear puncta in the RAW264.7 cell line.

Table 2. SIKE colocalizes with select markers in a cell type-dependent manner based on quantitative data.

Cell Structure	*Marker*	*epithelial*	*myeloid*
Cytoskeleton	Actin (Phalloidin)	+++	++
	Tubulin	++	+++
Endosomal Structures	Early (Rab5)	-	-
	Late (Rab7)	-	-
	Recycling perinuclear, Golgi, plasma membrane (Rab11a)	++	++
	Lysosomal (LAMP-1)	+	-
	Autophagosomal (LC3)	-	+
RNA-associated structures	Stress granules (Edc4)	-	-
	Processing bodies (PABP)	-	-
	Ribosome (S6)	++	++

Colocalization Strength	None	Weak	Strong	Very Strong
Symbol	-	+	++	+++
Colocalization coefficient	0	0<*Colocalization* <0.6	0.6<*Colocalization* <0.75	*Colocalization* >0.75

Table 2. SIKE colocalizes with select markers in a cell type-dependent manner based on quantitative data.

Summary of the quantitative analysis of SIKE colocalization with the original ten markers. The values analyzed here included data from Region of Interest derived Colocalization Coefficients 1 and 2 from the Zeiss Zen software. Colocalization Coefficient 1 was used when the total signal of marker in an image was significantly greater than the total signal of SIKE in that image and vice versa. Colocalization strength of the markers was categorized based on the range into which the values of the majority (greater than half) of the calculated coefficients fit.

3.2.5 Additional markers

After analysis of colocalization between SIKE and the first ten markers was completed, these results were used to select an additional six cytoskeletal markers in order to determine the specific colocalization partners of SIKE within the actin cytoskeleton. The additional six cytoskeletal markers were α-actinin, β-catenin, caveolin-1, ezrin, FAK, and MLC. In addition to the cytoskeletal markers, we also examined additional potential markers for the nuclear puncta seen in the RAW264.7 cell line and the cytosolic puncta observed in both cell lines. These puncta markers represented three types of cellular structures: RNA-associated markers that included fibrillarin (nucleolus) and nucleophosphomin-1 (nucleolus, nucleoplasma), endosomal markers that included PMP70 (peroxisome) and PSMA7 (proteasome), and one cytosolic protein, TBK1.

During this work, a previous error was discovered with our original images labeling for α-tubulin. An antibody approved for Western blot, but not immunofluorescence, was mistakenly used instead of the immunofluorescence approved antibody. Therefore, at the same time we examined these additional markers, we also repeated the labeling of the DOV13 and RAW264.7 cell lines for α-tubulin and collected our quantitative data from these images using the same z-stack image analysis techniques used for the analysis of the new cellular markers. All new images were collected as whole cell z-stack images. Visual observations made from these images showed that SIKE appeared to colocalize with α-actin, β-catenin, and ezrin in the actin cytoskeleton, but not with any of the potential puncta markers in either cell line (data not shown). Quantitative analysis of DOV13 images confirmed these observations, while also showing that SIKE weakly colocalized with FAK as well (Figure 13). Examination of how SIKE colocalized with the markers showed a trend similar to the one observed during quantitative analyses of

SIKE colocalization with the original ten markers. SIKE showed the strongest colocalization with components of the actin cytoskeleton, little colocalization with RNA-associated markers, and little to no colocalization with endosomal markers (Figure 13 A). When comparing this data to the data showing how the markers colocalize with SIKE, the same general trend is observed. Again, cytoskeletal markers colocalize with SIKE most strongly, while RNA-associated and endosomal markers colocalize with SIKE very little (Figure 13 B). Surprisingly, we did not confirm our original conclusion that SIKE colocalizes strongly with α-tubulin in epithelial cells (Figure 13 A-B). Although these data demonstrate that SIKE does colocalize with the tubulin cytoskeleton in epithelial cells, the strength of the interaction is weaker than the original data suggested. Overall, the Pearson's Correlation Coefficient (PCC) for tubulin indicates a negative correlation between the two channels (Figure 13 C). This indicates that SIKE and these markers localize in such a way that they exclude each other.

The same markers were studied in the RAW264.7 cell line. Additionally, we labeled these cells for fibrillarin in order to attempt to identify the nuclear puncta observed in RAW264.7 cells. Similar to observations made in the DOV13 cell line, visual examination of these images showed that SIKE appeared to colocalize with α-actinin, but did not appear to colocalize with the other markers in the RAW264.7 cell line (data not shown). Quantitative analysis of these images demonstrated that SIKE colocalized with more markers in myeloid cells than we initially thought, but did not colocalize with these markers strongly (Figure 14). Much like the trend seen in the epithelial cell line, SIKE colocalized more strongly with actin cytoskeleton markers, but colocalized little or not at all with RNA-associated markers and endosomal markers in the myeloid cell line (Figure 14 A). This trend continued when examining marker colocalization with SIKE, with cytoskeletal markers colocalizing more strongly with SIKE and puncta markers

colocalizing weakly with SIKE (Figure 14 B). As was seen in DOV13, analysis of SIKE colocalization with α-tubulin demonstrated that the strength of the interaction was weaker than we observed in our original experiments (Figure 14 A-B). The PCCs for SIKE colocalization with this collection of markers in the RAW264.7 cell line were more wide ranging than the values collected in the DOV13 cell line. Overall, the PCCs in RAW264.7 indicate a more random correlation between SIKE and these markers (Figure 14 C) than that observed in DOV13. Based on the quantitative data obtained from both cells lines, we confirmed the interactions between SIKE and the actin and tubulin cytoskeletons, but were unable to definitively identify the cytosolic puncta in either cell line, or the nuclear puncta in the myeloid cell line (Table 3). The comparison of SIKE colocalization with α-tubulin observed in both DOV13 and RAW264.7 confirmed that SIKE colocalizes with α-tubulin more strongly in myeloid cells than in epithelial cells (Table 3). These interactions led us to conclude that SIKE may play a role in cytoskeleton rearrangement through interactions with key proteins involved in maintaining the structure of actin filaments. Furthermore, the interaction with α-actinin seems to indicate that SIKE may play a role in the formation of additional actin filaments.

Figure 13. SIKE colocalizes with actin cytoskeleton markers, but not with puncta markers in DOV13.

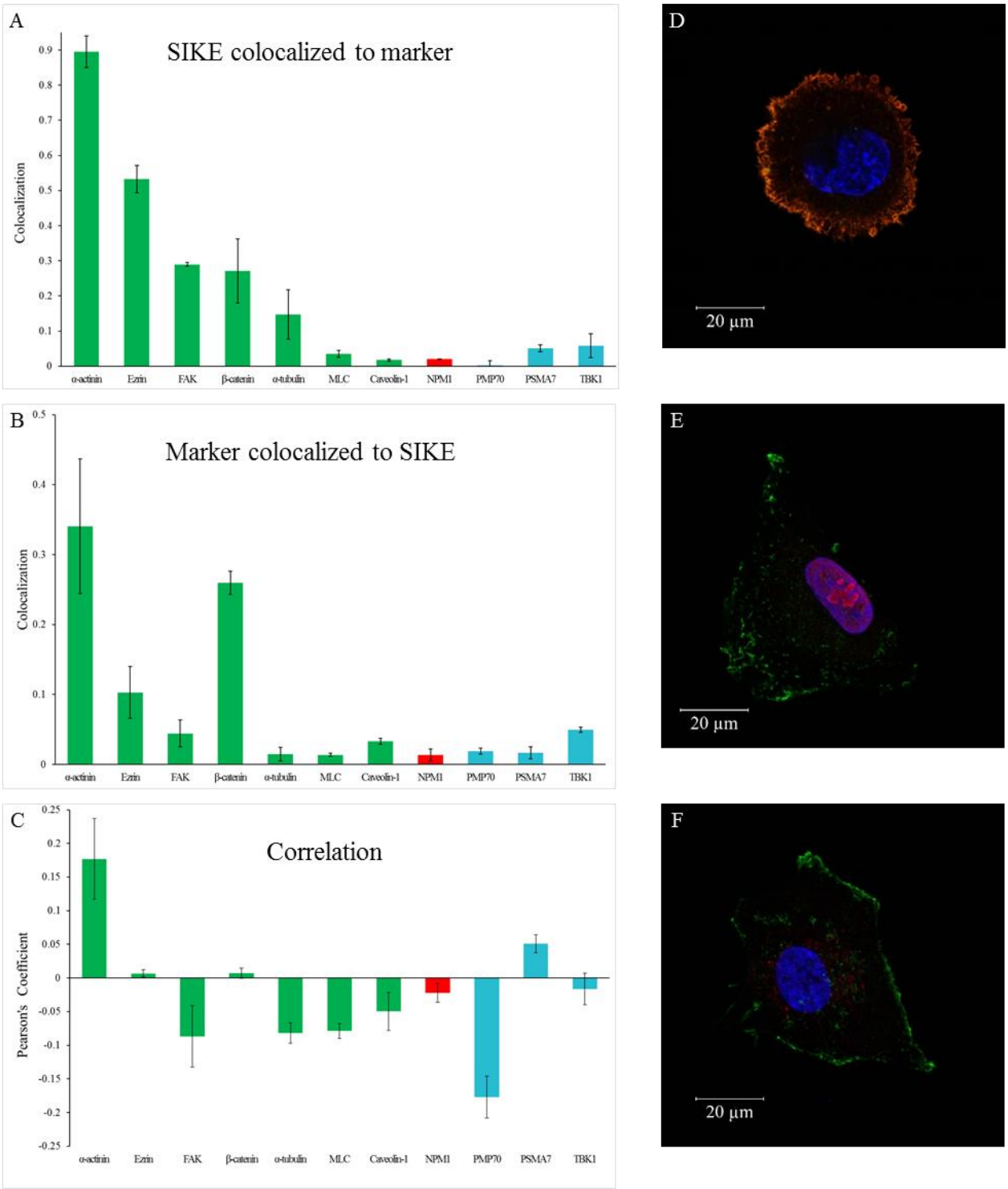

Figure 13. SIKE colocalizes with actin cytoskeleton markers, but not with puncta markers in DOV13.

Quantitative colocalization data from z-stack images of DOV13 labeled for SIKE and the indicated markers (cytoskeletal markers, green bars; RNA-associated markers, red bars; endosomal markers, light blue bars). (A)

SIKE colocalization with the indicated markers, calculated by dividing the colocalized signal volume by the total volume of SIKE signal in each image. (B) Marker colocalization with SIKE, calculated by dividing the colocalized signal volume by the total volume of marker signal in each image. Volume of each signal was calculated using the Volocity software, based on researcher determined threshold intensities. (C) PCC was calculated, by the Volocity software, for the intersecting population only in each image. Data represented in the above graphs are mean values of each coefficient, calculated from 5 fields ± SEM. Representative DOV13 labeled for SIKE (green), and either (D) α-actinin (red), (E) nucleophosphomin-1 (red) or (F) PMP70 (red). Yellow and orange signals are indicative of higher degrees of colocalization. Cells were counterstained for DNA (blue, Hoechst). Images were captured by confocal microscopy, using optimized gain and laser power settings for each image.

Figure 14. SIKE colocalizes with actin cytoskeleton markers, but not with puncta markers in RAW264.7.

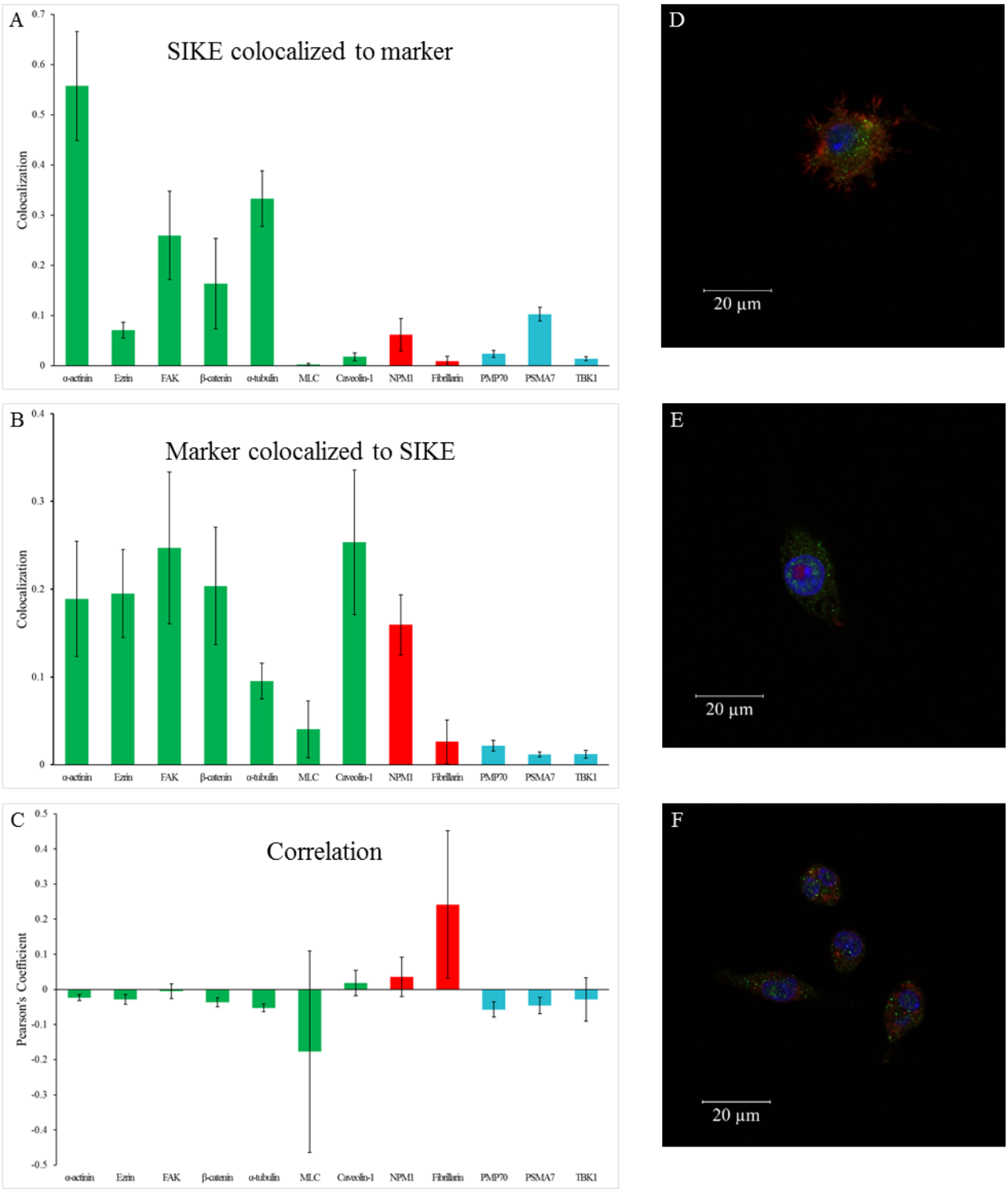

Figure 14. SIKE colocalizes with actin cytoskeleton markers, but not with puncta markers in RAW264.7.

Quantitative colocalization data from z-stack images of RAW264.7 labeled for SIKE and the indicated markers (cytoskeletal markers, green bars; RNA-associated markers, red bars; endosomal markers, light blue bars). (A)

SIKE colocalization with the indicated markers, calculated by dividing the colocalized signal volume by the total volume of SIKE signal in each image. (B) Marker colocalization with SIKE, calculated by dividing the colocalized signal volume by the total volume of marker signal in each image. Volumes of each signal were calculated using the Volocity software, based on researcher determined threshold intensities. (C) PCC was calculated, by the Volocity software, for the intersecting population only in each image. Data represented in the above graphs are mean values of each coefficient, calculated from 5 fields ± SEM. Representative RAW264.7 labeled for SIKE (green), and either (D) α-actinin (red), (E) fibrillarin (red), or (F) PMP70 (red). Yellow and orange signals are indicative of higher degrees of colocalization. Cells were counterstained for DNA (blue, Hoechst). Images were captured by confocal microscopy, using optimized gain and laser power settings for each image.

Table 3. SIKE colocalizes with actin cytoskeleton markers and NPM1 in a cell type-dependent manner.

Cell structure	*Marker*	*Epithelial*	*Myeloid*
Cytoskeleton	α-tubulin	+	+
	α-actinin	+++	+
	β-catenin	+	+
	Caveolin-1	-	+
	Ezrin	+	-
	FAK	+	+
	MLC	-	-
Endosomal Structures	Peroxisome (PMP70)	-	-
	Proteasome (PSMA7)	-	-
Cytosolic Protein	TBK1	-	-
RNA-associated Structures	Nucelophosphomin-1	-	+
	Fibrillarin	N/A	-

Colocalization Strength	None	Weak	Strong	Very Strong
Symbol	-	+	++	+++
Colocalization coefficient	0	0<*Colocalization* <0.6	0.6<*Colocalization* <0.75	*Colocalization* >0.75

Table 3. SIKE colocalizes with actin cytoskeleton markers and NPM1 in a cell type-dependent manner.

Quantitative analysis of SIKE colocalization with the panel of additional cellular markers. Data from Figure 13 and Figure 14 summarized, confirming that SIKE colocalizes with the cytoskeletal markers and does not colocalize with the puncta markers, with the exception of NPM1 in the myeloid cell line. Fibrillarin was not examined in DOV13 because it is expressed only in the nucleus and SIKE does not localize to the nucleus in epithelial cells. Colocalization was evaluated using the Volocity software as previously described. These colocalization values are based on signal volume rather than number of pixels (i.e. area), which was the basis for the coefficients provided by the Zeiss Zen software.

3.2.6 Super-resolution imaging

Based on the results obtained by quantitative analysis of dual-labeled confocal images, we selected four markers with which SIKE colocalized strongly for labeling and examination via Structured Illumination Microscopy. Both cell lines were labeled for SIKE and either α-actinin, α-tubulin, actin (via Alexa Fluor® 555 conjugated phalloidin), or S6. Although Rab11a was also determined to colocalize with SIKE at confocal microscopy resolution, this marker was not studied using SIM due to time restrictions. Analysis of colocalization in SIM images relied on the perception of a third indicator color (yellow) to signify colocalization. Little to no colocalization was observed between SIKE and these markers in the myeloid cell line (Figure 15), while α-actinin, actin, and S6 colocalized with SIKE in the epithelial cell line (Figure 16). Since the resolution of the SIM microscope is 85nm [27] versus 250nm in traditional confocal microscopy, we conclude that SIKE interacts with these proteins in epithelial cells at a distance no greater than 85nm. Similarly, we can also conclude that the markers with which SIKE did not colocalize interact with SIKE at a distance of greater than 85nm because these markers did colocalize with SIKE when imaged by confocal microscopy.

Figure 15. Super-resolution microscopy reveals that SIKE does not colocalize with selected markers in RAW264.7.

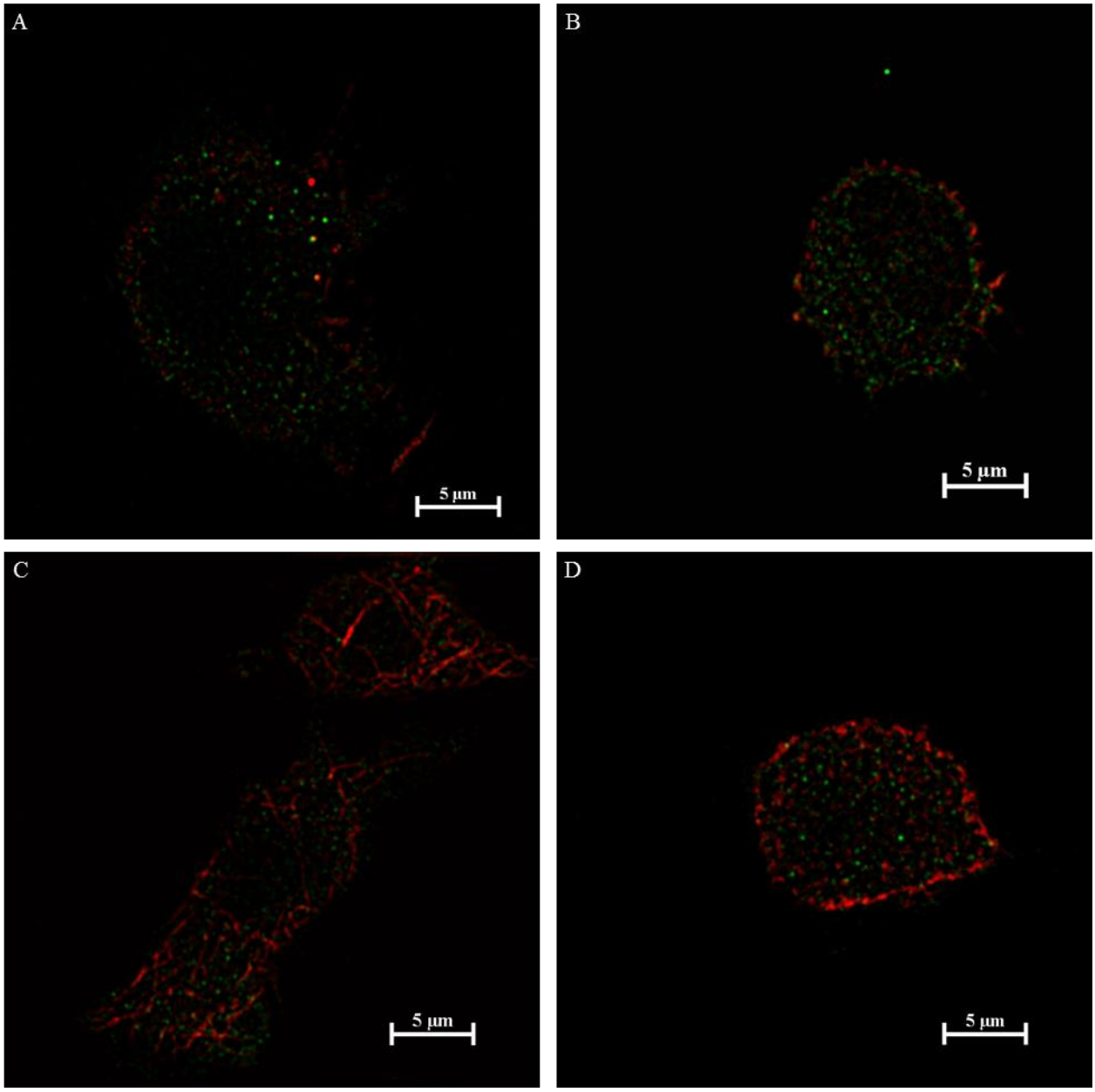

Figure 15. Super-resolution microscopy reveals that SIKE does not colocalize with selected markers in RAW264.7. Structured Illumination Microscopy of RAW264.7 labeled for SIKE (green) and markers (red). SIKE does not appear to colocalize with (A) α-actinin, (B) actin, (C) α-tubulin, or (D) S6. Images were captured by SIM, using optimized gain and laser power settings for each image. LUTs were applied to images using ImageJ based on LUT settings from Nikon Elements program.

Figure 16. Super-resolution microscopy reveals that SIKE colocalizes with α-actinin and actin, but not with α-tubulin and S6 in DOV13.

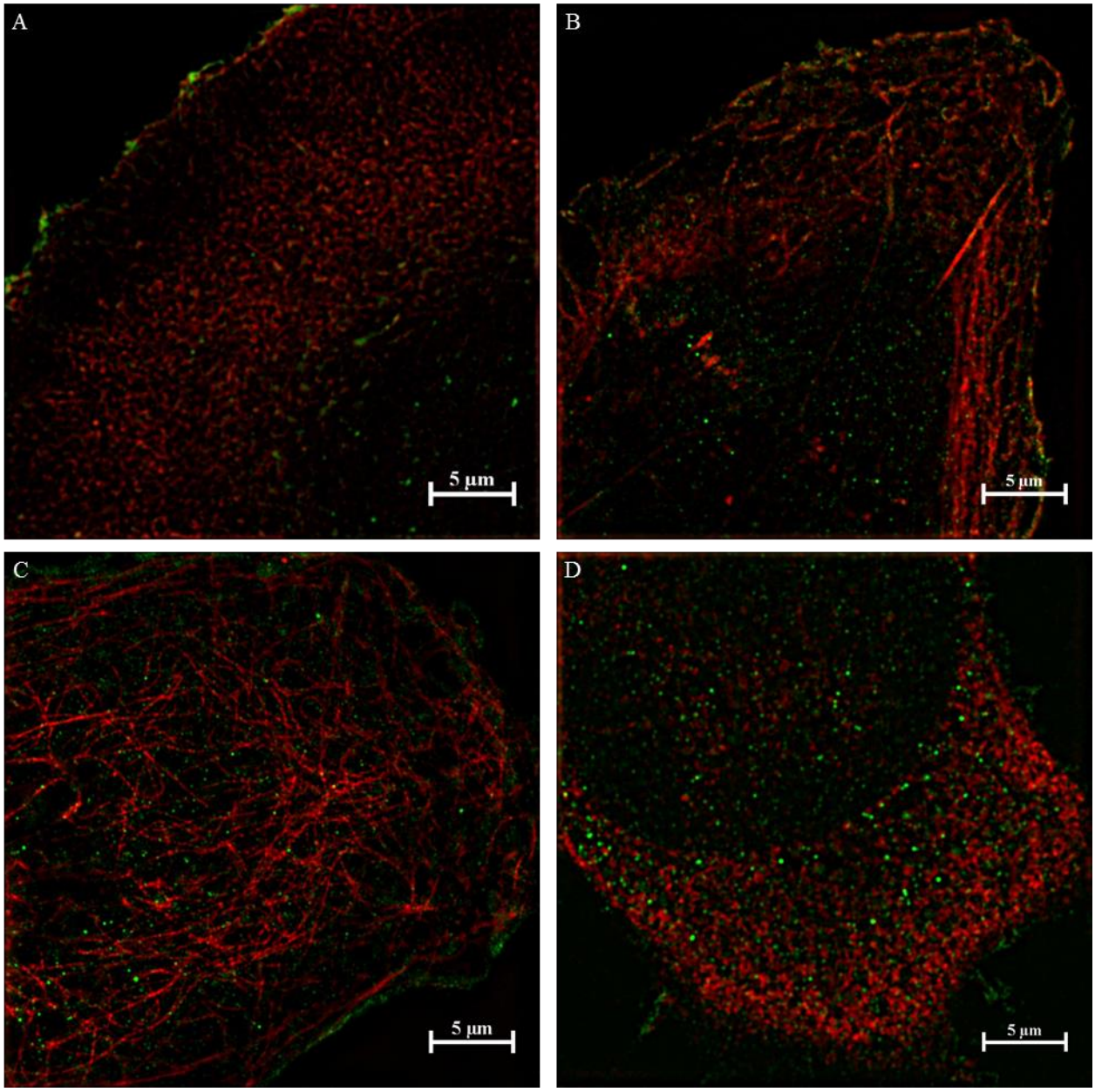

Figure 16. Super-resolution microscopy reveals that SIKE colocalizes with α-actinin and actin, but not with α-tubulin and S6 in DOV13. Structured Illumination Microscopy images of DOV13 labeled for SIKE (green) and markers (red). SIKE appears to colocalize with (A) α-actinin and (B) actin, but does not appear to colocalize with (C) α-tubulin or (D) S6. Images were captured by SIM, using optimized gain and laser power settings for each image. LUTs were applied to images using ImageJ based on LUT settings from Nikon Elements program.

3.3 Suppressor of IKK-ε trafficking and localization upon dsRNA challenge

We wanted to examine the effect of viral infection on the intracellular localization of SIKE. In order to determine this effect, we infected DOV13 and RAW264.7 cells with poly(I:C), a synthetic dsRNA molecule that mimics viral dsRNA and activates TLR3 signaling. Cells were infected, then fixed at 0 hours, 15 minutes, 30 minutes, 1 hour, 2 hours, 8 hours, 12 hours, and 24 hours after exchanging the infection media. Our first approach to analyze these images was to visually assess whether SIKE localization was altered over the course of infection. This assessment relied on visually detecting the formation of structures not previously observed when labeling for SIKE. However, we found no distinguishable differences among the images from the different time points in DOV13 (Figure 17) and RAW264.7 (data not shown). Since the visual assessment did not highlight any differences at the various stages of infection, we chose to alter our approach.

The next method we employed to determine the changes in SIKE localization during dsRNA challenge was segmentation analysis. The segmentation analysis was intended to assign parameters, using the Volocity software, which would segregate the SIKE signal in each image into groups which represented major categories of cellular structures. These parameters relied on the application of several filters (i.e. maximum volume of puncta, minimum length for fibers, minimum diameter for fibers, etc.) to separate the SIKE signal in each image into categories of structures. Segmentation analysis divided SIKE into four categories of cellular structures: plasma membrane, puncta, stress fibers, and other SIKE structures. The protocol for the segmentation analysis was adapted and refined by testing different settings for each parameter in a single test image until it yielded consistent, satisfactory results for each image.

We wanted to ensure this method would yield usable results before we imaged cells for all time points from the infection time course. Therefore, we collected z-stack images of DOV13 cells from two key time points during the course of dsRNA challenge. We imaged unchallenged cells to establish a baseline to which challenged cells could be compared. We imaged cells fixed two hours after dsRNA challenge because 2 hours was one of our immunologically relevant time points for TLR3 signaling. Two hours after activation of TLR3, phosphorylation of STAT1 can be detected [6]. Phosphorylation of STAT1 increases between 1 hour and 6 hours post-activation of TLR3 as a result of activation of kinase activity due to type I IFN production via TLR3 signaling [6]. Segmentation analysis of images of DOV13 cells from these time points showed that this analysis was unlikely to show significant differences in SIKE localization to the various structures due to wide variability in SIKE localization to each structure at given time points (Figure 18). These results, in combination with the results of the initial observations from single z-plane images from the full time course, led us to conclude that using cells fixed at specific time points during dsRNA challenge would not be beneficial in determining SIKE's function downstream of TLR3 activation. Instead, we decided that transfection of cells with fluorescently tagged SIKE and live cell imaging over the course of dsRNA challenge would prove more effective to follow the changes in SIKE localization during the antiviral response. We began preparations for making stable cell lines expressing the fluorescently tagged SIKE constructs, but halted this work after purifying the DNA. Future studies will complete the production of stable cell lines and live cell imaging of dsRNA challenged cells.

Figure 17. dsRNA challenge produces no gross changes in SIKE localization over time in DOV13 cells.

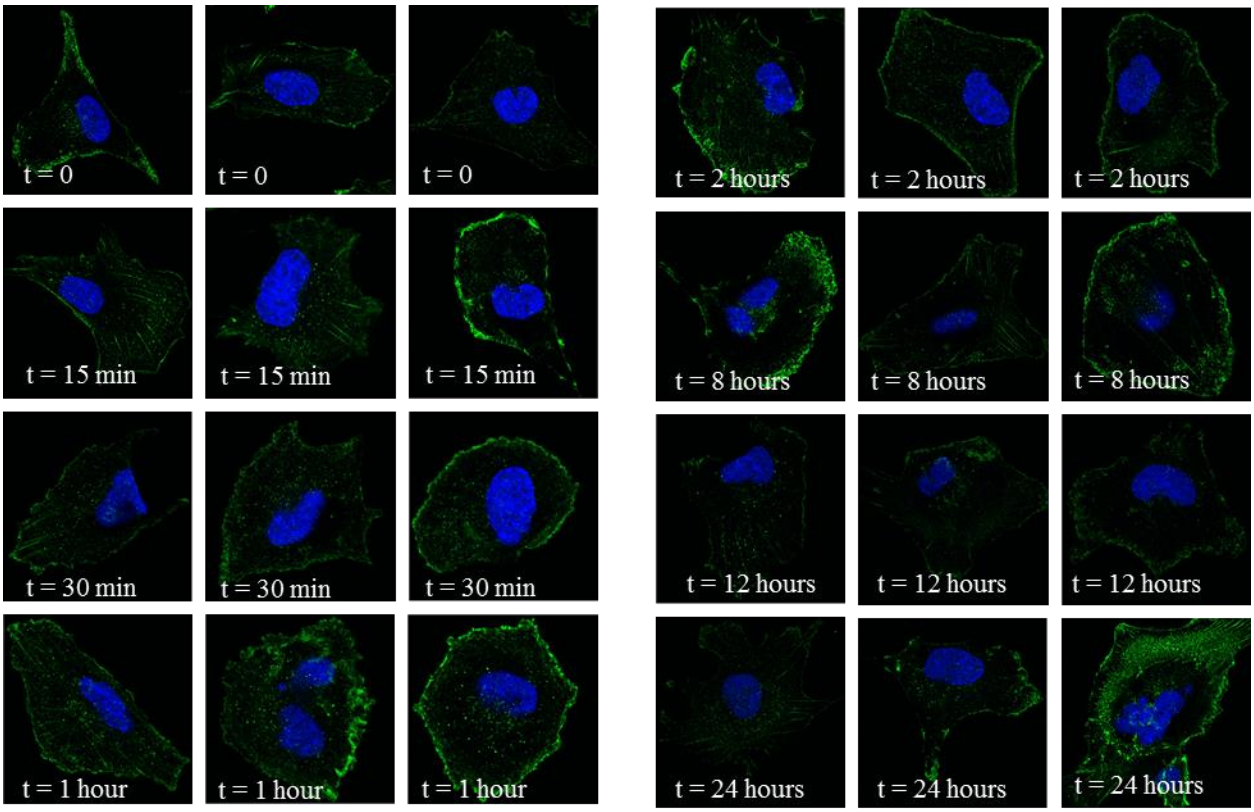

Figure 17. dsRNA challenge produces no gross changes in SIKE localization over time in DOV13 cells.

DOV13 at the indicated time points during dsRNA challenge. Each image shows the localization of SIKE (green) with respect to the nucleus (DNA, blue, Hoechst). Cells were grown on coverslips in 6-well plates and challenged with poly(I:C). After the infection media was removed, the cells were grown for the indicated lengths of time before being fixed with paraformaldehyde. Images were captured by confocal microscopy, using optimized gain and laser power settings for each image.

Figure 18. Segmentation analysis in DOV13 during dsRNA challenge does not demonstrate significant alterations of SIKE localization.

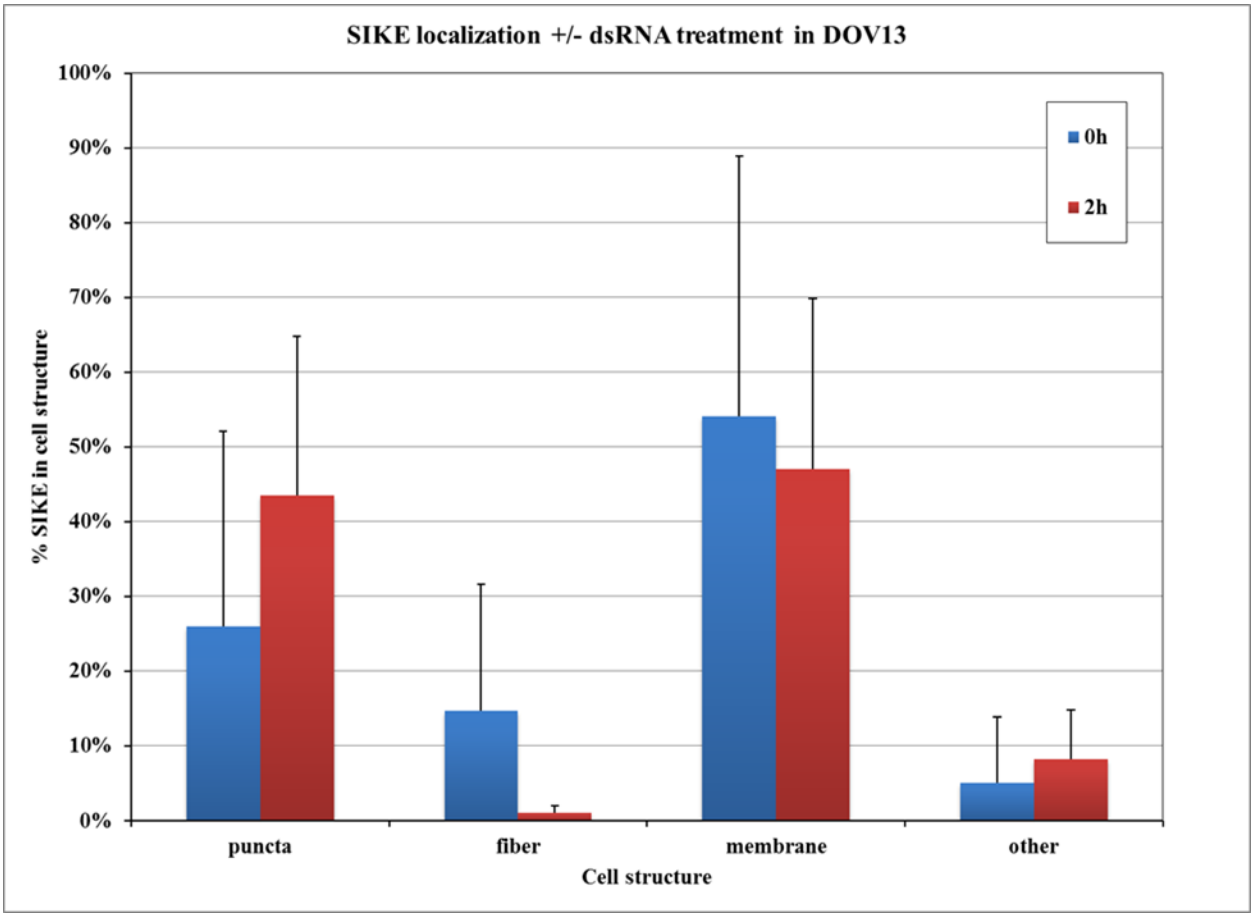

Figure 18. Segmentation analysis in DOV13 during dsRNA challenge does not demonstrate significant alterations of SIKE localization. Percent of total SIKE in each cell localized to various types of intracellular structures. For both time points, three z-stack images were captured from DOV13 microscope slides. Cells included in the t = 0 time point were not treated with poly(I:C) The images were analyzed with the Volocity software, using the protocol described previously (Section 2.6.1). Data represented in graphs are mean values of the percent of total SIKE localized to each structure, calculated from 3 fields ± SEM.

3.4 Suppressor of IKK-ε trafficking and colocalization upon *S. enterica typhimurium* infection

In addition to dsRNA challenge, changes in the SIKE interaction network during *Salmonella* infection were investigated. Because TBK1 is integral to the maintenance of many types of PCVs, including SCVs, it is plausible that SIKE also participates in this maintenance activity, through its interaction with TBK1. In order to answer this question, we chose to perform a time course infection of DOV13 and RAW264.7 cells using *Salmonella* strain SL1344. The red fluorescent protein (RFP) marker stably expressed in SL1344 was used to determine whether infection protocols were successful and permitted visualization of the potential relationship between SIKE and the SCV. RFP fluorescence also streamlined the process of locating the SCV in infected cells.

Previous work in our laboratory with this strain had not yielded strong enough fluorescence for detection by confocal microscopy. Therefore, we performed a selection procedure using streak plating of SL1344 on agar plates. The most vibrantly pink colonies were selected and plated individually on new agar plates. The selection was repeated multiple times to select for the greatest RFP expression prior to use in infection experiments. The pink color of the colonies was the indicator for strong production of RFP (Figure 19 A). For our initial infection, a colony was selected to start liquid broth cultures that were then used to infect our epithelial and myeloid cell cultures. Coverslips from 5 hours and 18 hours (DOV13, M.O.I. 20; RAW264.7 M.O.I. 50) indicated successful selection of SL1344 to express RFP strongly. However, the M.O.I was insufficient because few cells from either cell line were infected, and those cell that were infected bore relatively small infection load (Figure 19 B). A colony located

close to the one used to perform the infection was used to make glycerol stocks. These stocks were the source of SL1344 for the remaining infection experiments.

At this point in the experiment, the fluorescence of RFP in SL1344 was still not as strong as anticipated. We hypothesized that the problem may no longer have been an issue of low levels of RFP expression, but an issue of the cellular machinery of SL1344 struggling to fold the RFP protein appropriately during growth of the bacterial cultures. In order to determine if this was the case, the effect of temperature reduction on RFP folding was tested. However, continuous incubation of the liquid culture at 16°C impeded growth of SL1344 (data not shown), so we attempted growing an SL1344 culture at 37°C until the culture appeared turbid, then reducing the temperature to 16°C. Subsequent centrifugation of the liquid culture revealed that the pellet of bacterial cells was extremely pink, bordering on red, indicating elevated levels of properly folded RFP (data not shown). Subsequent imaging of cells infected with SL1344 grown by this method, at higher M.O.I. (DOV13, 1,000 M.O.I.; RAW264.7, 2,500 M.O.I.) demonstrated stronger RFP signal, as well as a greater number of infected cells bearing a greater infection load than previously observed (Figure 19 C).

Once the protocol for growing SL1344 with high RFP expression was established, changes to the network of SIKE colocalization during SL1344 infection were explored. In order to understand how the colocalization of SIKE with selected markers changed during *Salmonella* infection, cells were labeled for: Rab5 (early stage, 0-30 minutes [14, 15]); Rab11a (intermediate stage, 30 minutes-5 hours [14, 15]); and Rab7 and LAMP-1 (intermediate and late stage, > 5 hours [14, 15]). Since SL1344 expresses RFP, which fluoresces at the same wavelengths as the secondary antibodies previously used for the markers, a fluorophore that emitted in the far red range of wavelengths was used for the markers during infection. Imaging by confocal

microscopy, using the LSM700 equipped with long-pass filters, showed that the separation of the red RFP signal and far red marker signal was insufficient for accurate analysis (Figure 19 D). The insufficient distinction between these two signals was the direct result of overlap in the ranges of light wavelengths allowed to pass through the long-pass filters used for the red and far red channels. This problem was addressed through the use of a different confocal microscope system, the LSM710 (with lambda imaging and linear un-mixing capability). Subsequent imaging of SL1344 infection microscope slides was performed with this confocal microscope which used a spectral detector. The array of detectors and user-defined filters facilitated imaging of quadruple labeled images by enabling fine-tuning of the settings to appropriately separate red and far red fluorescence emission signals. Infected DOV13 labeled for LAMP-1 confirmed that this instrumentation allowed us to achieve sufficient separation amongst the four fluorescent labels (Figure 19 E).

In addition to Rab5, Rab7, Rab11a, and LAMP-1, for which we had already immunolabeled, we added labels for Rab4, Rab9, and α-tubulin when we conducted the SL1344 infection time course experiments. Rab4 was used as an additional marker for the early stage of SCV progression [14, 15], while Rab9 was used as an additional marker for the late stage of SCV progression [14]. α-Tubulin was used to indicate formation of Sifs at the late stage of *Salmonella* infection, which is indicated by rearrangement of the tubulin cytoskeleton [15]. SIKE colocalizes with the tubulin cytoskeleton in the absence of infection, and the aim was to determine whether SIKE's interaction with the tubulin cytoskeleton was altered during the course of SL1344 infection.

We performed two iterations of the infection time course experiment. The first time, we labeled for all seven markers in DOV13 and RAW264.7. During the second attempt, we labeled

each cell line for markers that were determined, by visual analysis, to have either strong colocalization with SIKE, or noticeable changes in the level to which they colocalized with SIKE over the course of infection (Table 4).

When examining the early markers for *S. typhimurium* infection, Rab4 and Rab5, we observed no change in SIKE colocalization in DOV13 (Figure 20). Although the ratio of colocalizing volumes did not change, we did observe a significant negative shift in the PCC of SIKE and Rab4 between 5 and 18 hours post-infection in DOV13 (Figure 20 E), showing that SIKE and Rab4 localize in a mutually exclusive manner at 18 hours post-infection. In RAW264.7, colocalization between SIKE and early *Salmonella* infection markers demonstrated significant changes over the course of infection (Figure 21). SIKE colocalization with Rab4 did not change as the infection progressed (Figure 21 C), while Rab4 colocalization with SIKE did experience a significant decrease from 30 minutes to 1 hour post infection and from 1 hour to 5 hours post infection (Figure 21 D). The PCC of SIKE and Rab4 across all time points in RAW264.7 was effectively zero, with the only significant change being a positive shift between 1 hour and 5 hours post-infection (Figure 21 E). Colocalization between SIKE and Rab5 in RAW264.7 decreased between 5 hours and 18 hours post-infection (Figure 21 F). However, the Rab5 colocalization decreased between 0 hours and 18 hours post-infection, with no difference between 0 hours and 30 minutes post-infection or 1 hour and 18 hours post-infection (Figure 21 G). The correlation between SIKE and Rab5 in RAW264.7 indicated a relatively random interaction between the two based on PCC values of roughly 0 for all the time points. In both DOV13 and RAW264.7, colocalization ratios observed between SIKE and early PCV markers did exhibit some significant changes over the course of infection. However, the magnitude of this colocalization was too low to be considered even weak colocalization with respect to our

previous criteria. Therefore, SIKE does not appear to play a role in the immune response during the early stage of *Salmonella* infection through interaction with the markers associated with this stage.

Based on the criteria for categorizing colocalization, Rab11a, the marker for the intermediate stage of *Salmonella* infection, does not colocalize with SIKE in either cell line (Figure 22 C-D, F-G). When these results are considered with respect to basal colocalization between SIKE and Rab11a in unchallenged cells (Figure 7 and Figure 8), it is apparent that a major decrease in colocalization between these two proteins occurs during *Salmonella* infection. Additionally, at examined time points, SIKE and Rab11a appear to be randomly correlated, exhibiting PCC values very close to 0 in both cell lines (Figure 22 E, H). The random correlation between SIKE and Rab11a, coupled with low ratios of colocalization in epithelial and myeloid cells, suggests that SIKE does interact with Rab11a to influence the immune response to *Salmonella* infection over time.

LAMP-1 and Rab7 are the markers we examined for both the intermediate stage and the late stage of *Salmonella* infection. In DOV13, SIKE and LAMP-1 did not demonstrate actual colocalization (Figure 23 C-D) and the PCCs indicated random correlation (Figure 23 E). Similarly, SIKE did not colocalize with Rab7 (Figure 23 F), but Rab7 demonstrated weak colocalization with SIKE (Figure 23 G). Overall, the PCC of SIKE and Rab7 in DOV13 suggested random correlation, although at 5 hours post-infection, they exhibit a positive correlation, indicating that they preferentially colocalize at this time point (Figure 23 H). SIKE demonstrated weaker colocalization with LAMP-1 in RAW264.7 than in DOV13, with the interaction abating between 30 minutes and 18 hours post-infection (Figure 24 C). Colocalization of LAMP-1 with SIKE was also weaker in RAW264.7 than in DOV13, but the

interaction between the two was reduced between 0 hours to 30 minutes and 0 hours to 5 hours post-infection (Figure 24 D). As was observed in DOV13, correlation between SIKE and LAMP-1 in RAW264.7 is random (Figure 24 E). SIKE did not colocalize with Rab7 in RAW264.7 (Figure 24 F) nor did Rab7 colocalize with SIKE (Figure 24 G) and any correlation between SIKE and Rab7 based on PCC appears random (Figure 24 H). In general, it does not seem likely that SIKE influences the immune response to *Salmonella* infection via interaction with LAMP-1 or Rab7, since SIKE does not colocalize with either marker during infection of epithelial or myeloid cells.

Rab9 and α-tubulin are markers we investigated as markers for the late stage of *Salmonella* infections. While examining the late stage markers in DOV13 (Figure 25), we observed that SIKE did not colocalize with Rab9 (Figure 25 C) and Rab9 did not colocalize with SIKE (Figure 25 D). In fact, PCCs of SIKE and Rab9 suggest that during the intermediate stages of infection, SIKE and Rab9 exclude each other, localizing independent of each other (Figure 25 E). Meanwhile, SIKE and α-tubulin did colocalize at the anticipated level (Figure 25 F-G), and the relationship appeared to display a random correlation (Figure 25 H). In RAW264.7, SIKE did not colocalize with Rab9 (Figure 26 C), but at 0 hours and 5 hours, Rab9 weakly colocalized with SIKE (Figure 26 D). Overall, the correlation between SIKE and Rab9 was random, but at 18 hours they almost seemed to preferentially colocalize with each other, when they were colocalized (Figure 26 E). SIKE colocalized with α-tubulin more strongly in RAW264.7 than in DOV13 during SL1344 infection, consistent with observations made in the absence of pathogen challenge. SIKE colocalization with α-tubulin increased between 0 hours and 30 minutes, then decreased significantly between 30 minutes and 18 hours (Figure 26 F). Colocalization of α-tubulin with SIKE demonstrated significant decreases at each time point compared to 0 hours

(Figure 26 G). The colocalization of SIKE and α-tubulin appears randomly correlated, trending toward a more negative correlation as the infection progressed (Figure 26 H). The relatively low level of colocalization between SIKE and Rab9 in both cell lines indicates that SIKE does not likely play role in the immune response to *Salmonella* infection via interaction with Rab9. Likewise, in DOV13, the decreasing ratio of colocalization between SIKE and α-tubulin coupled with random correlation indicate that SIKE does not interact with α-tubulin to impact the immune response. However, in RAW264.7, the decrease in colocalization between SIKE and α-tubulin over the course of infection, in tandem with the parallel trend toward a more negative correlation, suggests that SIKE associated with the tubulin cytoskeleton in myeloid cells dissociates as the infection develops, perhaps to influence the immune response elsewhere in the cell. In conclusion, it seems that SIKE may play a role in the innate immune response to *Salmonella* infection at the late stage, although the direct colocalization partners involved are yet to be identified.

Figure 19. Selection of SL1344 based on RFP-expression, refinement of liquid culture techniques, and use of optimized confocal microscopy parameters for imaging.

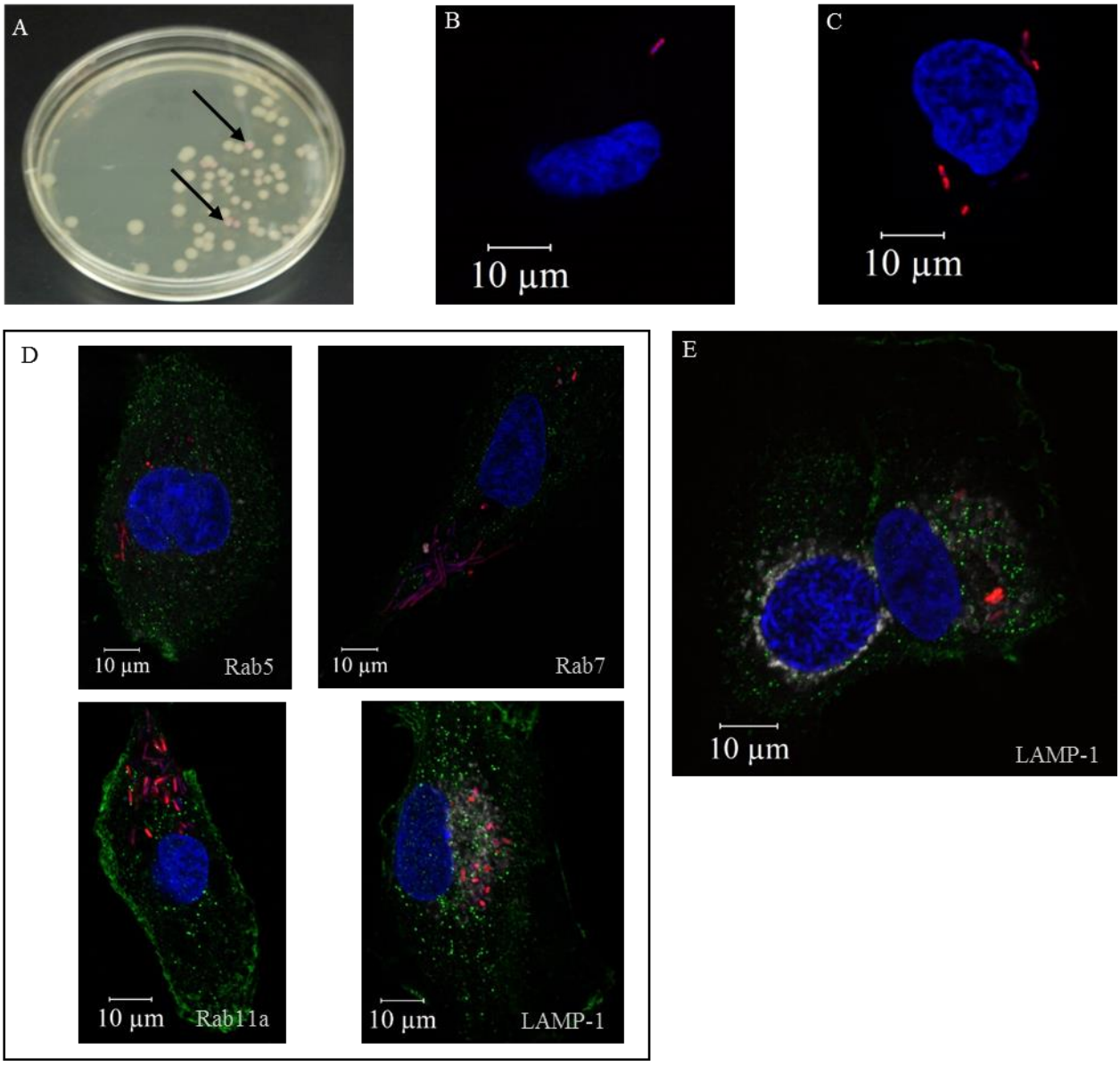

Figure 19. Selection of SL1344 based on RFP-expression, refinement of liquid culture techniques, and use of optimized confocal microscopy parameters for imaging. Steps taken to optimize the procedures for infecting cells with SL1344 and subsequent imaging of those cells. (A) A typical agar plate with SL1344. Based on the colony color, arrows indicate colonies considered to have high RFP expression. (B) SL1344 (red) grown at 37°C overnight was used to infect DOV13 at 20 M.O.I. for 18 hours. (C) SL1344 grown at 37°C until turbid, then overnight at 16°C was used to infect DOV13 at 1,000 M.O.I. for 17 hours. (D-E) After infection, cells were labeled for SIKE (green) and indicated markers (far red, shown as gray), counterstained, and imaged using confocal

microscopy that (D) did not achieve sufficient separation between red and far red signals, or (E) achieved sufficient separation between red and far red signals. Prior to imaging, cells were counterstained for DNA (blue, Hoechst). Gain and laser power settings were optimized for each image.

Table 4. Inclusion of cellular markers in SL1344 infection time course trials.

Cell Structure	*Stage of Infection*	*Marker*	*Epithelial*	*Myeloid*
Cytoskeleton	Late	α-tubulin	+	+
Endosomal Structures	Late	Rab9	+	–
	Intermediate/Late	Rab7	+*	+*
	Intermediate/Late	LAMP-1	+	+
	Intermediate	Rab11a	+	+
	Early	Rab4	–	–
	Early	Rab5	+	–

Number of trials	2 trials	1 trial
Symbol	+	–

Table 4. Inclusion of cellular markers in SL1344 infection time course trials. Summary of markers associated with progression of the SCV during *Salmonella* infection, and their inclusion in both trials of the experiment. The inclusion of markers in both trials was determined by visual observations regarding SIKE's interaction with each marker during the first trial. Only markers which visually demonstrated colocalization or noticeably different levels of colocalization with SIKE over the course of infection were repeated in the second trial.

Figure 20. SIKE colocalization with markers of early *Salmonella* infection remains constant as infection progresses in DOV13.

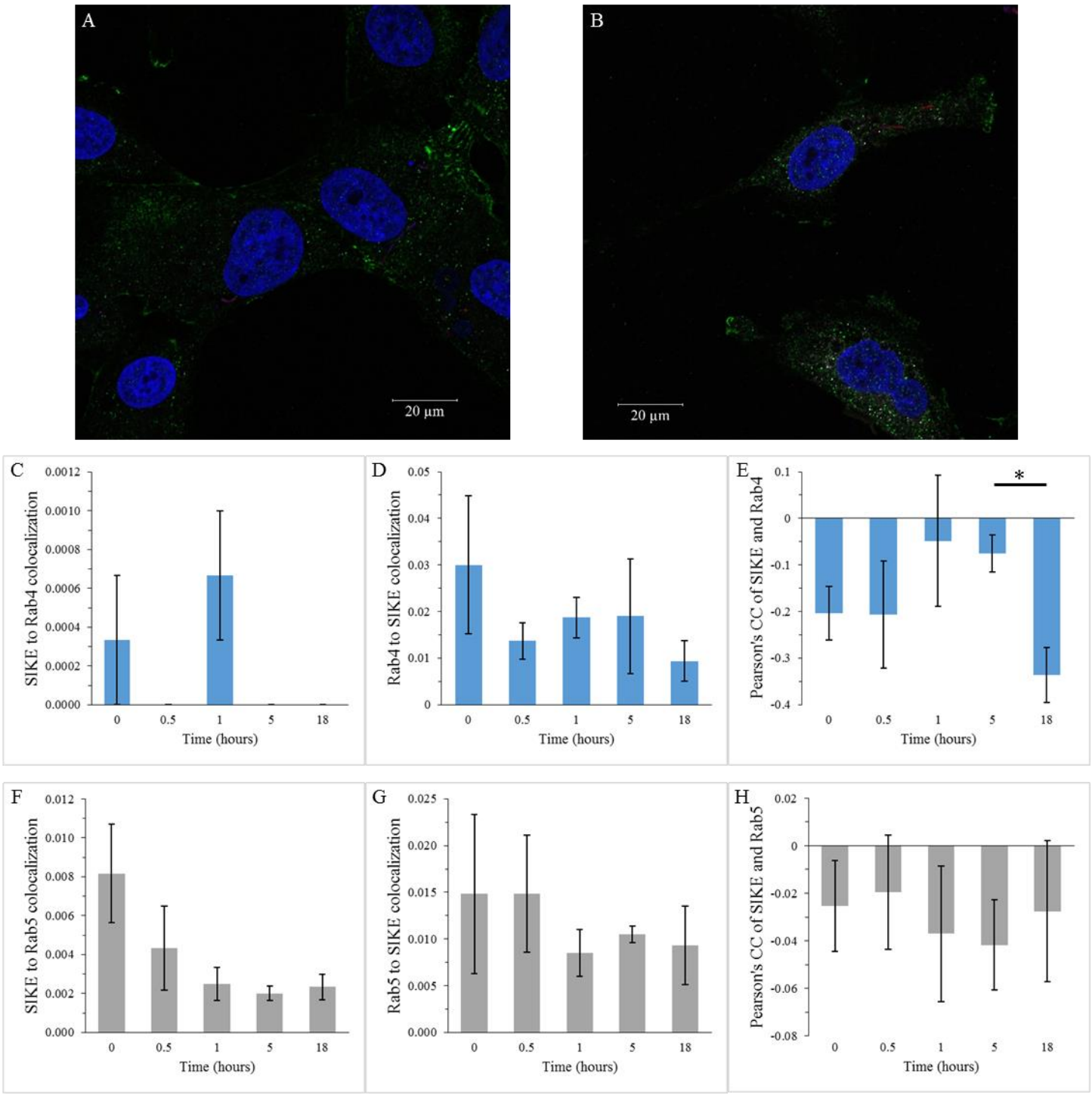

Figure 20. SIKE colocalization with markers of early *Salmonella* infection remains constant as infection progresses in DOV13. DOV13 infected for 18 hours at 1000 M.O.I. with SL1344 (red), and labeled for SIKE

(green) and either (A) Rab4 or (B) Rab5 (gray), then counterstained (DNA, blue). Images represent the single plane of a z-stack image that best represents SIKE/marker interaction observed, level of SL1344 infection similar to Figure 19D (LAMP-1). (C) Mean ratio of SIKE colocalized with Rab4 (colocalized signal volume/total SIKE signal volume). (D) Mean ratio of Rab4 colocalized with SIKE (colocalized signal volume/total Rab4 signal volume). (E) Mean PCC of SIKE and Rab4. Data in graphs represent mean values calculated from 3 fields ± SEM. (F) Mean ratio of SIKE colocalized with Rab5 (colocalized signal volume/total SIKE signal volume). (G) Mean ratio of Rab5 colocalized with SIKE (colocalized signal volume/total Rab5 signal volume). (H) Mean PCC of SIKE and Rab5. Data in graphs represent mean values calculated from 6 fields ± SEM. * denotes P value < 0.05, significance bars connect the two time points compared. Images were captured by confocal microscopy using optimized gain and laser power settings for each image

Figure 21. SIKE colocalization with markers of early *Salmonella* infection decreases as infection progresses in RAW264.7.

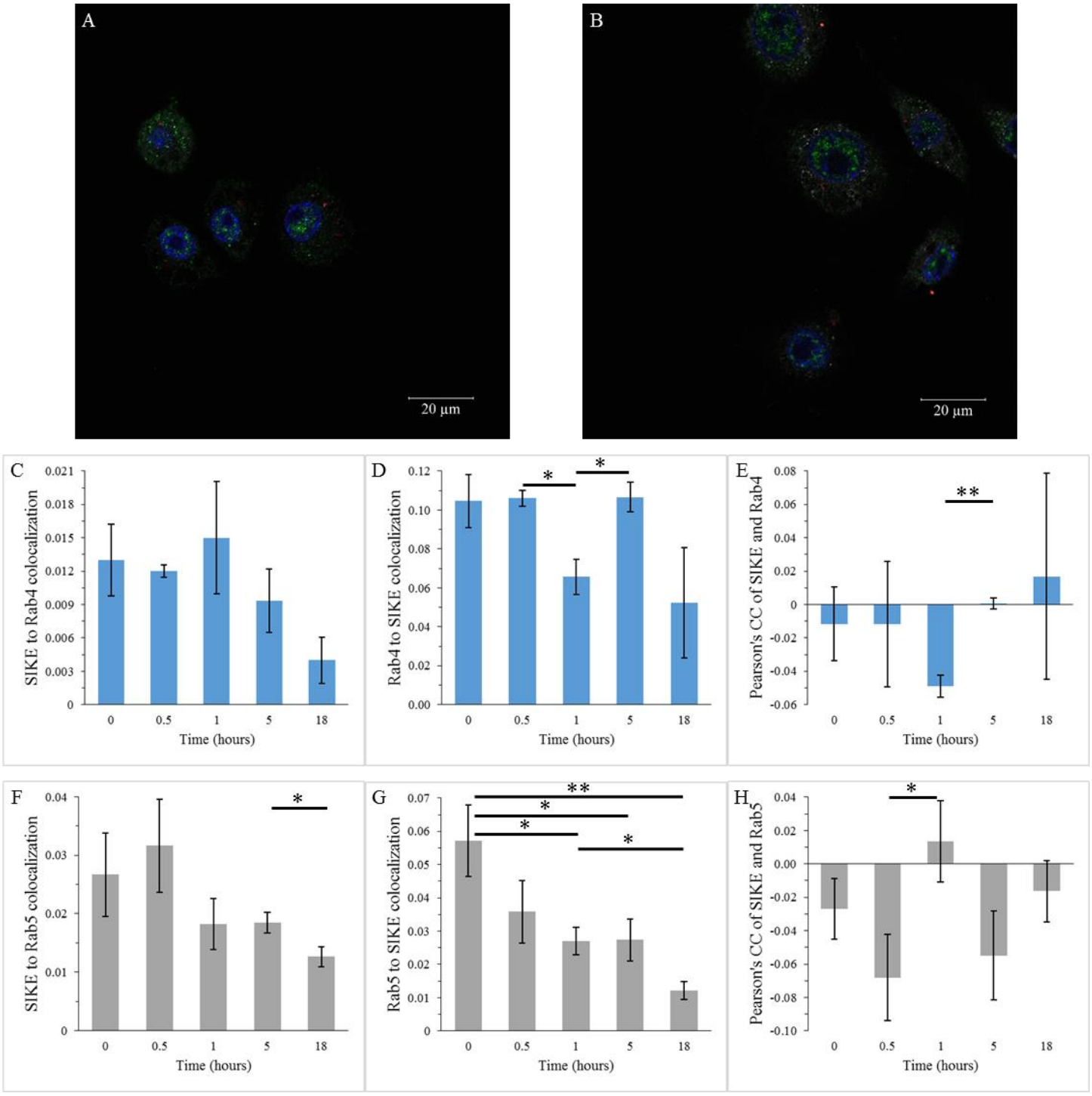

Figure 21. SIKE colocalization with markers of early *Salmonella* infection decreases as infection progresses in RAW264.7. RAW264.7 infected for 18 hours at 2500 M.O.I. with SL1344 (red), and labeled for SIKE (green)

and either (A) Rab4 or (B) Rab5 (gray), then counterstained (DNA, blue). Images represent the single plane of a z-stack image that best represents SIKE/marker interaction observed, level of SL1344 infection similar to Figure 19D (LAMP-1). (C) Mean ratio of SIKE colocalized with Rab4 (colocalized signal volume/total SIKE signal volume). (D) Mean ratio of Rab4 colocalized with SIKE (colocalized signal volume/total Rab4 signal volume). (E) Mean PCC of SIKE and Rab4. Data in graphs represent mean values calculated from 3 fields ± SEM. (F) Mean ratio of SIKE colocalized with Rab5 (colocalized signal volume/total SIKE signal volume). (G) Mean ratio of Rab5 colocalized with SIKE (colocalized signal volume/total Rab5 signal volume). (H) Mean PCC of SIKE and Rab5. Data in graphs represent mean values calculated from 6 fields ± SEM. * denotes P value < 0.05, ** denotes P value < 0.01, significance bars connect the two time points compared. Images were captured by confocal microscopy using optimized gain and laser power settings for each image.

Figure 22. SIKE colocalization with Rab11a, an intermediate stage marker for Salmonella infection does not change over time in DOV13 or RAW264.7.

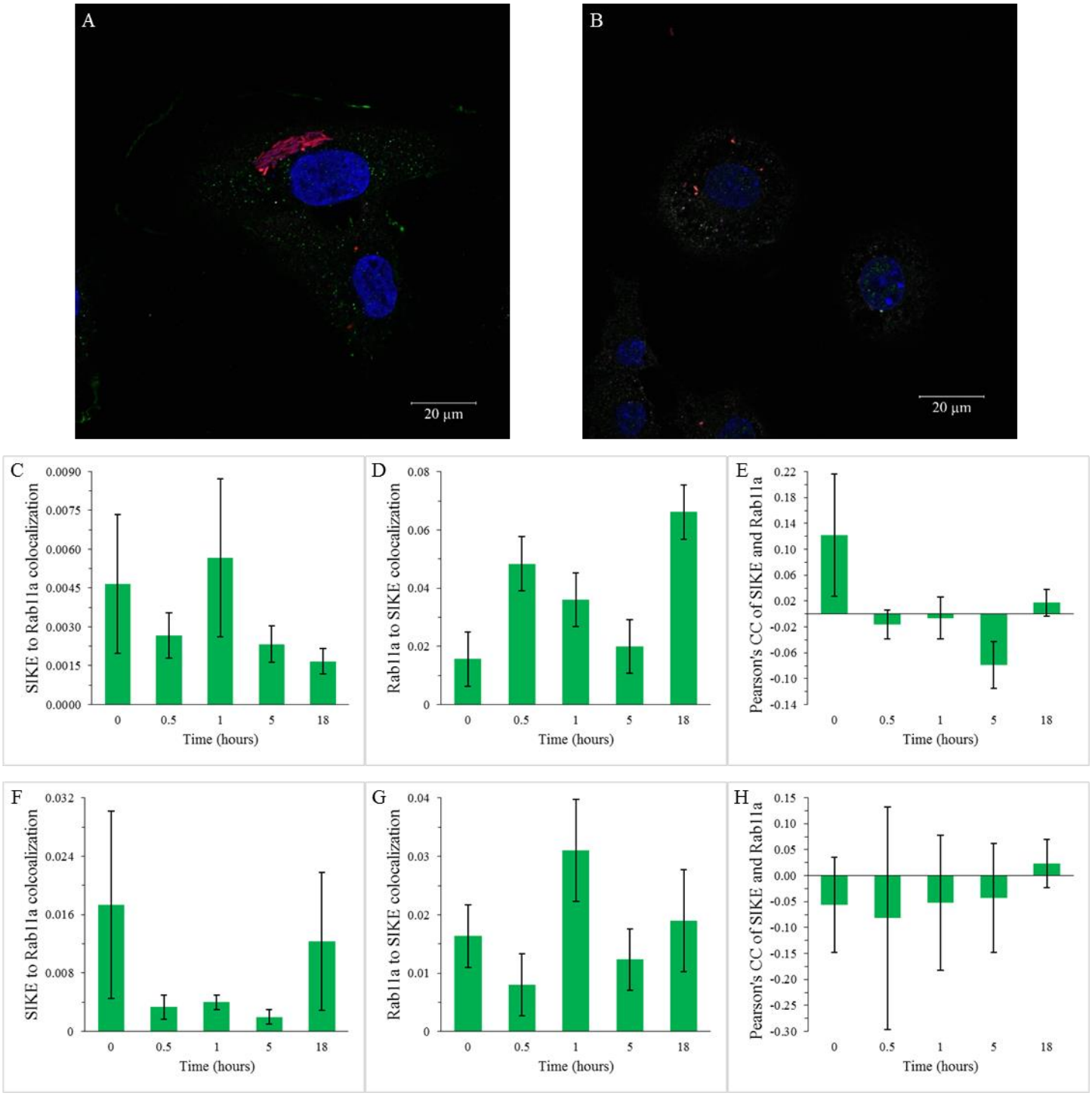

Figure 22. SIKE colocalization with Rab11a, an intermediate stage marker for *Salmonella* infection does not change over time in DOV13 or RAW264.7. (A) DOV13 infected for 18 hours at 1000 M.O.I. and (B) RAW264.7

infected for 18 hours at 2500 M.O.I. with SL1344 (red), and labeled for SIKE (green) and Rab11a (gray), then counterstained (DNA, blue). (C) Mean ratio of SIKE colocalized with Rab11a (colocalized signal volume/total SIKE signal volume) in DOV13. (D) Mean ratio of Rab11a colocalized with SIKE (colocalized signal volume/total Rab11a signal volume) in DOV13. (E) Mean PCC of SIKE and Rab11a in DOV13. Data in graphs represent mean values calculated from 6 fields ± SEM. (F) Mean ratio of SIKE colocalized with Rab11a (colocalized signal volume/total SIKE signal volume) in RAW264.7. (G) Mean ratio of Rab11a colocalized with SIKE (colocalized signal volume/total Rab11a signal volume) in RAW264.7. (H) Mean PCC of SIKE and Rab11a in RAW264.7. Data in graphs represent mean values calculated from 3 fields ± SEM. Images were captured by confocal microscopy using optimized gain and laser power settings for each image.

Figure 23. SIKE colocalization with markers of intermediate and late *Salmonella* infection do not change over time in DOV13.

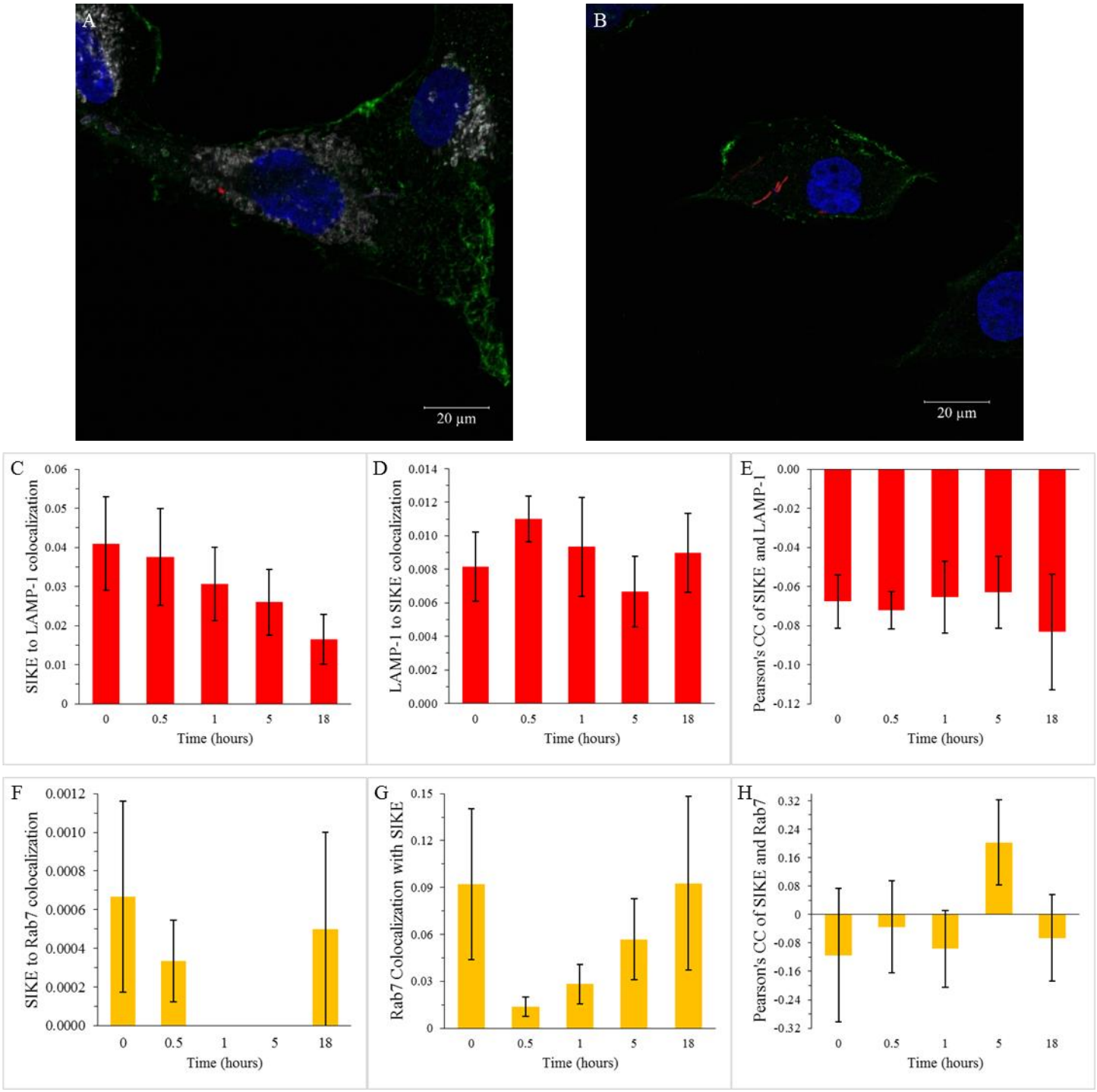

Figure 23. SIKE colocalization with markers of intermediate and late *Salmonella* infection do not change over time in DOV13. DOV13 infected for 18 hours at 1000 M.O.I. with SL1344 (red), and labeled for SIKE (green) and either (A) LAMP-1 or (B) Rab7 (gray), then counterstained (DNA, blue). (C) Mean ratio of SIKE

colocalized with LAMP-1 (colocalized signal volume/total SIKE signal volume). (D) Mean ratio of LAMP-1 colocalized with SIKE (colocalized signal volume/total LAMP-1 signal volume). (E) Mean PCC of SIKE and LAMP-1. (F) Mean ratio of SIKE colocalized with Rab7 (colocalized signal volume/total SIKE signal volume). (G) Mean ratio of Rab7 colocalized with SIKE (colocalized signal volume/total Rab7 signal volume). Data in graphs represent mean values calculated from 6 fields ± SEM. (H) Mean PCC of SIKE and Rab7 (t = 0, 1, 5, 18 means calculated from 5 fields ± SEM, t = 0.5 mean calculated from 3 fields ± SEM). Images were captured by confocal microscopy using optimized gain and laser power settings for each image.

Figure 24. SIKE colocalization with markers of intermediate and late *Salmonella* infection decreases over time in RAW264.7.

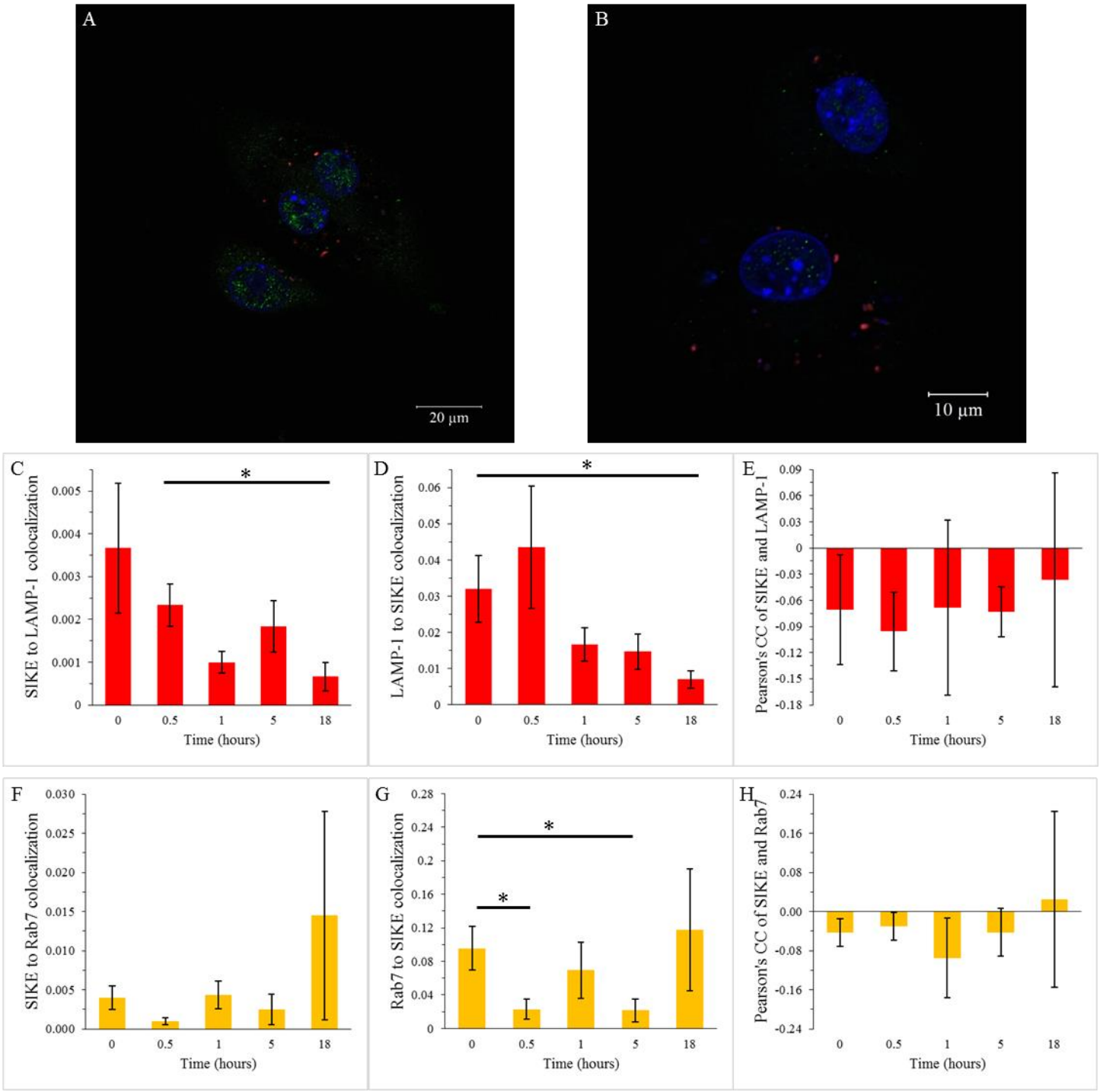

Figure 24. SIKE colocalization with markers of intermediate and late *Salmonella* infection decreases over time in RAW264.7. RAW264.7 infected for 18 hours at 2500 M.O.I. with SL1344 (red), and labeled for SIKE (green) and either (A) LAMP-1 or (B) Rab7 (gray), then counterstained (DNA, blue). (C) Mean ratio of SIKE

colocalized with LAMP-1 (colocalized signal volume/total SIKE signal volume). (D) Mean ratio of LAMP-1 colocalized with SIKE (colocalized signal volume/total LAMP-1 signal volume). (E) Mean PCC of SIKE and LAMP-1 (t = 0, 1, 18 means calculated from 5 fields ± SEM, t = 0.5, 5 means calculated from 6 fields ± SEM). (F) Mean ratio of SIKE colocalized with Rab7 (colocalized signal volume/total SIKE signal volume). (G) Mean ratio of Rab7 colocalized with SIKE (colocalized signal volume/total Rab7 signal volume). (H) Mean PCC of SIKE and Rab7 (t = 0 mean calculated from 6 fields ± SEM, t = 0.5, 1, 5 means calculated from 5 fields ± SEM, t = 18 mean calculated from 4 fields ± SEM). * denotes P value < 0.05, significance bars connect the two time points compared. Images were captured by confocal microscopy using optimized gain and laser power settings for each image.

Figure 25. SIKE colocalization with markers of late *Salmonella* infection does not change over time in DOV13.

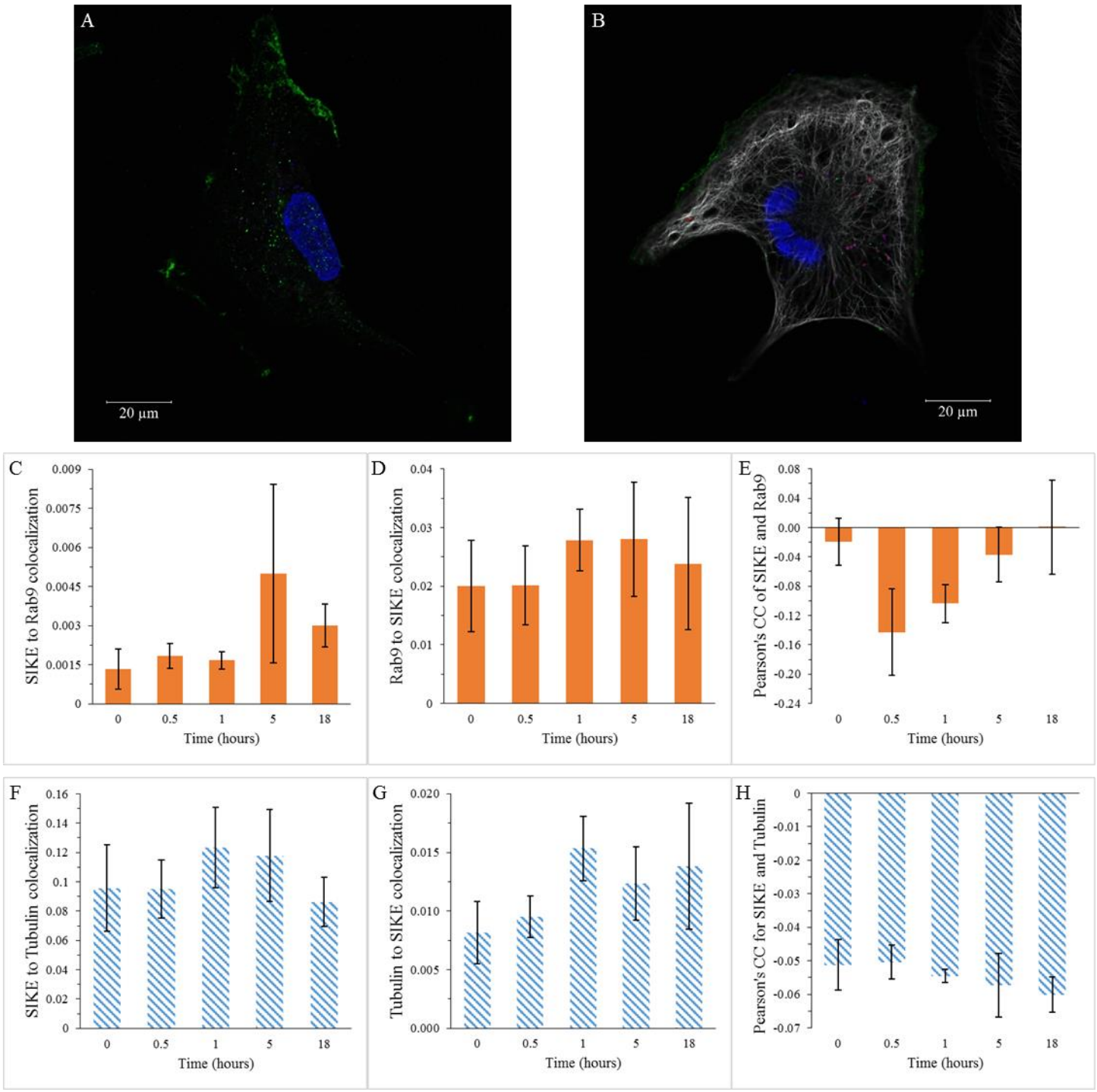

Figure 25. SIKE colocalization with markers of late *Salmonella* infection does not change over time in DOV13. DOV13 infected for 18 hours at 1000 M.O.I. with SL1344 (red), and labeled for SIKE (green) and either (A) Rab9 or (B) α-tubulin (gray), then counterstained (DNA, blue). Images represent the single plane of a z-stack

image that best represents SIKE/marker interaction observed, level of SL1344 infection similar to Figure 19D (LAMP-1). (C) Mean ratio of SIKE colocalized with Rab9 (colocalized signal volume/total SIKE signal volume). (D) Mean ratio of Rab9 colocalized with SIKE (colocalized signal volume/total Rab9 signal volume). (E) Mean PCC of SIKE and Rab9. (F) Mean ratio of SIKE colocalized with α-tubulin (colocalized signal volume/total SIKE signal volume). (G) Mean ratio of α-tubulin colocalized with SIKE (colocalized signal volume/total α-tubulin signal volume). (H) Mean PCC of SIKE and α-tubulin. Data in graphs represent mean values calculated from 6 fields ± SEM. Images were captured by confocal microscopy using optimized gain and laser power settings for each image.

Figure 26. SIKE colocalization with markers of late Salmonella infection decreases over time in RAW264.7.

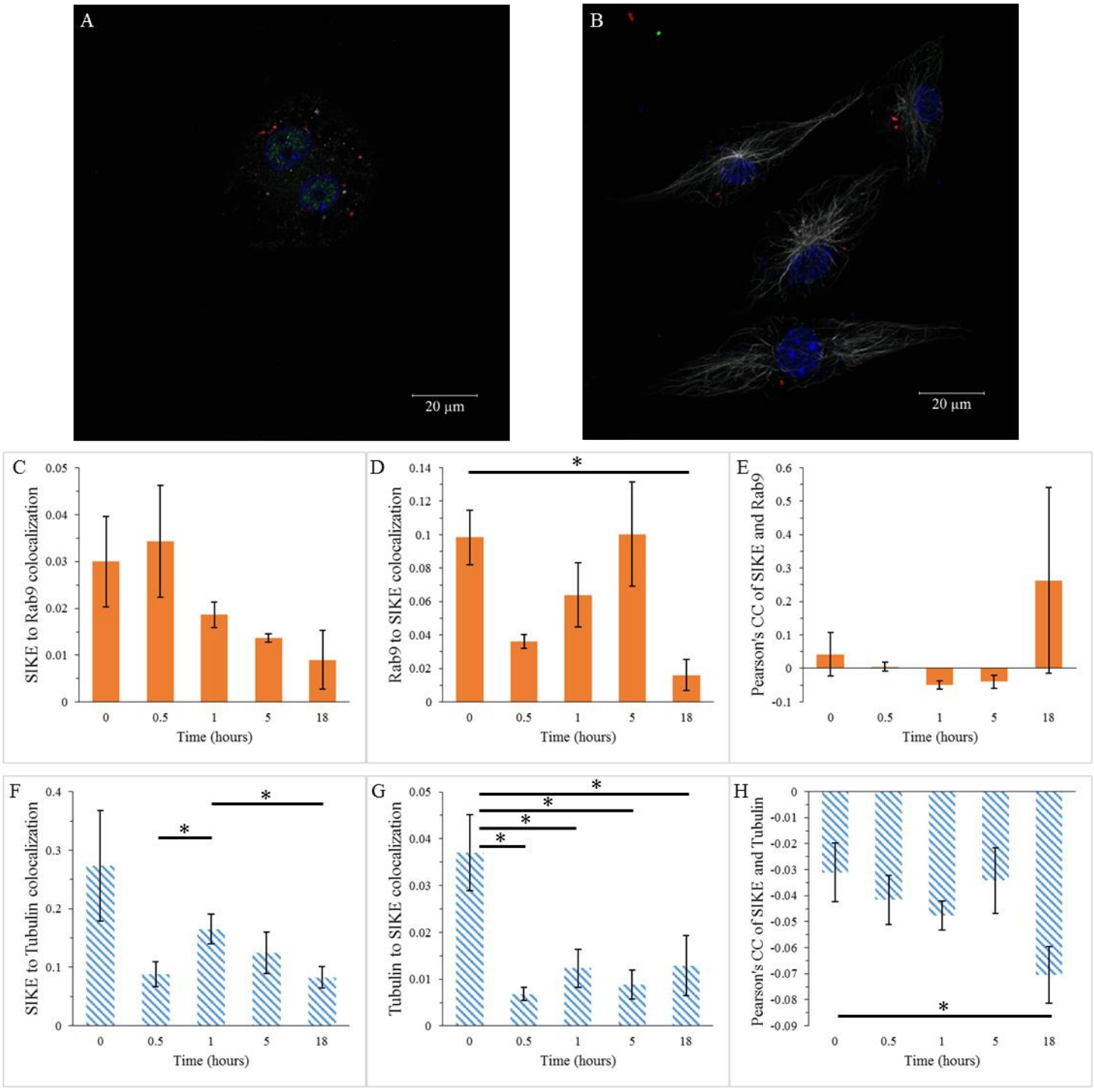

Figure 26. SIKE colocalization with markers of late *Salmonella* infection decreases over time in RAW264.7.

RAW264.7 infected for 18 hours at 2500 M.O.I. with SL1344 (red), and labeled for SIKE (green) and either (A) Rab9 or (B) α-tubulin (gray), then counterstained (DNA, blue). (C) Mean ratio of SIKE colocalized with Rab9 (colocalized signal volume/total SIKE signal volume). (D) Mean ratio of Rab9 colocalized with SIKE (colocalized

signal volume/total Rab9 signal volume). (E) Mean PCC of SIKE and Rab9. Data in graphs represent mean values calculated from 3 fields ± SEM. (F) Mean ratio of SIKE colocalized with α-tubulin (colocalized signal volume/total SIKE signal volume). (G) Mean ratio of α-tubulin colocalized with SIKE (colocalized signal volume/total α-tubulin signal volume). (H) Mean PCC of SIKE and α-tubulin. Data in graphs represent mean values calculated from 6 fields ± SEM. * denotes P value < 0.05, significance bars connect the two time points compared. Images were captured by confocal microscopy using optimized gain and laser power settings for each image.

CHAPTER 4: DISCUSSION AND FUTURE DIRECTIONS

4 Discussion and Future Directions

Originally, SIKE was declared to be an inhibitor of TBK1 [5]. Our lab demonstrated that SIKE is actually a high affinity substrate of TBK1, capable of outcompeting the typical TBK1 substrate, IRF3. SIKE is phosphorylated by TBK1 at sites that mimic the phosphorylation sites of IRF3 and IRF7. The function carried out by phosphorylated SIKE downstream in the TLR3 signaling pathway is unknown. In order to discern the function of SIKE, we sought to develop an understanding of SIKE's interactions in cells.

An interaction network for SIKE was originally identified by co-IP experiments performed in our lab. The experiments identified several proteins associated with RNA trafficking. Co-immunoprecipitation experiments are useful to determine the interactions a protein may have within a cell. However, two proteins may interact with each other directly, or be separated by a complex of several proteins, which may also pull down in a co-IP. Other methods to examine protein-protein interactions can determine interactions that occur across smaller distances.

Later work using immunofluorescence microscopy demonstrated the typical localization pattern for SIKE in epithelial and myeloid cell line. The observed localization of SIKE included cytosolic puncta in two cell types, as well as nuclear puncta in myeloid cells, and stress fibers in epithelial cells. The differential localization patterns observed for SIKE, dependent upon cell type, suggests that SIKE may play different roles in different cell types. Characterization of SIKE localization patterns in additional cell types would be useful in determining other physiologic functions SIKE perform. Based on the observations of SIKE localization, in conjunction with the interaction partners identified by co-IP, we set out to determine specific

colocalization partners of SIKE *in vivo*. Colocalization partners are important to identify because the function of a colocalization partner may provide insight into the function of a protein of interest [29]. In essence, colocalization studies allow for the interaction to be defined in complementary terms. The use of confocal microscopy to characterize colocalization defines the upper limit for distance between two interacting proteins. Typically, confocal microscopes are able to achieve a resolution approaching 250nm, although this figure is largely dependent upon the numerical aperture of the objective lens, the illumination wavelength, and the pin hole setting for each color channel, as well as a variety of other settings [30].

As previously mentioned, we selected a panel of ten standard markers with which to begin our colocalization analysis. As the research progressed, we transitioned from analyzing colocalization solely by visual observation and subjective assessment to quantitation using computer programs. Colocalization occurs when two signals in an image that are perceived as two different colors overlap at the pixel level, creating pixels which possess intensity values considered to be positive signal for both channels in question. The appearance of a third, indicator color occurs only when both signals are found in equal abundance within an image. During our original analysis, we identified colocalization mainly between SIKE, and actin, tubulin, recycling endosomes, and ribosomes. Differential colocalization, dependent on cell-type, was identified between SIKE, and LAMP-1 in epithelial cells or LC3 in myeloid cells. However, the colocalization observed with these markers was weak, and mainly identified only through analysis of colocalization within ROIs rather than whole images. Of the interactions identified, the interaction between SIKE and actin was particularly intriguing because IKKε, a known interaction partner of SIKE, has been shown to play roles in stimulating changes to actin filaments [31].

The markers selected to better understand SIKE's interaction with the actin cytoskeleton were chosen based on observed localization patterns and the function they performed in the actin cytoskeleton. α-Actinin is an actin cross-linking protein responsible for formation of bundles of actin fibers [32]. β-Catenin is a component of the focal adhesion complex known to anchor the actin cytoskeleton to the plasma membrane [33]. Caveolin-1 anchors plasma membrane invaginations, known as caveolae, to the actin cytoskeleton [34]. Ezrin is a protein associated with the plasma membrane and plays a role in anchoring the actin cytoskeleton to the plasma membrane [35]. FAK is a kinase that is integral to the process of cytoskeletal rearrangement at focal adhesions [37]. MLC is an actin interacting protein responsible for providing the mechanical force to move the actin cytoskeleton to facilitate cellular mobility [32]. Additionally, puncta markers were examined to identify the SIKE puncta observed in both cell lines. Fibrillarin was examined only in the RAW264.7 cell line because it is a protein expressed exclusively in the nucleus, specifically, the Dense Fibrillar Component of the nucleolus [36]. Nucleophosphomin-1 was examined in both cell lines because it was identified in the original co-IP experiments as a potential interaction partner of SIKE in both epithelial and myeloid cells. PMP70 (peroxisome) and PSMA7 (proteasome) were selected on the basis that they associate with unique cytosolic puncta for which we had not yet labeled. TBK1 was selected because it is known to interact with SIKE directly as the kinase which phosphorylates SIKE downstream of TLR3 activation.

The interaction between SIKE and the cytoskeleton suggests that SIKE may play a role in the trafficking along the cytoskeleton network. The cytoskeleton network is a major expressway for protein trafficking inside cells [37]. In particular, the actin cytoskeleton plays a critical role in protein transport throughout the cell [37]. This role is primarily facilitated through the action

of actin cytoskeleton-associated proteins, the myosin proteins, which play crucial roles in transport and cell motility [38]. Cell movement can be mediated by class II myosin proteins, which alter the structure of the actin cytoskeleton by performing contractile movements [38, 30]. Other classes of myosin proteins are crucial for trafficking along actin fibers, as they attach to and guide vesicles from one location to another in the cell [39]. However, the low levels of colocalization we observed between SIKE and myosin light chain indicate that SIKE does not directly act to stimulate mechanical changes to, or trafficking along the actin cytoskeleton via interaction with myosin proteins. One issue we noticed with the labeling by our MLC antibody was that the signal produced by the associated secondary antibody was very diffuse. It is possible that the time between labeling and imaging of these slides was too great, allowing the secondary antibody to begin to dissociate from the corresponding MLC primary antibody, although this is not the only explanation for the weak labeling observed with this antibody. Therefore, we were not confident that we observed appropriate myosin labeling and this particular label will need to be repeated.

SIKE exhibited strong colocalization with α-actinin in both cell lines when viewed using confocal microscopy. α-Actinin plays a major role in actin nucleation, facilitating the bundling of actin filaments in the leading edge of cells [32, 40], mainly through the cross-linking of actin filaments [41]. Additionally, α-actinin performs a crucial role in attaching actin filaments to the plasma membrane by binding to cytosolic domains of cadherin and integrin receptors [40]. Based on the functions of α-actinin, the strong colocalization between it and SIKE suggest that SIKE plays a role in cytoskeleton rearrangement associated with cellular motility in response to pathogen challenge.

Another important actin-associated protein with which SIKE colocalized was β-catenin. At cell-cell adhesions, β-catenin functions in a complex with many other adherens junction proteins to mediate the anchoring of the actin cytoskeleton to the plasma membrane [33]. The anchoring is mediated through an indirect interaction between β-catenin and cadherin family receptors [33]. Although the synapses formed between cells at adherens junctions are typically thought of as forming among similar cell types, i.e. two epithelial cells, the junctions may also form between a pathogen and an immune cell [42]. In part, the critical role of β-catenin at adherens junctions explains the interesting interaction observed with SIKE. When imaging cells that had no cell-cell contacts, β-catenin signal was relatively scarce and as a result, we only observed colocalization with SIKE at cell-cell contacts. Adherens junctions are known to play a role in cell-cell signaling [42]. Therefore, the weak colocalization observed between SIKE and β-catenin suggests a possible role in which SIKE acts to induce these cell-cell signaling pathways.

In epithelial cells, we observed colocalization between SIKE and ezrin. Ezrin is a protein in the ezrin-radixin-moesin family of proteins, all of which are highly homologous to each other [35]. Much like α-actinin and β-catenin, ezrin plays an important role in attaching the actin cytoskeleton to the plasma membrane [35]. Additionally, ezrin has been shown to participate in cellular signaling involved with immune responses through interactions with transmembrane receptors [43]. Although the interaction between SIKE and ezrin in epithelial cells was weak, it was extremely close to being considered strong based on our criteria. On average, SIKE colocalized with ezrin at a ratio of 0.533 (colocalizing signal volume/total SIKE signal volume). Colocalization observed with ezrin supports the conclusion that SIKE activates immune response signaling related to the actin cytoskeleton.

SIKE also colocalized with FAK, another key protein in the formation of focal adhesions. FAK is activated by the formation of adhesions [44], and plays an important role in the turnover of focal adhesions [45]. FAK participates in the regulation of cell-cell and cell-matrix adhesions and has been implicated in the pathology of many diseases, including metastatic cancers [45]. Through interactions with FAK, SIKE may potentially facilitate or stimulate reorganization of focal adhesions and the actin cytoskeletal network in order to augment the innate immune signaling or the general innate immune response. Additionally, SIKE may activate cell-cell communication in response to pathogen challenge as a result of its interaction with FAK. Interestingly, we observed SIKE colocalization with many key proteins involved with focal adhesion formation and maintenance. SIKE was also observed to be present in high quantities at the leading edge of many cells examined from the epithelial cell line.

In addition to actin and actin cytoskeleton-associated proteins, SIKE also colocalized with α-tubulin in our cell lines. α-Tubulin is one component of the α- and β-tubulin heterodimers that compose microtubules and make up the tubulin cytoskeletal network [46]. Microtubules provide a major avenue for the transport of cellular components, as motor proteins are capable of using microtubules as "tracks" along which they move their cargo [46]. With respect to this function of tubulin, SIKE may participate in trafficking along the tubulin cytoskeleton. Tubulin and microtubule-associated proteins (MAPs) have also been shown to play pivotal roles in many diseases, often through their dysregulation [47]. Additionally, tubulin is acetylated upon activation of the anti-inflammatory response mediated by interleukin-10 (IL-10) in macrophages stimulated with lipopolysaccharide (LPS), and this interaction is crucial to the proper activation of the IL-10 response [48]. Because the anti-inflammatory response is a crucial part of the body's response to viral infection, the interaction between SIKE and tubulin would be consistent

with a role for SIKE in immune modulation, through an interaction with tubulin, helping to regulate the anti-inflammatory response downstream of TLR3. A striking observation becomes apparent when the colocalization between SIKE and α-tubulin is considered alongside the interactions observed between SIKE and the actin cytoskeletal proteins associated with focal adhesions as well as the localization of SIKE to the leading edge of epithelial cells. This observation suggests that SIKE associates with highly dynamic cytoskeletal structures (i.e. microtubules, focal adhesion networks, actin cytoskeleton at the leading edge). It is possible SIKE plays some role in signaling within these highly dynamic networks or possibly stabilizes the cytoskeleton, preventing excess change through mechanisms yet to be determined.

During our evaluation of SIKE colocalization with puncta markers, we found colocalization between SIKE, and Rab11a and S6. Rab11a is a marker for recycling endosomes, which traffic between the plasma membrane and the *trans*-Golgi apparatus [49]. Rab11a also directs endosomes to the apical plasma membrane in polarized epithelial cells [49]. The interaction between SIKE and Rab11a would support a role for SIKE in signaling the trafficking of endosomes in response to TLR3 signaling.

S6 ribosomal protein is a subunit of ribosomes that, when phosphorylated, correlates to increased translation of messenger RNA [27]. We observed strong colocalization between SIKE and S6 in both cell lines. The strong colocalization observed indicates that SIKE could function to stimulate activation of translation of proteins which are important effectors in the anti-viral response downstream of TLR3 signaling. Overall, the identified interactions between SIKE and the cytoskeleton, recycling endosomes, and ribosomes support our hypothesis that SIKE functions to facilitate trafficking in response to TLR3 activation.

We wanted to expand our understanding of SIKE's interactions with actin, tubulin, and ribosomes. We observed that SIKE colocalized with these markers in both cell lines. Therefore, we hoped to understand what distance separated SIKE from these proteins when they interacted. Based on colocalization observed by confocal microscopy, we were able to conclude that the distance separating SIKE from these proteins was no more than 250nm, the typical resolution associated with confocal microscopy. However, 250nm still covers a rather large range. Therefore, we sought to evaluate SIKE's colocalization with these markers using a super-resolution microscopy technique, Structured Illumination Microscopy. SIM offers improved resolution compared to traditional confocal microscopy due to the increases in effective spatial resolution through the use of patterned light to excite fluorophores on labeled specimens [50].

Colocalization only occurs when the sources of the two signals, the fluorophores, are within close enough proximity to one another that the resolving power of the microscope used to visualize the object is not able to separate the two signals. Because colocalization is dependent upon the resolving power of an imaging tool, it is possible for two proteins to colocalize when viewed under one microscope, but not the other. The relationship between colocalization and the resolution of an instrument explains our desire to look at colocalization by both confocal microscopy and SIM. For example, in our work we identified colocalization between SIKE and α-actinin in both DOV13 and RAW264.7 using confocal microscopy. However, when we observed these cells using SIM, we found that SIKE still colocalized with α-actinin in the epithelial cells, but not in the myeloid cells. We examined the interactions between SIKE, and actin, α-actinin, α-tubulin, or S6 by SIM. These interactions demonstrated some of the strongest colocalization that we observed by confocal microscopy. We observed that SIKE did not colocalize with these markers in RAW264.7. This suggests that while SIKE and α-actinin do

interact in the myeloid cells, they interact in such a way that they are separated by a distance greater than 85nm, the resolution of the SIM microscope [27].

The benefit to using super-resolution microscopy when colocalization is identified using confocal microscopy is that researchers can better understand how two proteins interact based on how far apart they are in the cell. To this end, SIM becomes an even more powerful tool when coupled to resonance energy transfer [51]. The combination of SIM with resonance energy transfer can provide even greater insight into the distance separating two interacting proteins. One experiment which could further develop our understanding of SIKE's function would be to examine fluorescence resonance energy transfer (FRET) for SIKE and identified colocalization partners. The resolution of FRET coupled with traditional confocal microscopy is greater than 20Å and less than 100Å, a vast improvement over the resolution of SIM. FRET experiments coupled with traditional confocal microscopy could help to more accurately define the distance at which SIKE interacts with these markers.

We relied primarily on quantitative evaluation of colocalization in order to define the colocalization network of SIKE. Quantitative analysis of our images presented a unique set of quirks and challenges. Optimized laser power and gain settings for each image prevented us from being able to use any colocalization expressions which relied on intensity because the intensity in images collected with different settings could not be compared to each other. These settings were optimized for each image, meaning that the only coefficients we could consider to characterize colocalization were those coefficients that were independent of intensity. Additionally, we were unable to analyze SIM images by quantitative means because the manipulations involved in reconstructing the data to generate a SIM image alter the image such that any analysis involving signal intensity would be irrelevant. Another challenge was selecting

relevant coefficients for interpretation. Each coefficient has advantages and disadvantages based on the question a researcher is asking. We were able to eliminate any variables dependent upon signal intensity immediately. Following this criterion, the choice was made to focus on coefficients that provided us with a ratio of colocalized signal to total signal of that particular marker.

We also focused on the Pearson's Correlation Coefficient, which enabled us to better understand the colocalization events we observed. The PCC indicates the correlation between the signals of two channels in an image, based on a scale ranging from -1 to 1 [17]. A PCC equal to 1 indicates that the signals from these channels preferentially colocalize with each other; anywhere signal from one channel in an image is present, signal from the other channel will also be present. On the other hand, a PCC equal to -1 indicates that the signals in the two channels are mutually exclusive; anywhere signal from one channel is present, signal from the other channel will never be present. When PCC equals 0, the correlation is random and predicting the presence of signal from one channel based on the presence of signal from the other channel is impossible. In our experiments, we never observed PCC values equal to 1 or -1. For most part, our data indicated that the correlation between signals from the green and red channels was random or slightly negative. However, a major problem with PCC is the extreme sensitivity of this coefficient to different levels of signals. Pearson's can be skewed toward a negative correlation if the relative abundance of signal from one channel greatly outweighs the relative abundance of the signal from the other channel. A prime example of this phenomenon was our work with SIKE and α-tubulin. Typical volume measurements for total α-tubulin signal in our epithelial cell line were greater than 1000μm^3, while typical volume for total SIKE signal in these cells was approximately 200μm^3. The roughly five-fold difference in signal volume

between SIKE and α-tubulin may partially explain the abundance of negative PCC values, even though we observed colocalization in these cells. This was the case for almost all the markers we examined, as SIKE was rarely present in the same volumes as our markers. SIKE was occasionally the minority compared to the marker, as was the case with most of the cytoskeletal markers, and other times, such as with RNA-associated and most endosomal markers, SIKE was the majority relative to the markers. This observation compels us to consider these differences in relative abundance of SIKE and markers when interpreting all colocalization coefficients, not only the PCC.

After defining the colocalization partners of SIKE in cells that were not exposed to pathogen challenge, we wanted to explore how SIKE localization was altered by the activation of TLR3 signaling. TLR3 is activated in response to binding of double-stranded viral RNA [11]. Activation of this signaling pathway leads to the production of type I interferons. For both viral infections and certain bacterial infections, the production of type I IFNs can instigate the activation of programmed cell death pathways [52]. In order to further explore the role of SIKE in the innate immune response to viral infections, we challenged our two cell lines with poly(I:C) to mimic a viral challenge. We decided to fix challenged cells at eight time points over the course of the poly(I:C) challenge. Unstimulated (0h) was selected to establish an unchallenged baseline for SIKE localization, to which we could compare SIKE localization at the other time points. At 15 minutes following TLR3 activation, TRIF speckles, which are TRIF/TBK1 complexes, can be observed in challenged cells [53]. At 2 hours, phosphorylated STAT1 indicates that the TLR3 signaling pathway has been fully activated, since this phosphorylation event is up-regulated by type I IFN produced via TLR3 mediated signaling [6]. Between 15 minutes and 2 hours post-challenge, we also examined 30 minutes and 1 hour, because type I

IFN, which is detected 6 hours to 18 hours post-challenge, is actually produced before STAT1 is phosphorylated (at 2h) [6]. The reason STAT1 is detected before type I IFN is STAT1 collects inside the cell, allowing detection by Western blot, but interferon-β is secreted from the cell, and must therefore reach concentrations in the surrounding environment at which it can be detected. We examined SIKE localization at 8 hours and 12 hours after dsRNA challenge because these time points fall within the established time frame during which interferon-β is released from cells. Finally, SIKE localization at 24 hours post-challenge provided a reference for SIKE localization following full activation and detection of the components of the TLR3 signaling pathway.

We faced several challenges in our attempts to discern SIKE's function in the antiviral response. Primarily, we were interested in how SIKE interacted with other proteins in the cell. Therefore, we elected to track changes in SIKE localization over the course of a simulated viral challenge. In tracking these changes, we sought to identify potential changes to SIKE localization using cells labeled for SIKE and counterstained for DNA. In our earliest attempts, we wanted to determine if SIKE localization changed drastically enough during dsRNA challenge to be observed visually. However, we found that cells labeled for SIKE after challenge, fixing, and labeling were visually consistent across all time points we observed.

The next step we took was to explore quantitative methods of analyzing our fixed time point imaging of dsRNA challenged cells. We undertook the process of segmentation analysis, wherein we used image analysis software on 3-dimensional images to assign SIKE signal to a variety of structures within the cell. 3-dimensional images were analyzed in order to eliminate the bias in the analysis resulting from the use of single z-plane images. Analyzing single z-plane images is problematic, in that it becomes very difficult to guarantee that all images represent

comparable planes within each cell. We began this analysis unsure that it would provide meaningful data. We therefore decided to test this procedure using only images collected from the DOV13 cell line. We thought that the greater cell size would better enable us to accurately assign SIKE to structures in the cell, enabling us to evaluate the practicality of this approach for our study. SIKE was assigned to different cell structures as percentages of total SIKE in that cell. We chose to use percentages because the volume of SIKE present in any one cell was largely dependent upon the size of the individual cell. Therefore, it seemed reasonable that percent of total SIKE would account for the variability in the amount of SIKE due to cell size.

Making use of software which measured the volume of SIKE based upon different user defined criteria, we calculated percent of total SIKE localized to each of our four structure categories. We used three images of DOV13 challenged with poly(I:C) at each time point. For the segmentation analysis, we chose to examine the zero time point to establish an unchallenged baseline with which to compare and the two hour time point because we wanted to test the segmentation analysis at a time point at which a meaningful immunological change could be detected. Segmentation analysis segregated intracellular SIKE signal into fibers, puncta, membrane-associated, and other SIKE. This analysis showed that the amount of SIKE localized to each structure was highly variable among cells. Based on this discovery, we concluded that we would not be able to determine statistically relevant differences in SIKE localization using fixed cell imaging.

Rather than relying on fixed cell imaging to track SIKE localization during dsRNA challenge, we concluded that live cell imaging would prove more successful. We set out to establish stable cell lines expressing fluorescent tagged constructs of SIKE. We planned to repeat our dsRNA challenge time course in these cells, while utilizing spinning disk confocal

microscopy to image the cells over the course of the challenge. Thus far, we have selected a stable pCDNA3.1mTURQ cell line in DOV13 and RAW264.7 cell types. Future work to define the changes in SIKE localization during dsRNA challenge will focus on testing the stable cell lines and performing the challenge time course with live cell imaging.

We also examined SIKE interactions during infection with *Salmonella typhimurium*. TBK1, the kinase which phosphorylates SIKE, is critical to the maintenance of SCVs [13]. Knockdown of TBK1 in macrophages demonstrated that TBK1-deficient cells are unable to partition the bacteria from the cytosol [13]. We hypothesized that SIKE may also contribute to the proper maintenance of the SCV, through its interactions with TBK1.

In order to address this question, we began by establishing our protocol for infecting our cells with *Salmonella*. Our experiments made use of SL1344, a strain of *S. typhimurium* which has been transformed to express RFP. Initial work with SL1344 in our lab was unable to infect cells with bacteria expressing RFP strongly enough for detection by confocal microscopy. We performed selection of SL1344 colonies, based on colony color, for high RFP-expression. The resulting SL1344 glycerol stocks, made from colonies with the highest expression of RFP, were used to infect our cell lines. Early successful infections used M.O.I.s that were too small to establish useful infections. Once appropriate M.O.I. was determined for both cell lines, we performed infections, fixing cells at set time points over the course of infection. It of interest to note that although we infected RAW264.7 at an M.O.I. that was 2.5 fold greater than the M.O.I. used to infect DOV13, our images indicate that RAW264.7 cells, in general, carried smaller infection loads at each time point than DOV13 cells from the same time point. The likely explanation for this observation is that RAW264.7 is a mouse macrophage cell line, meaning

these cells are professional phagocytic cells. Therefore, these cells likely activated a more robust response to clear the SL1344 infection than their epithelial cell counterparts.

During the SL1344 infection time course experiments, we labeled cells for SIKE and markers associated with each of the three stages of the progression of *Salmonella* infection and quantified the colocalization between them. Overall, the interaction between SIKE and the various endosomal markers we examined suggested nothing which would indicate SIKE functions in the immune response to *Salmonella* infection. However, we did observe a marked decrease in colocalization between SIKE and α-tubulin over the course of infection. We opted to examine SIKE colocalization with α-tubulin during SL1344 infection because at the late stage of infection, *Salmonella* stimulates the reorganization of endosomes associated with microtubules and the MTOC to form Sifs [15, 54]. Possibly, this indicates that signaling via the tubulin network stimulates SIKE localized to the tubulin cytoskeleton to dissociate and move elsewhere in the cell. Once located to these other regions, SIKE may stimulate other signaling involved with the innate immune response to *Salmonella* infection.

One issue we noticed during the labeling for the SL1344 infection time course was the peculiar labeling pattern observed for Rab7. Even in uninfected cells, the pattern of Rab7 labeling appeared inconsistent with the observed pattern from our original experiments with this primary antibody. Therefore, we were hesitant to draw conclusions from this Rab7 data until it has been confirmed using a fresh primary antibody against Rab7 that has been shown to function properly.

The function of SIKE as it pertains to *Salmonella typhimurium* infection remains to be fully delineated. Moreover, changes to expression levels and localization of SIKE over the course of infection remain to be determined. The importance of SIKE as a component of the

innate immune response to this infection is largely unknown, although this could be determined via infection of SIKE knockdown or knockout cell lines. By evaluating the ability of SIKE knockdown or knockout cells to cope with *Salmonella* infection, the importance of SIKE to the proper functioning of this immune response can be defined. Changes to SIKE localization during infection can be confirmed by live cell imaging of *Salmonella* infected stable cell lines expressing fluorescent tagged SIKE constructs. Additionally, co-immunopreciptiation of SIKE following infection could also help to identify other potential interaction partners of SIKE related to the infection. Since, the panel of markers we examined for *Salmonella* infection was not all-inclusive, further interaction partners of SIKE can be identified by labeling for additional markers. Labeling for actin during infection would also prove interesting, as we found that SIKE colocalized strongly with the actin cytoskeleton in the absence of pathogen challenge. Also, the colocalization of SIKE with SL1344 in infected cells was not examined. By analyzing the images already collected or collecting new images, we could quantitatively evaluate whether SIKE colocalizes with SL1344, thereby enabling us to posit potential functions SIKE may fulfill in response to this infection. Based on qualitative observation of colocalization, SIKE does not colocalize with SL1344.

In order to develop greater understanding of SIKE's role in the innate immune response to *Salmonella* infection, future experiments will also need to confirm the observed interaction between SIKE and α-tubulin over the course of infection. This confirmation can be achieved through Western blotting and co-immunoprecipitation protocols. Performing co-IP experiments on lysates from cells infected with *S. typhimurium*, wherein SIKE is immunoprecipitated and α-tubulin is pulled down, can outline the interaction between the two proteins. By using lysates

from cells exposed to infection for different lengths of time, the degree of interaction between these proteins can be characterized for the stages of infection progression.

Overall, the results of our research supported our hypothesis that SIKE plays a role in trafficking related to the innate immune response. Interactions with the cytoskeleton indicate that SIKE may function in the cytoskeletal networks. This interaction could alter signaling capacity to stimulate formation of new cytoskeleton rearrangements within the cell to facilitate innate immune responses. Interactions between SIKE and recycling endosomes suggest SIKE may participate in the activation of endosome mediated trafficking of effector molecules throughout the cell. The interaction between SIKE and ribosomes provides strong evidence that SIKE may play a role in the translational regulation of genes necessary for host immune response. During pathogen challenge, several important questions regarding SIKE's function during the immune response remain. However, it appears that SIKE is performing an unknown function during response to *Salmonella typhimurium* infection based on altered colocalization of SIKE with the tubulin cytoskeleton during infection. In conclusion, SIKE appears to play a role in trafficking and signaling related to the innate immune response both downstream from TLR3 activation, and in the response to intracellular pathogenesis by *Salmonella enterica* serovar *typhimurium*.

References

1. Murphy K.M., Travers, P., Walport, M. (Eds.) (2010) Janeway's Immunobiology. 8th Edition. New York: Taylor & Francis, Inc.
2. Willey, J.M., Sherwood, L.M., Woolverton, C.J. (2014) Prescott's Microbiology. 9th Edition. New York: McGraw-Hill Companies, Inc.

3. Keating, S.E., Baran, M., Bowie, A.G. (2011) Cytosolic DNA sensors regulating type I interferon induction. *Trends in Immunology*. **32 (12)**, 574-581
4. Pandey, R.K., Yu, F., Kumar, A. (2013) Targeting Toll-like receptor signaling as a novel approach to prevent ocular diseases. *Indian J. Med. Research*. **138 (5)**. 609-619.
5. Huang, J., Ting, L., Xu, L.G., Chen, D., Zhai, Z., Shu, H.B. (2005) SIKE is an IKKε/TBK1-associated suppressor of TLR3- and virus-triggered IRF-3 activation pathways. *EMBO J*. **24**, 4018-4028.
6. Salaun, B., Coste, I., Rissoan, M.C., Lebecque, S.J., Renno, T. (2006) TLR3 Can Directly Trigger Apoptosis in Human Cancer Cells. *Journal of Immunology*. **176**, 4894-4901.
7. Marion, J.D., Roberts, C.F., Call, R.J., Forbes, J.L., Nelson, K.T., Bell, J.E., Bell, J.K. (2013) Mechanism of Endogenous Regulation of the Type I Interferon Response by Suppressor of IκB Kinase ε (SIKE), a Novel Substrate of TANK-binding Kinase 1 (TBK1). *J. Biol. Chem.* **288 (25)**, 18612-18623.
8. Alexopoulou, L., Holt, A.C., Medzhitov, R., Flavell, R.A. (2001) Recognition of double-stranded RNA and activation of NF-κB by Toll-like receptor 3. *Nature*. **413**, 732-738
9. Bell, J.K., Botos, I., Hall, P.R., Askins, J., Shiloach, J., Segal, D.M., Davies, D.R. (2005) The molecular structure of the Toll-like receptor 3 ligand-binding domain. *PNAS*. **102 (31)**, 10976-10980.
10. Van, D.N., Roberts, C.F., Marion, J.D., Lépine, S., Harikumar, K.B., Schreiter, J., Dumur, C.I., Fang, X., Spiegel, S., Bell, J.K. (2012) Innate immune agonist, dsRNA, induces apoptosis in ovarian cancer cells and enhances the potency of cytotoxic chemotherapeutics. *FASEB J*. **26**, 3188-3198.

11. Zhang, S., Herman, M., Ciancanelli, M.J., Diego, R.P., Sancho-Shimizu, V., Abel, L., Casanova, J. (2013) TLR3 immunity to infection in mice and humans. *Curr. Op. in Immunology*. **25 (1)**, 19-33.

12. Piao, W., Song, C., Chen, H., Diaz, M.A.Q., Wahl, L.M., Fitzgerald, K.A., Li, L., Medvedev, A.E. (2009) Endotoxin tolerance dysregulates MyD88- and Toll/IL-1R domain-containing adapter inducing IFN-β-dependent pathways and increases expression of negative regulators of TLR signaling. *J. Leukocyte Biol*. **86**, 863-875.

13. Radtke, A.L., O'Riordan, M.X.D., (2008) Homeostatic maintenance of pathogen-containing vacuoles requires TBK1-dependent regulation of aquaporin-1. *Cellular Micro.* **10 (11)**, 2197-2207.

14. Steele-Mortimer, O. (2008) The *Salmonella*-containing vacuole – Moving with the times. *Curr. Op. in Micro.* **11**, 38-45.

15. Brumell, J.H., Scidmore, M.A. (2007) Manipulation of Rab GTPase Function by Intracellular Bacterial Pathogens. *Micro. and Molec. Biol. Reviews*. **71 (4)**, 636-652.

16. Zinchuk, V., Wu, Y., Grossenbacher-Zinchuk, O. (2013) Bridging the gap between qualitative and quantitative colocalization results in fluorescence microscopy studies. *Scientific Reports*. **3 (1365)**, doi: 10.1038/srep01365.

17. Manders, E.M.M., Verbeek, F.J., Aten, J.A. (1993) Measurement of co-localization of objects in dual-color confocal images. *Journal of Microscopy*. **169 (3)**, 375-382.

18. Dunn, K.W., Kamocka, M.M., McDonald, J.H. (2011) A practical guide to evaluating colocalization in biological microscopy. *Am. J. Physiol. Cell Physiol*. **300**, C723-C742.

19. Cavalli, V., Corti, M., Gruenberg, J. (2001) Endocytosis and signaling cascades: a close encounter. *FEBS Letters*. **498**, 190-196.

20. Hyttinen, J.H.T., Niittykoski, M., Salminen, A., Kaarniranta, K. (2013) Maturation of autophagosomes and endosomes: A key role for Rab7. *Biochimica et Biophysica Acta*. **1833**, 503-510.

21. Baetz, N.W., Goldenring, J.R. (2014) Distinct patterns of phosphatidylserine localization within the Rab11a-containing recycling system. *Cellular Logistics*. **4**, http://dx.doi.org/10.4161/cl.28680

22. Mambula, S.S., Stevenson, M.A., Ogawa, K., Calderwood, S.K. (2007) Mechanisms for Hsp70 Secretion: Crossing Membranes Without A Leader. *Methods*. **48 (3)**, 168-175.

23. Wild, P., McEwan, D.G., Dikic, I. (2014) The LC3 interactome at a glance. *Journal of Cell Science*. **127**, 3-9.

24. Rzeczkowski, K., Beuerlein, K., Müller, H., Dittrich-Breiholz, O., Schneider, H., Kettner-Buhrow, D., Holtmann, H., Kracht, M. (2011) c-Jun N-terminal kinase phosphorylates DCP1a to control formation of P bodies. *J. Cell Bio.* **194 (4)**, 581-596.

25. Vance, C., Scotter, E.L., Nishimura, A.L., Troakes, C., Mitchell, J.C., Kathe, C., Urwin, H., Manser, C., Miller, C.C., Hortobágyi, T., Dragunow, M., Rogelj, B., Shaw, C.E. (2013) ALS mutant FUS disrupts nuclear localization and sequesters wild-type FUS within cytoplasmic stress granules. *Human Molecular Genetics*. **22 (13)**, 2676-2688.

26. Peterson, R.T., Schreiber, S.L. (1998) Translational control: Connecting mitogens and the ribosome. *Current Biology*. **8**, R248-R250.

27. Cooper, J.A. (1987) Effects of Cytochalasin and Phalloidin on Actin. *The Journal of Cell Biology*. **105**, 1473-1478.

28. Nikon Instruments Inc. N-SIM Super-Resolution Microscope system. Nikon Instruments - Microscopes. [Online]. Available: http://www.nikoninstruments.com/Products/Light-Microscope-Systems/Inverted-Microscopes/N-SIM-Super-Resolution [18 Nov. 2014].

29. Zinchuk, V., Zinchuk, O., Okada, T. (2007) Quantitative Colocalization Analysis of Multicolor Confocal Immunofluorescence Microscopy Images: Pushing Pixels to Explore Biological Phenomena. *Acta Histochem. Cytochem.* **40 (4)**, 101-111.

30. Cox, G., Sheppard, C.J.R. (2004) Practical Limits of Resolution in Confocal and Non-Linear Microscopy. *Microscopy Research and Technique*. **63**, 18-22.

31. Oshima, K., Takeda, M., Kuranaga, E., Ueda, R., Aigaki, T., Miura, M., Hayashi, S. (2006) IKKε Regulates F Actin Assembly and Interacts with *Drosophila* IAP1 in Cellular Morphogenesis. *Current Biology*. **16**, 1531-1537.

32. Le Clainche, C., Carlier, M. (2008) Regulation of Actin Assembly Associated with Protrusion and Adhesion in Cell Migration. *Physiology Review*. **88**, 489-513.

33. Nelson, W.J. (2008) Regulation of cell-cell adhesion by the cadherin-catenin complex. *Biochem. Soc. Trans.* **36 (Pt 2)**, 149-155.

34. Navarro, A., Anand-Apte, B., Parat, M. (2004) A role for caveolae in cell migration. *FASEBJ*. **18**, 1801-1811.

35. Clucas, J., Valderrama, F. (2014) ERM proteins in cancer progression. *Journal of Cell Science*. **127**, 267-275.

36. Sobol, M., Yildirim, S., Philimonenko, V.V., Marášek, P., Castaño, E., Hozák, P. (2014) UBF complexes with phosphatidylinositol 4,5-bisphosphate in nuclear organizer regions regardless of ongoing RNA polymerase I activity. *Nucleus*. **4 (6)**, 478-486.

37. Lodish, H., Berk, A., Kaiser, C.A. and Krieger, M. (2007) Molecular Cell Biology, 6th edition. New York: W.H. Freeman & Co

38. Betapudi, V. (2014) Life without double-headed non-muscle myosin II motor proteins. *Frontiers in Chemistry*. **2 (45)**, doi:10.3389/fchem.2014.00045.

39. Papadopulos, A., Tomatis, V.M., Kasula, R., Meunier, F.A. (2013) The cortical acto-myosin network: from diffusion barrier to functional gateway in the transport of neurosecretory vesicles to the plasma membrane. *Frontiers in Endocrinology*. **4 (153)**, doi: 10.3389/fendo.2013.00153.

40. Bois, P.R.J., Borgon, R.A., Vonrhein, C., Izard, T. (2005) Structural Dynamics of α-Actinin-Vinculin Interactions. *Molecular and Cell Biology*. **25 (14)**, 6112-6122.

41. Foley, K.S., Young, P.W. (2014) The non-muscle functions of actinins: an update. *Biochem. J*. **459**, doi:10.1042/BJ20131511.

42. Yamada, S., Nelson, W.J. (2007) Synapses: Sites of Cell Recognition, Adhesion, and Functional Specification. *Annual Rev. Biochem.* **76**, 267-294.

43. Neisch, A.L., Fehon, R.G. (2011) Ezrin, Radixin, and Moesin: Key regulators of membrane-cortex interactions and signaling. *Curr. Op. Cell Biol*. **23 (4)**, 377-382.

44. Leask, A. (2012) Focal Adhesion Kinase: A Key Mediator of Transforming Growth Factor Beta Signaling in Fibroblasts. *Advances in Wound Care*. **2 (5)**, 247-249.

45. Yeatman, T.J. (2004) A renaissance for SRC. *Nature Reviews*. **4**, 470-480.

46. Parker, A.L., Kavallaris, M., McCarroll, J.A. (2014) Microtubules and their role in cellular stress in cancer. *Frontiers in Oncology*. **4 (153)**, doi:10.3389/fonc.2014.00153.

47. Tang, E.I., Mruk, D.D., Cheng, Y.C. (2013) MARKs (MAP/microtubule affinity-regulating kinases), microtubule dynamics and spermatogenesis. *Journal of Endocrinology*. **217 (2)**, doi: 10.1530/JOE-12-0586.

48. Wang, B., Rao, Y.H., Inoue, M., Hao, R., Lai, C.H., Chen, D., McDonald, S.L., Choi, M.C., Wang, Q., Shinohara, M.L., Yao, T.P. (2014) Micortubule acetylation amplifies p38 kinase signaling and anti-inflammatory IL-10 production. *Nature Communications*. **5 (3479)**, doi: 10.1038/ncomms4479.

49. Thuenauer, R., Hsu, Y.C., Carvajal-Gonzalez, J.M., Deborde, S., Chuang, J.Z., Römer, W., Sonnleitner, A., Rodriguez-Boulan, E., Sung, C.H. (2014) Four-dimensional live imaging of apical biosynthetic trafficking reveals a post-Golgi sorting role of apical endosomal intermediates. *PNAS*. **111 (11)**, 4127-4132.

50. O'Holleran, K., Shaw, M. (2014) Optimized approaches for optical sectioning and resolution enhancement in 2D structured illumination microscopy. *Biomedical Optics Express*. **5 (8)**, 2580-2590.

51. Choi, H., Wadduwage, D., Matsudaira, P.T., So, P.T.C. (2014) Depth resolved hyperspectral imaging spectrometer based on structured light illumination and Fourier transform interferometry. *Biomedical Optics Express*. **5 (10)**, 3494-3507.

52. Dhariwala, M.O., Anderson, D.M. (2014) Bacterial programming of host responses: coordination between type I interferon and cell death. *Frontiers in Microbiology*. **5 (545)**, doi:10.3389/fmicb.2014.00545.

53. Funami, K., Sasai, M., Ohba, Y., Oshiumi, H., Seya, T., Matsumoto, M. (2007) Spatiotemporal Mobilization of Toll/IL-1 Receptor Domain-Containing Adaptor Molecule-1 in Response to dsRNA. *The Journal of Immunology*. **179**, 6867-6872.

54. Krieger, V., Liebl, D., Zhang, Y., Rajashekar, R., Chlanda, P., Giesker, K., Chikkaballi, D., Hensel, M. (2014) Reorganization of the Endosomal System in *Salmonella*-Infected Cells: The Ultrastructure of *Salmonella*-Induced Tubular Compartments. *PLOS Pathogens*. **10 (9)**, e1004374. doi: 10.1371/journal.ppat.1004374.

55. Marion, J.D. (2013) The activation, receptor complexing and endogenous regulation of the type-1 interferon response as it pertains to innate immunity. Ph.D. dissertation. Virginia Commonwealth University, Richmond, VA.

56. Sasikumar, A.N., Perez, W.B., Kinzy, T.G. (2012) The Many Roles of the Eukaryotic Elongation Factor 1 Complex. *Wiley Interdiscip. Rev. RNA*. **3 (4)**, 543-555.

57. Costes, S.V., Daelemans, D., Cho, E.H., Dobbin, Z., Pavlakis, G., Lockett, S. (2004) Automatic and Quantitative Measurement of Protein-Protein Colocalization in Live Cells. *Biophysical Journal*. **86**, 3993-4003.

Vita

Kenneth F. Lawrence was born in Washington, D.C., U.S.A. on January 26, 1989. Following graduation from Brentsville District High School, he attended Bridgewater College, graduating with a Bachelor of Science in Biology and a minor in Philosophy and Religion in May 2013. He received his Master of Science degree in Microbiology and Immunology from Virginia Commonwealth University in December 2013. He plans to pursue a career in microbiology, immunology, or biomedical research.